MULTIFUNCTIONAL GRAPHITE NANOPLATELETS (GNP) REINFORCED CEMENTITIOUS COMPOSITES

HUANG SIXUAN

(B. Eng., Tsinghua University)

A THESIS SUBMITTED

FOR THE DEGREE OF MASTER OF ENGINEERING

DEPARTMENT OF CIVIL ENGINEERING

NATIONAL UNIVERSITY OF SINGAPORE

2011/2012

Acknowledgements

I wish to express my sincere thanks to Dr. Pang Sze Dai and Professor Quek Ser Tong under whose supervision this study was carried out. Their dedication, invaluable guidance and constructive advices make this research a success.

I am very grateful to the staff in the Concrete and Structural Engineering Laboratories of the Department of Civil Engineering in NUS for their kind assistance and support throughout the whole project.

Special thanks go to former undergraduate student Wang Peng for her great help in sharing this project. Thanks also go to my colleagues and friends, Jin Jiangang, Zhang Yang, Fu Yingfei, Lin Kunpeng, Chen Jianghang, Du Hongjian and others for their encouragement and friendship all along the way.

Finally, deepest appreciation goes to my parents and my girl friend He Nanxi for their endless love, understanding and support.

Table of Contents

Abstract

Construction materials have evolved from materials that are mechanically strong to materials that are both strong and smart. This study investigates the feasibility of using GNP (Graphite nanoplatelets) as a novel conductive admixture for developing multifunctional cementitious composites, aiming at both enhancing their mechanical and electrical properties as well as making them sensible to their internal damage by showing electrical resistance increase. Introducing Darex Super 20 as a novel dispersant and applying ultra-sonication technique facilitated effective dispersion of GNP particles in the cement matrix.

For the tests on mechanical properties, up to 1.5% (by total weight of cement and sand) of GNP was added and increases of up to 20% and 17% were observed in compressive strength and flexural strength respectively for the mortar specimens. For the cement paste batches, an increase of up to 82% in flexural strength was observed. The enhancements in mechanical properties of the composites are due to the small size effect, surface effect, filler effect, crack arresting effect of the GNP particles and the improvement in the interfacial transition zone of the cement matrix. However, more significant enhancements in mechanical properties of the cementitious nanocomposites are desired before they can be attractive in construction industry.

For the tests on electrical properties, mortar with a dose of GNP as high as 5% was successfully fabricated guided with a non-conventional processing technique. Decrease in resistivity of the cementitious composites to the kΩ*cm's level was

observed and the conducting mechanisms were discussed. Parametric studies were performed on the factors having effects on electrical resistance of the specimens, to serve as knowledge preparation for the studies on their self damage memorizing properties. In the self crack memorizing tests, the relations between electrical resistance increase and growth of a traction-free crack at the center of the specimens were studied and a model based on the law of electrical resistance was proposed. The electrical resistance curves for specimens under repeated uniaxial compression showed their ability in monitoring internal damage development and the advantages of the damage memorizing method over the real-time damage sensing method.

This study serves as a preliminary development for smart construction materials that can monitor the integrity of the structures. Further researches are needed before the test results in this study can be applied into the real structures.

List of Tables

List of Figures

List of Notations

ASTM	American society for testing and materials
BS	British Standard
CB	Carbon black
CF	Carbon fiber
CFRC	Carbon fiber reinforced concrete
CNT	Carbon nanotube
DC	Direct Current
GNP	Graphite nanoplatelet
MWNT	Multi-walled nanotube
ITZ	Interfacial transition zone
SEM	Scanning electron microscope
SWNT	Single-walled nanotube
ε	Strain
π	Pi
σ	Stress
ρ	Resistivity
α	Angle
Δ	Differential
∞	Infinity

A_r	Residual cross section area
a	Constant got from Linear Regression
b	Constant got from Linear Regression
d	Crack depth
d/D	Relative crack depth
d_0	Original crack depth
d_f	Final crack depth
$d_{1\text{-}2}$	Dividing point for the two segments in the curve of f(d/D) versus d/D
f(d/D)	A function modifying the electrical resistance
D	Height of the specimen
k	Constant got from Linear Regression
k_1	A constant in the model
L	Length of the specimen
n	Number of equivalent layers in the thickness direction
R	Electrical resistance
R_0	Original electrical resistance
R_f	Final measured electrical resistance
R_{li}	Longitudinal electrical resistance
R_{ti}	through-thickness electrical resistance
s/c	Sand to cement ratio
T	Temperature
W	Width of the Specimen
w/c	Water to cement ratio

CHAPTER 1 INTRODUCTION

1.1 Background

Progress in research of material directly affects social development and the degree of progress in human civilization. With the rapid development of modern science and technology, materials used in civilian industries have been required for higher and higher performance that individual materials cannot satisfy. Developing designable composite materials has become one of the inevitable trends (Luo J., 2009).

Composite materials, often shortened to composites, are engineered or naturally occurring materials made from two or more constituent materials with significantly different physical or chemical properties which remain separate and distinct at the macroscopic or microscopic scale within the finished structure (Wikipedia, 2011). There are two categories of constituent materials: matrix and reinforcement. The matrix material surrounds and supports the reinforcement materials by maintaining their relative positions. The reinforcements impart their special mechanical and physical properties to enhance the matrix properties.

For smart multifunctional composites, usually not only conventional mechanical properties are enhanced, but also some new physical, chemical or biological properties are provided. As modern concrete structures become large-scale and smart, cementitious composites have also evolved from materials that are mechanically strong to materials

that are both strong and smart. One of the methods achieving this is by adding conductive admixtures. When cement-based matrix is intrinsically a material with poor conductivity, incorporating conductive admixtures significantly improves its electrical properties and provides it self-sensing ability shown by the response of electrical resistance change (Chung D. D. L., 2003). This smart behavior shows the potential of cementitious composites to be used in monitoring structural integrity. Comparing to other smart materials such as optical fibers, piezoelectric sensors, etc., cementitous composites are themselves structural materials and have the advantages of low cost, good durability, large sensing volume, good compatibility with concrete structure and absence of mechanical property degradation due to embedded sensors (Chacko R. M. et al., 2007).

Nowadays, carbon-based particles are the most common used conductive admixtures for fabricating multifunctional cementitious composites, because of their high conductivity, high strength, high elastic modulus, as well as high resistance to corrosion. Carbon fiber (CF), carbon nanotube (CNT) and carbon black (CB) have been used in previous researches, with which both strength enhancements as well as self-sensing behaviors of the cementitious composites have been widely reported.

1.2 Literature Review

1.2.1 Carbon Fiber Reinforced Cementitious Composites

Developed since the 1960s, carbon fiber (CF) is the first carbon-based material used to develop multifunctional cementitious composites. The effects of CF on improving properties of cementitious composites will be reviewed in this section.

1.2.1.1 Mechanical Properties

CF is considered to be a good substituent for steel bar in concrete, to solve the corrosion problem met by conventional steel. Researches on carbon fiber reinforced cement concrete (CFRC) started in the beginning of the 1970s and developed rapidly since the 1990s (Wang Y., 2007). Judging from the test results it is concluded that CF can effectively enhance the mechanical properties of concrete.

It is well known that concrete has a low tensile strength, which is usually only 1/8 to 1/17 of its compressive strength. The tensile strength of pitch-based CF is 300 to 500 times higher than that of plain concrete, and its elastic modulus is 1.5 to 2 times higher. When CF with a fraction of 3% by volume was added, the tensile strength and flexural strength of concrete were increased by up to 56% and 138% respectively (Toutanji H. A. et al., 1994).

The failure of concrete is closely related to the development of internal micro cracks. Adding CF to constrain the transverse deformation of concrete, and in turn limit the

development of internal micro cracks, is a way to increase its compressive strength. It was found that the compressive strength of CFRC was 20% to 50% higher than the compressive strength of plain concrete (Chung D. D. L., 1998).

It is widely accepted that there are two effects which help to improve mechanical properties in CFRC: the strengthening effect and the toughing effect (Gong S., 2008). For the first effect, since elastic modulus of CF is higher than that of concrete, when stress is applied, load will transfer at the interface of CF and the cement matrix. In the case of a same strain, CF will carry a greater load and thereby sharing the load borne by the matrix, resulting in enhancement of the overall strength. For the second effect, the existence of CF greatly prevents crack propagation by bridging the cracks as they are about to open, this delays the failure of concrete and increases its toughness.

1.2.1.2 Electrical and Self-sensing Properties

CFRC is the first carbon-based cementitious composite whose electrical properties were studied. Chung D. D. L. first found in 1989 (Chiou J.-M. et al., 1989) that when short CFs were added into the cement matrix, the composites became conductive. Furthermore, when the original electrical resistance of the composite was decreased to a certain range, the change of its resistivity had a good corresponding relationship with the compressive stress it suffered, which means a self-sensing ability towards the change in its internal stress, strain and damage (Chen P.-W. and Chung D. D. L., 1993). Subsequently, research group of Chung D.D.L. conducted a series of studies on the self-sensing properties of CFRC, including using CFRC as a stress sensor for real-time self-monitoring of concrete

structures, response of CFRC under static and dynamic loads; relationships between damage and resistivity change of CFRC, etc. (Chung D. D. L., 2003).

Other researchers also started to be interested in the self-sensing properties of CFRC. Particularly, electrical properties of CFRC were widely studied. Banthia, N. et al. (Banthia N. et al., 1992) found that under the same fiber fraction, resistivity of CF reinforced cement was lower than that reinforced with steel fiber. Furthermore, there was a percolation threshold for CF with which the composite had the lowest resistivity. Reza F. et al. (Reza F. et al., 2001) summarized the factors affecting electrical resistance of CFRC, including CF fraction, CF length, curing age, ambient temperature, relative humidity, etc.

At present there are basically two explanations for the self-sensing mechanism of CFRC. (1) Professor Chung D.D.L. (Chung D. D. L., 2003) proposed that during loading or unloading processes, CF is “push-in” the cement matrix or is “pull-out”, ending in decrease or increase of the contact resistance between CF and the matrix. Therefore in the macroscopic scale, these “push-in” and “pull-out” effects are reflected by the corresponding decrease or increase in overall electrical resistance of the composite. (2) Some other researchers (Hussain M. et al., 2001; Li G. Y. et al., 2007) tended to explain the self-sensing mechanism with “tunneling effect” which come from quantum mechanics. It is considered that when compressive stress is applied, the spacing among CF is reduced, resulting in decrease of the barrier width and increase of the tunnel current, which are reflected by decrease of electrical resistance of CFRC at the macro level. On

the other hand, during unloading the electrical resistance of CFRC increases. Although the two proposed mechanisms explain the self-sensing behavior of CFRC from different viewpoints, they come to a same conclusion: electrical resistance of CFRC decreases when the compressive force is applied, and increases during the unloading process.

1.2.2 Carbon-based Cementitious Nanocomposites

1.2.2.1 Introduction of Nanomaterials and Nanocomposites

Nanomaterials are characterized by at least one dimension in the nanometer ($1nm=10^{-9}$ m) range. Due to the significant change in surface electronic structure and crystal structure, materials reduced to the nano-scale can show distinctly different physical and chemical properties compared to what they exhibit at macro scale, enabling unique applications (Gogotsi Y., 2006). For instance, opaque substances become transparent (copper); inert materials attain catalytic properties (platinum); stable materials turn combustible (aluminum); and insulators become conductors (silicon).

A nanocomposite is a multiphase solid material where one of the phases has one, two or three dimensions in nanometer range (Ajayan P. M. et al., 2003). Thanks to the unique properties of nano-particles, together with their large surface area and strong interfacial interaction with the matrix, nanocomposites may have novel properties and functions that traditional macro composites do not possess. This provides new ways and new ideas for preparing high-performance multifunctional materials. For example, adding nano metal particles significantly improved mechanical properties of ceramic materials, and

introducing nano-alumina particles enhanced dielectric properties of rubber. Observing the advantages of nanocomposites, their applications are also to be exploited in the construction industry.

1.2.2.2 Benefits of Nano-reinforcement in Cementitious Composites

Although CF has been proved to be beneficial for enhancing properties of concrete, there are still some disadvantages with CFRC. Firstly, fractures of the CFs usually occur during casting of the mixture because they are usually as long as 5mm (Luo J., 2009). Secondly, entanglement problem may lead to poor dispersion of CFs and introduce additional air voids in the cement matrix (Mindess S. et al., 2003). Finally, SEM (Scanning Electron Microscope) images have shown that the interfacial bonding between CF and cement matrix is weak (Li G. Y. et al., 2005). The small gaps at the interface can lead to stress concentration and accelerate crack propagation. Meanwhile, it also prevents satisfactory load transfer between CF and the matrix.

In order to solve these problems, other conductive reinforcing particles that have good compatibility with cement matrix, as well as have the ability to improve both mechanical and electrical properties of the composites are to be found. Nanotechnology provides a choice and carbon-based nano-particles are considered to be the suitable candidates. Firstly, the nano size of nano-particles eliminates the fracture and entanglement problems during cement casting. Although agglomeration of the nano-particles may occur due to van de Waals force, it can be easily dealt with by using dispersant and applying ultra-sonication technique (Li J. et al., 2005). Besides, nano-particles have stronger adsorption

capacity due to the higher percentage of surface atoms. This together with their large surface area solves the bonding problem between reinforcing particles and the cement matrix.

Carbon-based nano-particles still have other advantages over CF. Mechanically, they bridge the cracks in the nano scale at a very preliminary stage of crack propagation (Shah S. P. et al., 2009). Furthermore, they fill up the voids in the cement matrix up to the nano scale, which effectively decreases porosity and reduces stress concentration and in turn, increases strength and corrosion resistance of the composites (Wang Y., 2007). For electrical properties, nano-particles are easier to be dispersed, leading to a better self-sensing property of the materials. Besides, the bridge effect of nano-particles is limited to a scale close to their largest dimension. Compared to CFRC, conductive networks in the nanocomposites are much easier to be cut off during crack propagation and larger electrical resistance change will occur, which also means a better self-sensing ability for the nanocomposites (Xiao H. and Li H., 2006).

1.2.2.3 Research Overview on Carbon-based Cementitious Nanocomposites

Introduction of Carbon Nanotube and Carbon Black

Studies on cementitious nanocomposites started since the 1990s. Two kinds of carbon-based nano-particles have been used: carbon nanotube (CNT) and carbon black (CB). CNTs are categorized as single-walled nanotubes (SWNTs) and multi-walled nanotubes (MWNTs) (Grobert N., 2007). As shown in Fig. 1.1 (Luo J., 2009), the structure of a SWNT can be conceptualized by wrapping a graphene (graphene is a single two-

dimensional layer of carbon atoms bonded together in the hexagonal graphite lattice) into a seamless cylinder, while MWNTs consist of multiple rolled layers (concentric tubes) of graphene. The typical diameter and length for SWNTs are 0.75~3nm and 1~50μm, while for MWNTs, they are 2~30nm and 0.1~50μm respectively. Different to CNTs, CB particles have a ball shape nanostructure, with a typical diameter of 30~120nm.

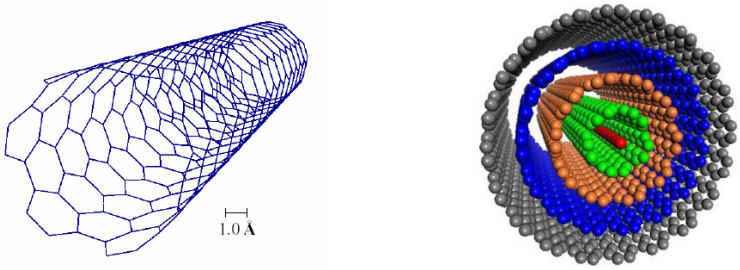

Fig.1.1. Structures of single-walled nanotubes (SWNTs) and multi-walled nanotubes (MWNTs) (Luo J., 2009).

Mechanical properties of cementitious nanocomposites

It has been found that both CNT and CB can effectively serve as nano-reinforcements in cementitious nanocomposites. For the composites reinforced with CNT, Li G. Y. et al. (Li G. Y. et al., 2007) found that cement added with acidic treated MWNTs showed 19% increase in compressive strength and 25% increase in flexural strength. Konsta-Gdoutos M. S. et al. (Konsta-Gdoutos M. S. et al., 2010) improved the dispersion of CNTs by applying ultrasonic energy in combination with the use of surfactant, achieving an increase of 25% in flexural strength for cement paste with only 0.048% CNTs by weight of cement. For the composites reinforced with CB, an increase of 15.14% in compressive strength and an increase of 44.32% in flexural strength were observed in mortar specimens when 0.75% CB by weight of cement were added (Wang Y., 2005). Wang Y.

F. (Wang Y., 2007) and S. Q. Gong (Gong S., 2008) also confirmed the effect of CB in enhancing mechanical properties of cementitious composites.

However, reinforcing mechanisms for CNT or CB reinforced cementitious composites are different. CNTs act as nano-fibers and increase the strength of the composites mainly by the bridge effect, controlling the initiation and propagation of the cracks in the nano-scale (Luo J., 2009). On the other hand, the ball-shape CB particles act as efficient nano-fillers. They decrease the porosity and the size of air voids in the cement matrix, which in turn reduce stress concentration and slow down crack propagation (Wang Y., 2005).

Electrical and self-sensing properties of cementitious nano-composites

As conductive admixtures, CNTs and CB also enhance electrical properties of cementitious composites, showing their potential in preparing self-sensing construction materials. For CNT, Li G. Y. et al. (Li G. Y. et al., 2007) found that adding 0.5% MWNTs by weight of cement not only decreased the resistivity of cementitious composites to be less than 150 Ωcm, but also led to distinct enhancement in their compressive sensitivity. Saafi M. (Saafi M., 2009) developed cement-CNT sensors and embedded them into concrete beams. By monitoring the sudden change in electrical resistance, crack initiation in the beam was able to be detected. For CB, researhcer group in Harbin Institute of Technology of China have studied electrical properties of CB reinforced cementitious composites since the year of 2006. They reported that the cementitious composites contained 15% amount of CB which was in the percolation threshold also showed good self-sening ability (Li H. et al., 2008).

The self-sensing mechanism for CNT reinforced cementitious composites is similar to that of CFRC, except that the "push-in" and "pull-out" effect, tunneling effect and degration of conductive network due to damage occur since the nano scale. On the other hand, the "push-in" and "pull-out" effect are eliminated in CB reinforced cementitious composites due to the ball-shape nanostructure of CB. The much simpler self-sensing mechanism provides much more regular relations between compressive stress level and the change of electrical resistance for CB reinforced cementitious composites. When the curves showing compress stress level verus electrical resistance change are non-linear for CF or CNT reinforced cementitious composites, they are nearly linear for the composites reinforced with CB (Xiao H. and Li H., 2006).

Compared to CFRC, CNT or CB reinforced cementitious composites can sense their internal damage at a much smaller scale, and therefore have higher gage factors (the fraction change in resistivity per unit strain). Especially, conductive networks formed by the ball-shape CB particles are through point to point connections which are very sensitive to damage. A gage factor of 5525.7 was reported for CB reinforced cementitious composites (Xiao H. and Li H., 2006), compared to 700 which is the highest that has been reported for CFRC (Chung D. D. L., 1998).

1.2.3 GNP Reinforced Polymer Composites

1.2.3.1 Morphology and Properties of GNP

Graphite nanoplatelet (GNP) is another type of carbon-based conductive nano-particles that is produced from graphite. Natural graphite is a layered compound comprising a series of stacked parallel two-dimensional (2D) graphene layers (Pierson H. O., 1993), as shown in Fig.1.2. These graphene layers can be readily separated to form thin GNPs via intercalation and exfoliation (Viculis L. M. et al., 2005), the corresponding processes of which are schematically illustrated in Fig.1.3.

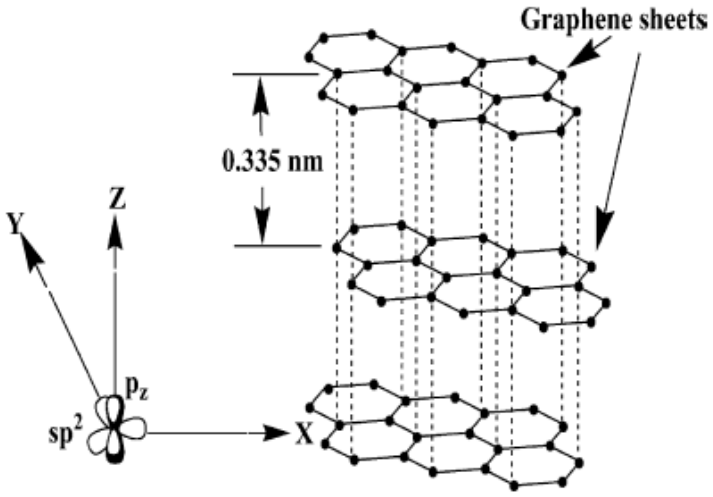

Fig.1.2. Layered structure of graphite showing the sp^2 hybridized carbon atoms tightly bonded in hexagonal rings (Sengupta R. et al., 2010).

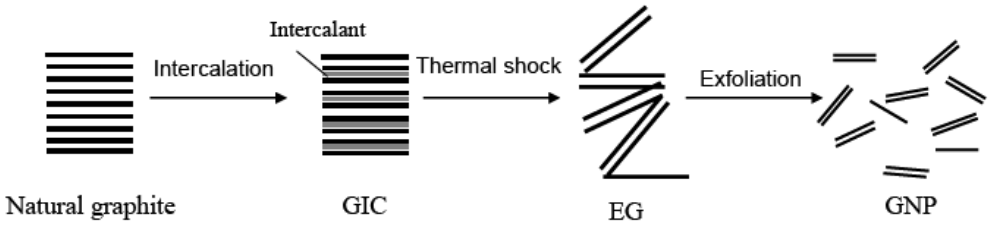

Fig.1.3. Schematic illustration of GNP production

GNP is a 2D platelet consisting of a few to several graphene layers with an overall thickness in nanometer scale and the particle diameter ranging from submicron up to 100μm. They possess a large surface area and a high aspect ratio, which are the properties favorable for mechanically reinforcement and forming conductive network in composites with low filler content. Properties of GNP are summarized in Table 1.1. It can be seen that GNP preserves the anisotropic feature as graphite and has excellent mechanical and electrical properties along the basal plane. Because of these unique properties, GNP has been considered as an alternative to conventional fillers, such as carbon fiber, carbon black and metallic particles, for conductive polymer composites.

1.2.3.2 Advantages of GNP in Fabricating Composites

Properties of GNP and CNT are compared in Table 1.1. Elastic modulus and strength of GNP are comparable to those of CNT, indicating its outstanding mechanical properties. This along with the high surface area and high aspect ratio of GNP shows its possibility in being also used as effective strength reinforcement. However, thanks to the platelets feature, GNP is exempted from entanglement problem that is very common for CNT. Furthermore, according to the self-sensing property, conductive network formed by GNP particles are more sensitive to damage than the network formed by CNT, since their dimension in the longitudinal direction is much smaller than that of CNT. At last, the biggest hurdle for extensive use of CNT is its exorbitant price. MWNTs are priced at ~$8/g and SWNTs are ~$170/g, while GNPs are priced at only $2/kg (Li J. et al., 2007).

Table 1.1. Properties of GNP and CNT

Property	Unit	GNP	CNT
Elastic modulus	TPa	1 (in-plane)	~1 for SWNT, ~0.3-1 for MWNT
Strength	GPa	~10-20	50-500 for SWNT, 10-60 for MWNT
Resistivity	μΩcm	50 (in-plane)	~5-50
Dimensions	-	Diameter: 1-20μm Thickness: ~30nm	Diameter: 0.75~3nm for SWNTs, 2~30nm for MWNTs. Length: 1~50μm for SWNTs, 0.1~50μm for MWNTs
Surface area	m^2/g	~2630	>400
Aspect ratio	-	50-300	~500

Reference: (Luo J., 2009); (Hilding J. et al., 2003); (Nanoamor, April 14, 2010); (Drzal L. T. and Fukushima H., 2006); (Yu A. et al., 2008); (Wu X. et al., 2010).

The advantages of GNP over CB mainly lie in the electrical properties of the nanocomposites. Because of their ball-shape nanostructure, CB particles have an aspect ratio of approximately one. The conductive paths in CB filled composites are formed by point to point connection, which leads to a high percolation threshold varying in the range of 3-15%, depending on the type of polymer matrix(Jia W. et al., 2005). On the other hand, the high aspect ratio of GNPs provides them percolation threshold values one order of magnitude lower than those of CB (Pike G. E. and Seager C. H., 1973; Seager C. H. and Pike G. E., 1973; Nan C.-W., 1993). Since the prices of CB and GNP are almost the same, a higher percolation threshold for CB means higher cost for nano-particles as well as more time and energy in dispersing them throughout dispersants and ultra-sonication. Besides, a higher amount of nano-particles means more water is absorbed, harming workability and hardening process of fresh mixtures, which further affect mechanical and electrical properties of the composites.

Although GNP reinforced cementitious materials have not been studied in previous literature, the advantages of GNP over other nano-particles have been proven in polymer composites. An increase of 300% in modulus and about 10 order of magnitude reduction in electrical resistance were achieved in Nylon66 nanocomposite with 15% of GNP by volume (Drzal L. T. and Fukushima H., 2006). The GNP/epoxy composites prepared by Mohammad A. Rafiee M. A. et al. (Balberg I. et al., 1984) showed 31% increase in elastic modulus and 40% higher tensile strength over the pristine epoxy matrix, compared to only 3% and 14% improvements respectively for CNTs. Electrical conductivity measurement indicated that room temperature conductivity of GNP/epoxy composites was around two orders of magnitude higher than that of SWNT/epoxy composites (Yu A. et al., 2008). All these results show the potential of GNP to be used as an alternative in preparing multifunctional cementitious nanocomposites.

1.2.4 Real-time Damage Monitoring and Damage Memorizing

Concerning the self-sensing properties of multifunctional cementitious composites, it is found that in previous literatures, damage of the materials was monitored by real-time sensing systems, which means electrical resistance was measured continuously, its curve was plotted versus the applied stress level, and the extent of damage was judged by observing the shape of the curve. Fig. 1.4 (Beer F. C. d. et al., 2004) shows the relation between applied compressive stress level and fractional change of electrical resistance for CFRC. It can be divided into three segments, indicating the three successive stages: no damage, minor damage and occurring of failure. At low stress level, the decrease of electrical resistance is mainly due to the “push-in” effect, tunneling effect with smaller

gap among the fibers and higher chance for CFs to contact each other. A plateau appeared when the stress level reached 57% indicated the development of minor damages. At last, the sharp increase of the curve indicated rapid accumulation of damages and failure of the material. Fig. 1.5 (Xiao H. and Li H., 2006) shows the same curve for CB reinforced cement composite. The perturbation on the linearity of the curve indicated the occurrence of micro cracks.

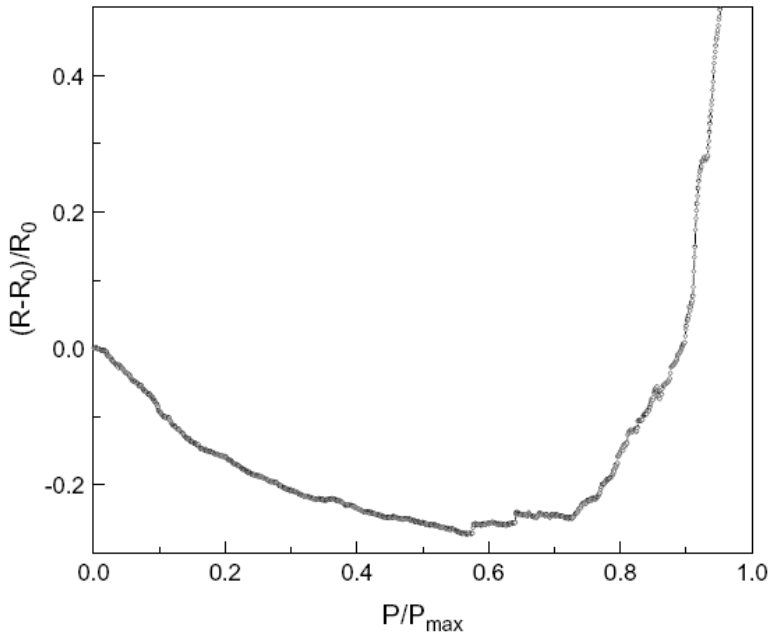

Fig. 1.4 Resistivity change for CFRC under compression (Beer F. C. d. et al., 2004)

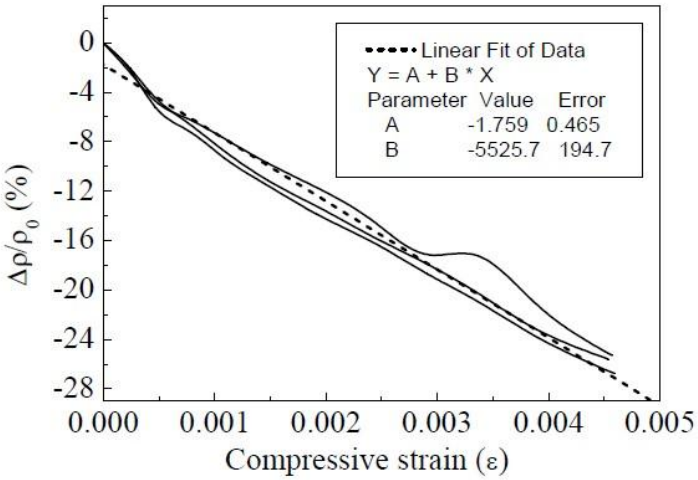

Fig.1.5. Fractional change in resistivity of CB reinforced cement composite as a function of compressive strain (Xiao H. and Li H., 2006).

However, the real-time monitoring systems must be operated continuously in order to detect any unexpected problems. These complex systems usually cause an increase in the costs and hence limit usage of such monitoring techniques. Therefore, a monitoring technique with the ability to memorize damage histories, which means the damage is still detectable even when the applied stress is removed is expected in order to introduce a simple system without permanent installations for data measurements and storages.

Yoshiki Okuhara et al. have studied the damage memorizing ability of carbon-based polymer composites since the year of 2003. They replaced CF with CB particles and increased the damage sensitivity of the composites (Hugh, 1993). Fig. 1.6 shows the relation between electrical resistance change and maximum applied tensile strain in history for CB reinforced polymer composites. It can be seen that in the unloading state, the maximum electrical resistance change occurred in the loaded state was almost totally retained, therefore the damage level could be assessed even after the load was removed.

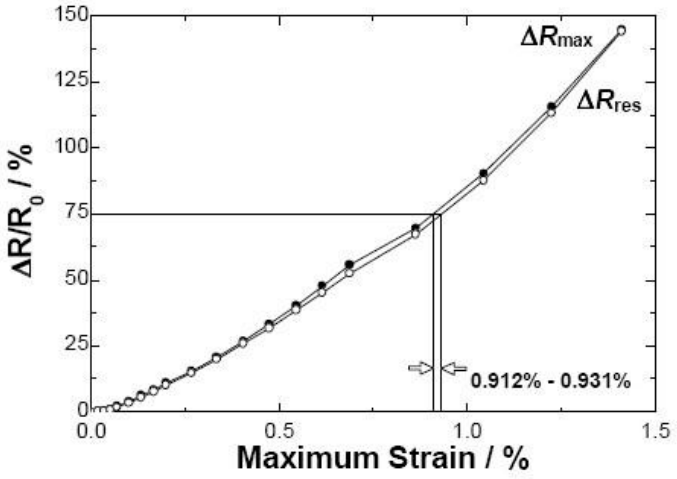

Fig.1.6. Residual resistance change (ΔR_{res}) after unloading and maximum resistance change ($\Delta R_{\max}$) as a function of maximum applied strain in the loaded state for each cycle for polymer composite containing carbon black (Hugh, 1993).

The damage memorizing ability of the materials provides a method to judge the damage after an unexpected problem such as an earthquake. Although has not been studied on purpose, the damage memorizing ability of cementitious composite can be observed from the real-time sensing curves under loading-unloading cycles. Fig. 1.7 (Reid R., 2000) shows the change of electrical resistance of CFRC under repeated compressive loading with highest stress amplitude higher than 60% of the compressive strength. It can be seen that there are residual electrical resistance changes at the points where stress returns to zero, indicating the damage memorizing ability of CFRC. It is expected that the sensitivity to damage can be enhanced if CFs are replaced with carbon-based nano-particles, since the nano-particles are easier to be dispersed and the "bridge effect" is reduced to a smaller scale, making the conductive network easier to be cut off.

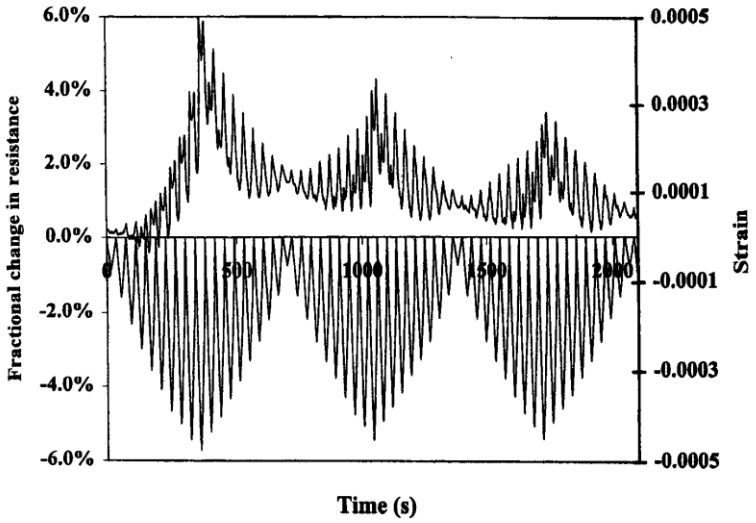

Fig. 1.7. Fractional change in electrical resistance and strain during repeated compressive loading at increasing and decreasing stress amplitudes, the highest of which was >60% of the compressive strength, for CFRC at 28days of curing (Reid R., 2000).

1.3 Observations Arising from Literature Review

The outstanding properties of GNP have shown its advantages over other carbon-based nano-particles. Also, experimental results from existing literatures have demonstrated the effect of GNP on improving both mechanical and electrical properties of polymer-based materials. All these show the potential of GNP to be used as an alternative conductive admixture for developing multifunctional cementitious nanocomposites.

Self damage sensing is one important property for the multifunctional composites that are to be developed. Damage memorizing is preferred to real-time damage monitoring in that it requires simpler systems and lower cost. The damage memorizing ability of carbon-based cementitious composites can be observed from the performance of CFRC under repeated compressive stress. This ability is to be improved by replacing CF with carbon-

based nano-particles, since the bridge effect will occur at a much smaller scale and the conductive networks are more sensitive to internal micro cracks.

1.4 Objectives and Scopes of This Study

The objective of this study is to investigate the feasibility of using GNP as a novel conductive admixture for preparing multifunctional cementitious nanocomposites. The GNP particles will be added into the cement matrix aiming at improving both the mechanical and electrical properties of the materials, and also activating their self damage sensing property. In particular, the self damage sensing property studied here refers to damage memorizing which does not require continuous real-time measurement for electrical resistance.

There are three main scopes in this research:

1. Fabrication technique of cementitious composites incorporating GNP particles with dosages from low to high will be studied. Especially, to achieve good dispersion of GNP inside the cement matrix, study on various dispersants and ultra-sonication technique will be carried out.
2. Experimental testing will be carried out to study the effects of GNP particles on the mechanical properties of the cementitious composites. Compressive strength, flexural strength and stiffness of each batch will be compared and discussed. Furthermore, the strengthening mechanism in these nanocomposites will be analyzed.

3. For electrical properties, the conducting mechanism of the GNP reinforced cementitious composites will be studied. Furthermore, the effects of polarization, age and dimensions of the specimen, temperature and moisture on electrical resistance will be investigated. Based on these results, self damage memorizing properties of the nanocomposites will also be studied and discussed by carrying out experimental tests.

CHAPTER 2 EXPERIMENTAL PROGRAME

In this chapter, materials used for fabricating specimens for experimental tests will be introduced in section 2.1. To solve the agglomeration problem of the nano-particles, study on dispersants and ultra-sonication technique will be made in section 2.2. The last two sections in this chapter will introduce the specimens and experimental set-ups for mechanical property tests and electrical property tests respectively.

2.1 Materials

2.1.1 Cement and Sand

ASTM Type I Ordinary Portland cement (Asia Cement) with a specific gravity of 3.15 was used in this study. For mechanical property tests, all the cement paste batches and the first five mortar batches were prepared with the same batch of cement; the rest of the mortar batches were produced with a new batch of cement, due to using up of the old batch in the structure lab. The two batches of cement have the same brand and the same type; therefore they have the same chemical composition, mineral composition, and fineness of cement particles etc. However, the first batch of cement had been kept in the lab for a long time, it absorbed the moisture in the air and some hydrated cement particles had been found. The inconsistency in cement properties may affect the consistency of the experimental results in the mechanical property tests, since the hydrated cement particles

in the first batch of cement could no longer perform as a cementitious material. For electrical property tests, all the specimens were fabricated with cement of the same batch.

Natural sand with a fineness modulus of 2.52, surface moisture of 0.13% and a maximum size of 4.75mm was used as fine aggregates. Calculation of sand fineness modulus is shown in Table 2.1. The grading of the sand satisfied the requirements in ASTM. The grading curve of sand particles is shown in Fig. 2.1.

Table 2.1 Calculation of sand fineness modulus

Sieve size	Weight retained (g)	Amount retained (wt. %)	Cumulative amount retained (%)	Cumulative amount passing (%)
4.75mm	0	0	0	100
2.36mm	47	9	9	91
1.18mm	92	18	27	73
600 μ m	103	23	50	50
300 μ m	118	24	74	26
150 μ m	90	18	92	8
Sample wt.	500		∑ =252	
Fineness modulus = 252/100 = 2.52				

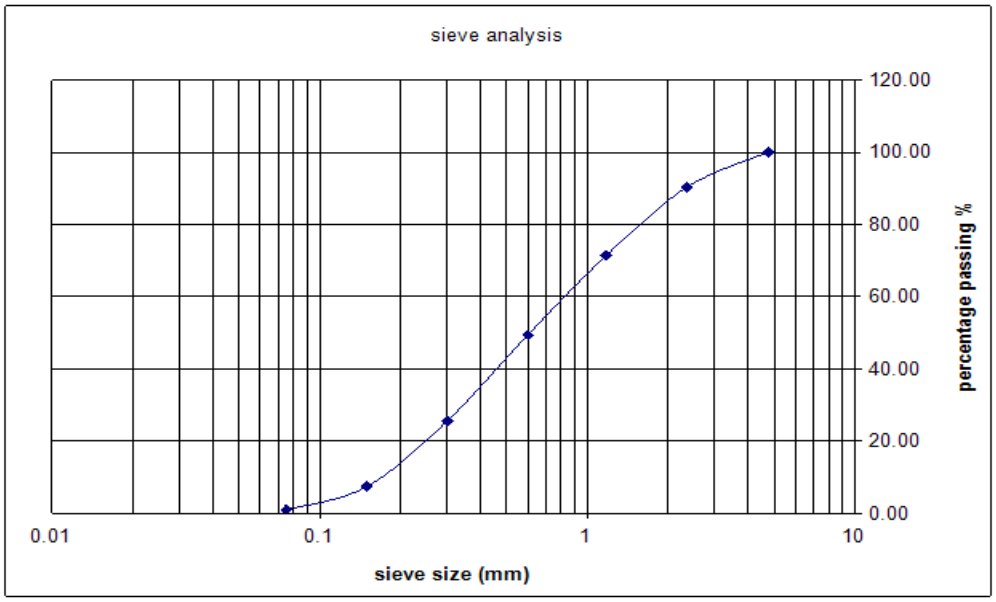

Fig. 2.1. Grading curve of sand particles

2.1.2 GNP Particles

Three types of expanded GNP were used in this study. Asbury TC307 and Asbury 3775 were from Asbury Graphite Mills, USA and Timrex T15 was from TIMCAL Graphite & Carbon, Switzerland. Their physical properties are tabulated in Table 2.2. Information on density, particle size and surface area were extracted from the product sheets. The "size passing" columns in Table 2.2 show the GNP particle sizes, where "50% size passing" means the average effective diameter of the GNP particles, and "90% size passing" means that 90% of the GNP particles have an effective diameter smaller than the value in the corresponding column. Although the thickness and aspect ratio are not available in the product sheets, they can be estimated from the available data as follows:

Assuming the platelets to be circular with effective thickness t, and the effective diameter D to be the 50% passing size in Table 2.2, the surface area $A_{s,p}$ and volume V_p of each platelet can be calculated as

$$A_{s,p} = \frac{\pi D^2}{2} + \pi D t \tag{2-1}$$

$$V_p = \frac{\pi D^2 t}{4} \tag{2-2}$$

From Equations (2-1) and (2-2), the ratio of surface area to volume of the nano-platelets can be determined as

$$\frac{A_{s,p}}{V_p} = \frac{2}{t} + \frac{4}{D} \tag{2-3}$$

From the bulk properties, which are surface area per unit weight A and the density ρ, the surface area per unit volume of the platelets can be estimated, assuming no voids between them

$$\frac{A_{s,p}}{V_p} \approx A\rho \tag{2-4}$$

Equating equations (2-3) and (2-4) can get the expressions for the estimated thickness t and aspect ratio χ

$$t = \frac{2D}{AD\rho - 4} \tag{2-5}$$

$$\chi = \frac{AD\rho - 4}{2} \tag{2-6}$$

Table 2.2. Physical properties of GNP particles

Type of GNP	Density ρ (g/cc)	Size Passing (μm)		Surface area A (m^2/g)	Estimated thickness *t* (nm)	Estimated aspect ratio *x*
		50%	90%			
Asbury 3775	2.26	8.0	18.1	24	37	215
Asbury TC307	2.16	2.6	5.0	352	3	986
Timrex T15	2.24	8.5	17.7	13	70	122

Physical properties of GNP were examined through SEM analysis. Fig. 2.2 shows the physical appearance of different types of GNP particles under the same magnification of x16, 000. All types of GNP present considerable degree of intercalation showing great needs for dispersion and ultra-sonication (see section 2.2). Asbury TC307 was characterized by the small particle size and the large surface area indicating high potential as efficient filler. T15 and Asbury 3775 were observed as large particles consisting of many layers of graphene sheets indicating good reinforcing effects if sufficient exfoliation can be achieved.

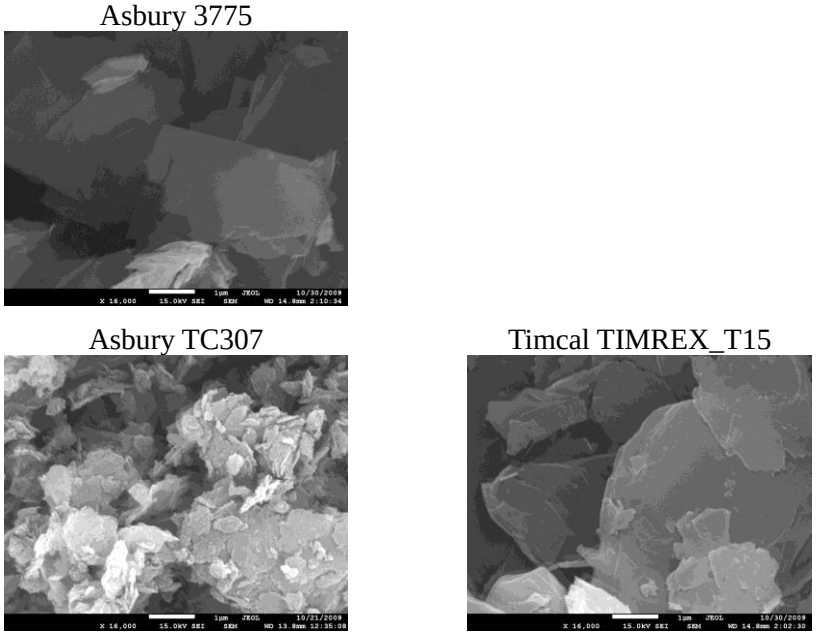

Fig. 2.2 SEM images of GNP particles at the same magnification of x16, 000.

2.1.3 High Range Water Reducing Admixture

The commercially available naphthalene sulfonate based high range water reducer Darex Super 20 was used as the water reducing agent in this study. The density of Darex Super 20 is approximately 1.2 ± 0.02 kg per liter conforming to BS 5075: Part 3: 1985. As will be discussed in section 2.2.1, Darex Super 20 was also used as the dispersant for GNP particles in this study. For specimens in mechanical property tests, the adopted amount of Darex Super 20 was kept constant as 0.45ml per kilogram of cement for cement paste batches and 1.54ml per kilogram of cement for mortar batches, with which both satisfactory workability of the fresh mixtures and uniform dispersion of GNP could be achieved. Specimens in electrical property test were all prepared with mortar (see section 2.3.1); the adopted amount of Darex Super 20 was 3.63ml per kilogram of cement during ultra-sonication of GNP suspension and about 8.00ml per kilogram of cement during mortar casting for increasing the workability of the fresh mixtures.

2.2 Studies on Dispersion of GNP

Poor dispersion is the major challenge involved in fabricating cementitious nanocomposites, because the strong van de Waals force causes agglomeration of the nano-particles (Grobert N., 2007). This leads to the formation of defects in the matrix and limits the effect of the nano-reinforcements (Hamann C. H. et al., 1998). To improve the dispersion of GNP particles in the cement matrix, the effect of different types of dispersants and the ultra-sonicaiton technique will be studied in this section.

2.2.1 Study on Dispersants

2.2.1.1 Selection of Dispersant through Experimental Study

Due to the non-suspensibility of GNP particles in water, dispersant is needed to obtain stable liquid suspension, preventing precipitation or floating of GNP particles. In previous literature various dispersants such as acetone, ethanol, nitrite acid, sulphate acid, gum arabic, alcohol and formic acid (Hamann C. H. et al., 1998; Lee C.-Y. and Wang S.-R., 2010; Sengupta R. et al., 2010) have been adopted in preparing liquid suspensions containing carbon-based nano-particles such as carbon nanotube. Based on the literature, and taking safety as well as availability into considerations, acetone, gum arabic and Darex Super 20 were selected as the candidates of GNP dispersant in this study. Among these dispersant candidates, gum arabic is a natural polysaccharide extracted from the Acacia tree. It is used primarily in the food industry as a stabilizer. It is also a key ingredient in traditional lithography and is used in printing, paint production, glue, cosmetics and various industry applications, including viscosity control in inks and in textile industries (Wikipedia, 2012). Gum arabic used in this study is from TIC GUMS, with the product sheet appended in Appendix E. When received the gum arabic product was in a form of white powders. It is extremely soluble in water and the solution can be used to prepare GNP suspensions.

Preliminary test was carried out in order to select the most effective GNP dispersant from the candidates. The stability of GNP suspensions made with different dispersants was tested by visually observing their homogeneity versus time.

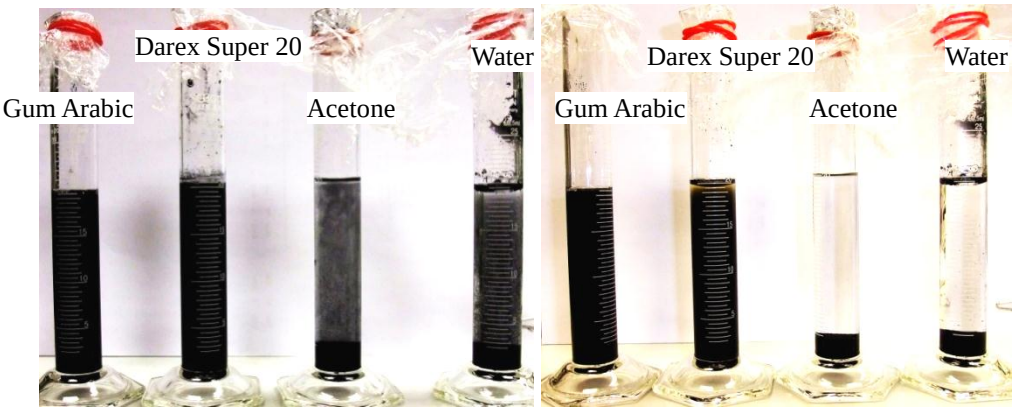

(a) 5 minutes after mixing (b) 30 minutes after mixing

Fig. 2.3. Stability test for GNP suspension in various dispersants

As shown in Fig. 2.3, the stability of a GNP suspension could be easily judged by looking at the distribution of the black color in a test tube, since the black color was displayed by the GNP particles, while the dispersant solutions without GNP particles are either colorless (gum arabic and acetone) or only with slight color and transparent (Darex Super 20 mixed with water in a volume ratio smaller than 1/10). It can be seen that GNP suspension in gum arabic showed the best stability because the black color remained going through the liquid even after 30 minutes. GNP suspension in Darex Super 20 solution also showed good stability; only little segregation phenomenon was observed on the surface of the liquid after 30 minutes. Considering that during cement casting, the GNP suspension only needed to be kept stable for about 10 minutes before being added to the cement mixture, which time period is far less than 30 minutes, Darex Super 20 had been able to keep GNP suspension stable for a long enough time. On the other hand, GNP suspensions could last no longer than 5 minutes in acetone or tap water. Apart from instability, the efficiency of acetone as a dispersant is also limited by its high evaporability, which makes it require repetitive supplement and in total nearly 150ml of

undiluted acetone to ultra-sonicate per gram of GNP. For gum arabic, its weak acidity makes it reactive in alkaline cementitious environment, which has resulted in generation of excess water during mixing, and in turn, brought about watery mixture with light GNP particles floating on top. Besides, it needs a long time stirring to make the gum arabic powder dissolved in the water. In comparison, sonication and dispersion of GNP particles throughout Darex Super 20 have resulted in suspension with good stability and minimal alteration on fresh mixtures. Therefore, Darex Super 20 was selected as the only dispersant through the whole study. Based on the knowledge of the author, this is the first time that Darex Super 20 is used as a dispersant for carbon-based nano-particles in cement matrix.

2.2.1.2 Dispersing Mechanism

Darex Super 20 is conventionally a high range water reducer based on naphthalene sulfonate for cement mixtures. In this study, it is also used as the dispersant for GNP particles. The dispersing mechanism of Darex Super 20 is similar to its mechanism for water reduction. Darex Super 20 consists of negatively charged organic molecules that absorb primarily at the GNP particle-water interface. Initially GNP particles carry residual charges on their surfaces, which may be positive, negative, or both. In liquid suspension, opposing charges on adjacent particles of GNP can exert considerable electrostatic attractions, causing the particles to flocculate (Fig. 2.4a). Molecules of Darex Super 20 interact to neutralize these surface charges and make all the GNP surfaces carry uniform charges of like sign. GNP particles now repel each other, rather than attract, and remain fully dispersed in the liquid suspension (Fig. 2.4b).

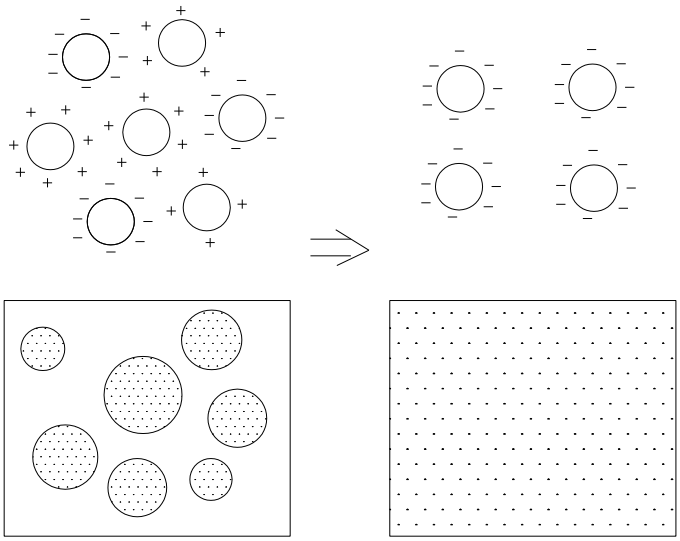

(a) Flocculated GNP particles. (b) Dispersed GNP particles.
Fig. 2.4. Dispersing action of Darex Super 20 for GNP particles

2.2.2 Study on Ultra-sonication Technique

2.2.2.1 Mechanism of Ultra-sonication

GNP particles prepared from bulk graphite consist of a series of stacked parallel two-dimensional (2D) graphene layers with nano-scale thickness (Li J. et al., 2007). This multi-layer nanostructure indicates that by separating the graphene layers and therefore obtaining smaller GNP particles further dispersion of GNP particles can be desired. Applying ultra-sonication technique is a method to achieve this.

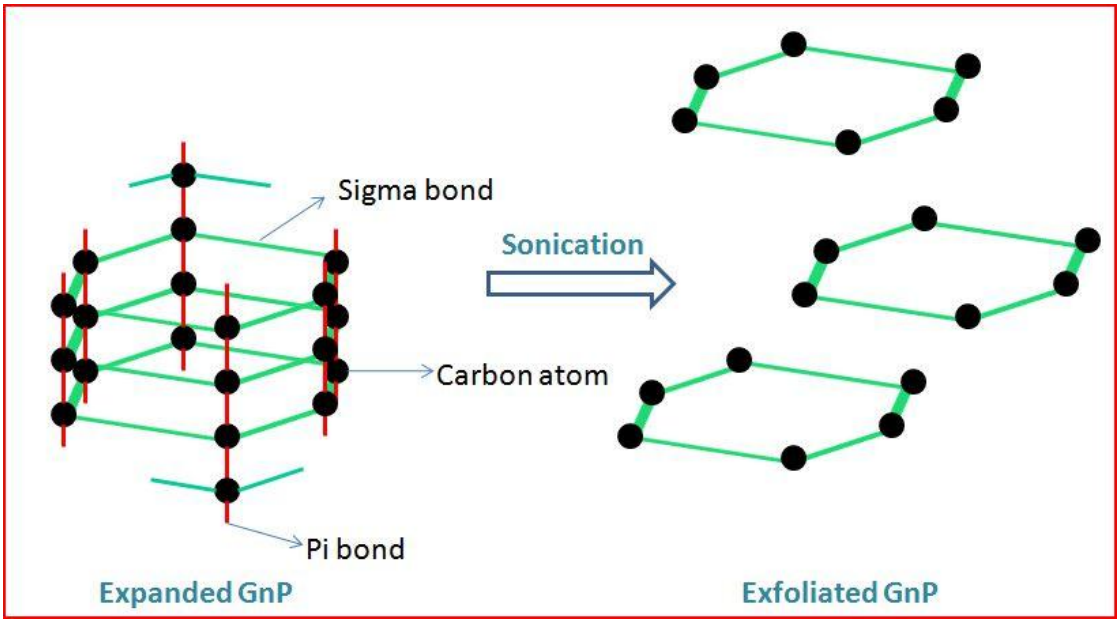

Fig.2.5. Mechanism of ultra-sonication

The mechanism of ultra-sonication for GNP is shown in Fig. 2.5. Ultra-sonication is identified as an important process to get exfoliated nano-sized particles with ultra-high surface area, large aspect ratios, and excellent mechanical properties (Li J. et al., 2007). It is commonly performed in liquid suspensions. It generates alternating low-pressure and high-pressure waves in liquids, leading to the formation and violent collapse of small vacuum bubbles. This phenomenon is termed cavitation and causes high speed impinging liquid jets and strong hydrodynamic shear-forces. The energy imparted into GNP particles results in the breakage of the weak interlayer pi-bonds, therefore exfoliated GNP particles with reduced thickness, increased aspect ratio and surface area, and enhanced particle mobility can be obtained.

2.2.2.2 Effect of Ultra-sonication Verified by Experimental Study

There are two major methods for delivering ultrasonic energy into liquids: the ultrasonic bath, and the ultrasonic horn or wand (Hilding J. et al., 2003). The ultra-sonication bath has a higher frequency (40-50 kHz) than the ultra-sonication horn or wand (about 25 kHz). The frequency of the ultrasound determines the maximum bubble size in the liquid. Low frequencies (about 20 kHz) produce large bubbles, and high energy forces are generated as the large bubbles collapse. Increasing the frequency reduces bubble size and nucleation, so that cavitation is reduced. Therefore, in this study, ultra-sonication horn was opted because of its lower frequency.

An ultra-sonication time of 2 hours was used in previous literature because it was found that 2 hours has been beyond the sonicaiton threshold for carbon nano-particles (Qizhao M. et al., 1997). To verify this an ultra-sonication time of 2 hours was used in this study. Besides, up to 8 hours' sonication was also performed to see the effect of the prolonged sonication. The ultra-sonication was performed in the GNP suspension made with Darex Super 20, which was selected as the dispersant. A 750W-20kHz ultrasonicator was used, with the ultra-sonication setup shown in Fig. 2.6.

Fig. 2.6. Ultra-sonication setup

GNP particles were collected from the liquid suspension both before and after ultra-sonication, and they were taken for SEM characterization. The effect of ultra-sonication is shown in Fig. 2.7.

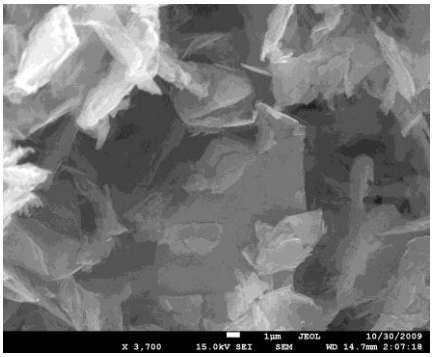

(a) Without ultra-sonication

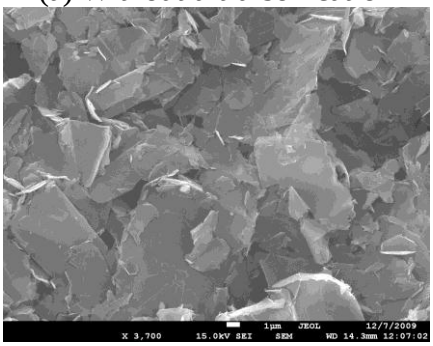

(b) After 2 hours' sonication

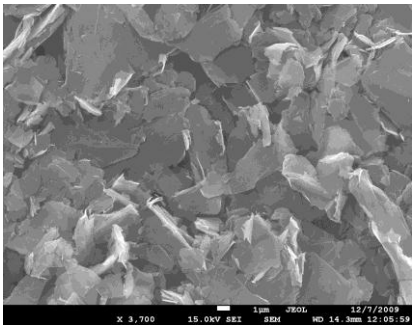

(c) After 8 hours' sonication

Fig. 2.7 SEM images showing the effect of ultra-sonication

It can be seen that GNP particles no longer show severe particle agglomeration and entanglement after ultra-sonication of more than 2 hours. Expansion, peeling and fractionation of the GNP particles can be observed. Comparing Fig. 2.7 (b) and (c) it is also found that a sonication time of 2 hours has been beyond the sonication threshold, since the prolonged sonication did not result in better effectiveness. Therefore, an ultra-sonication time of 2 hours was adopted in this study.

2.3 Specimens and Experimental Set-up for Mechanical Property Tests

2.3.1 Fabrication of Specimens

10 batches of cement paste specimens and 9 batches of mortar specimens were fabricated for mechanical property tests, in order to study the effect of the type of GNP, the amount of GNP, the dispersant and ultra-sonication technique on mechanical properties. For each batch, 6 small cubes with the dimensions of 50mm*50mm*50mm were prepared for the compressive tests, and 6 prisms with the dimensions of 40mm*40mm*160mm were prepared for the flexural tests.

For cement paste batches, the water to cement ratio (w/c) was chosen as 0.365, because the test results obtained with this w/c could be comparable to the established results in literatures where a w/c of 0.365 or 0.45 (Li G. Y. et al., 2005; Sanchez F. and Ince C., 2009) has been adopted. Moreover, this w/c has been proven to be adequate for this study, not only because it gives an adequate flowability for the fresh mixtures during casting, but also the desired strength is high enough for studying the effects of nano-

reinforcement in relatively high strength concrete, for which the compressive cube strength is greater than 40MPa. GNP of TC307 and T15 were used with the amount of 0% to 0.5% by weight of cement, which was also selected based on the existing literature on cementitious nanocomposite added with nano-particles such as carbon nanotube (Ibarra Y. S. d. et al., 2006).

For mortar batches, the water to cement ratio was 0.485, which is according to the recommendation in ASTM C109. Besides, this is the lowest w/c possible for mortar mixture without adding a water reducing agent, to facilitate casting of the control batch. In fact, it is possible to choose a higher w/c ratio but it will defeat the purpose of studying the effects of GNP reinforcement on concrete with relatively high strength. Also based on the suggestion in ASTM C109, the sand to cement ratio for all the mortar batches was selected as 2.75. Only GNP of TC307 was used in the mortar batches, in view of its potential to be efficient filler due to its small size and high aspect ratio. GNP with the amount ranging from 0% to 1.5% by total weight of cement and sand particles were added in different mortar batches.

General procedures of casting cement paste mixtures are outlined as follows:

1. For the batches that GNP particles were added, GNP suspension was prepared with mixing water and dispersing agent (except for the control batches that dispersing agent was not added) before mixed with cement, either with or without sonication. During sonication, the beaker containing the GNP suspension was kept in a water bath to lower the temperature. Furthermore, the beaker was

covered to prevent evaporation of water. The dispersing agent (Darex Super 20) used for preparing GNP suspension in this step also served as the water-reducing agent for the cement mixture.

2. During casting, firstly cement was placed into the 5-liter rotary mixer and dry mixed for 1 min at a low mixing speed.
3. GNP suspension and water were added slowly to the mixture with the mixing speed unchanged.
4. Finishing mixture was further mixed for 1min at a higher speed. Generally, workability of the cement mixtures in each cement paste batches was high enough to prevent consolidation problem, therefore no additional water-reducing agent was added at this step.

The procedures of casting mortar batches are basically the same as those for cement paste batches, except that in step 2 cement and sand were simultaneously placed into the mixer and dry mixed for 3 minutes, to achieve homogeneous mixture. All specimens were cast using steel molds. Besides workability control by adding water-reducing agent during casting, the following measures were taken to prevent consolidation problem in the specimens: ready mixtures were cast in three layers and were consolidated using a vibration table; after placement of each layer, tamping as guided by ASTM C109/C109M-08 was performed before each round of vibration. All specimens were covered with a plastic sheet immediately after casting to reduce the loss of moisture and thus reduce drying shrinkage. All specimens were kept in the molds until hardened and demolding was started after 24 hours. Demolded specimens were cured in the fog room

until testing after 28 days. Pure cement paste batch and plain mortar batch were cast as control batches for comparison. Control batches containing only the dispersant were also cast to study the effect brought about by the dispersant. The detailed specifications for each cement paste batch are summarized in Table 2.3, while those for each mortar batch are summarized in Table 2.4.

Table 2.3 Mixture compositions of cement paste batches

Paste	GNP Type	GNP Amount	Dispersant	Sonication
P1	-	-	-	-
P2	-	-	2mL	-
P3	TC307	0.05%	-	-
P4	TC307	0.05%	2mL	-
P5	TC307	0.05%	2mL	2 h
P6	TC307	0.25%	2mL	-
P7	T15	0.05%	2mL	-
P8	T15	0.05%	2mL	2 h
P9	T15	0.25%	2mL	-
P10	T15	0.50%	2mL	-

Table 2.4 Mixture compositions of mortar batches

Mortar	GNP Type	GNP Amount	Dispersant	Sonication
M1	-	-	-	-
M2	-	-	2mL	-
M3	TC307	0.5%	-	-
M4	TC307	0.5%	2mL	-
M5	TC307	0.5%	2mL	2 h
M6	TC307	1.0%	-	-
M7	TC307	1.0%	2mL	-
M8	TC307	1.0%	2mL	2 h
M9	TC307	1.5%	-	-

2.3.2 Experimental Set-up and Instrumentation

Uniaxial quasi-static compressive test was performed on the 114 small cubes using servo-hydraulic testing machine (see Fig.2.8) adopting an auto-generated loading rate of 800N/s. Three-point bending test at a loading rate of 20N/s was performed on the 114 flexural prisms using an Instron machine with a specially designed setup (see Fig.2.9). All specimens were rotated to have the load and support resting on the smooth surfaces in order to minimize the stress concentration.

Fig.2.8. Setup for compressive strength test

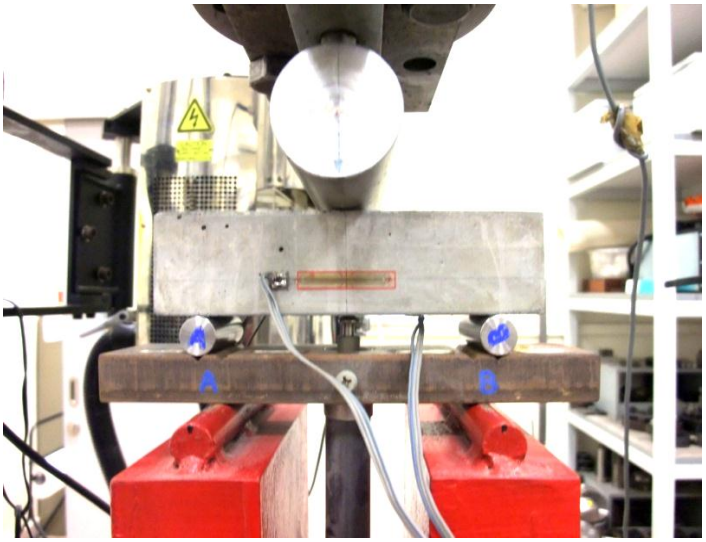

Fig.2.9. Setup for flexural strength and stiffness test

2.4 Specimens and Experimental Set-up for Electrical Property Tests

2.4.1 Composition of the Specimens

The materials used for fabricating specimens for the electrical property tests remain the same as those used in the mechanical property tests (see section 2.1). However, in view of the more consistent results for mortar specimens in mechanical property tests (see section 3.1), as well as the fact that cementitious composites with aggregates are more preferable in real application due to high cost of cement (Mindess S. et al., 2003), for electrical property tests only mortar specimens were prepared.

50mm mortar cubes were fabricated which include specimens with Asbury TC307 and Asbury 3775 GNP, which are termed as TC307 cubes and 3775 cubes respectively in this thesis, and a control with plain mortar for comparison. Prism specimens of 40mmx40mmx160mm were also fabricated with both Asbury TC307 and Asbury 3775

GNP, which are termed as TC307 prism and 3775 prism respectively. The cement to sand (c/s) ratio for all the mortar specimens was 1:1, which is higher than that for mechanical test. The amount of cement was increased to make up for some of the workability loss due to the high dose of GNP required to achieve high conductivity. This resulted in a high absorption of mixing water and low workability of the fresh mixtures was observed. Also, this c/s ratio is commonly used in literature (Chen P.-W. and Chung D. D. L., 1996), facilitating comparison between test results in this study and those in the literature. The water to cement (w/c) ratio for all the mortar batches was 0.6, which was kept high to avoid workability loss.

The forming of a closed loop circuit during measurement of electrical resistance will result in electric polarization in the cementitious composites, causing the electrical resistance to increase. In order to diminish the effect of electric polarization, a conductive network is desired inside the cementitious composite (Wen S. and Chung D. D. L., 2008), meaning that the amount of GNP added should be higher than its percolation threshold. The experimentally determined percolation thresholds for cement reinforced with CNT and CB are 0.5%~1.0% and 3%~15% by weight of cement respectively (Jia W. et al., 2005; Saafi M., 2009). Considering that the aspect ratio of GNP is smaller than CNT and is much larger than CB, it is estimated that percolation threshold for GNP reinforced mortar should be less than 5%. This estimation is also supported by the calculations based on the percolation theory, which are shown as follows.

According to the concept of excluded volume and average field approximation, the value of percolation threshold υ_c (by volume) can be expressed as (Nan C.-W., 1993)

$$\nu_c = 1 - exp\left(-\frac{B_c V}{V_{ex}}\right) \quad (2\text{-}7)$$

Where V is the volume of a conductive particle, V_{ex} is the proper average of the object's excluded volumes, and B_c is the average critical number of bonds per site which is invariant for a given objective shape (Pike G. E. and Seager C. H., 1973). The numerical value of B_c is $B_c = 2.7$ for spheres (3d) and $B_c = 4.0$ for disks (2d). Due to the platelet shape of the GNP particles, here B_c is selected approximately as 4.0.

The excluded volume V_{ex} can be defined as the volume around an object into which the center of another object is not allowed to enter if overlap of these two objects is to be avoided (Balberg I. et al., 1984). The excluded volume V_{ex} for objects with a plate shape can be calculated by taking the average of two extreme conditions. In the first condition (see Fig. 2.10 (a)) the two plates form a 90 degree angle and the excluded volume can be obtained simply by moving the other two plates around the first two and registering the center of the moving plates. In this condition the excluded volume can be calculated as

$$V_{ex1} = A_{ex1} \times L = (2L^2 + 6Lt) \times L = 2L^3 + 6L^2 t \quad (2\text{-}8)$$

In the second condition (see Fig. 2.10 (b)) the two objects form a 0 degree angle and the excluded volume can be calculated as

$$V_{ex2} = A_{ex2} \times L = 8Lt \times L = 8L^2 t \quad (2\text{-}9)$$

Taking the average of V_{ex1} and V_{ex2}, V_{ex} can be expressed as

$$V_{ex} = L^3 + 7L^2 t \quad (2\text{-}10)$$

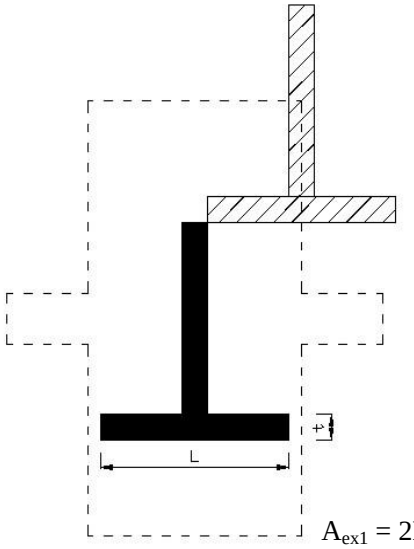

$A_{ex1} = 2L^2+6Lt$

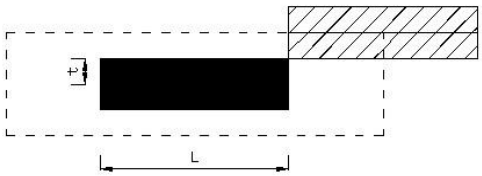

$A_{ex2} = 8L^2t$

(a) Two plates form a 90 degree angle (b) Two plates form a 0 degree angle

Fig.2.10. Excluded volumes (the plates have a length of L into the page)

Substitute equation (2-10) and $B_c = 4.0$, $V = 2L^2t$ into equation (2-7), we get

$$V_c = 1 - exp\left(\frac{-8t}{L+7t}\right) \tag{2-11}$$

As have been shown in Table 2.1, for GNP particles of TC307, their average L is 2.6μm and their average t is 3nm, therefore υ_c for TC307 particles is

$$V_c(TC307) = 1 - exp\left(\frac{-8\times3}{2600+7\times3}\right) = 0.92\% \tag{2-12}$$

For 3775 particles, their average L is 8.0μm, and their average t is 37nm, therefore

$$V_c(3775) = 1 - exp\left(\frac{-8\times37}{8000+7\times37}\right) = 3.58\% \tag{2-13}$$

Since the density of GNP (see Appendix C) and the density of mortar (see Table 3.4) are close, i.e. they are both in the range of 2.15~2.30g/cm^3, the results obtained in equation (2-12) and (2-13) can be considered as the fraction of GNP particles by weight of mortar. In the condition that the cement to sand ratio is 1:1 and the water to cement ratio is 0.6, it can be calculated that the fractions of GNP by weight of the solid particles (cement and sand particles) are

$$V_c(TC307)' = 0.92\% \times \frac{1+1+0.6}{1+1} = 1.19\% \quad (2\text{-}14)$$

$$V_c(3775)' = 3.58\% \times \frac{1+1+0.6}{1+1} = 4.65\% \quad (2\text{-}15)$$

These results confirm that the values of percolation threshold for GNP reinforced mortar are less than 5% by weight of the solid particles. Since the electrical property tests in this project are only preliminary tests which serve as proof of concept, instead of performing a series of tests to decide the optimum content for GNP, a dose as high as 5% was selected to ensure good conductivity.

By using the same concept above, the effect of good dispersion on getting low percolation threshold of GNP can also be manifested. Assume overlapping of GNP particles occurs, and the thickness in Figure 2.10 actually contains *n* layers of GNP particles, by substituting the thickness *t* in Equation (2-11) with *nt*, the percolation threshold υ_c (by volume) becomes

$$V_c = 1 - exp\left(\frac{-8nt}{L+7nt}\right) \quad (2\text{-}16)$$

If consider the GNP fractions by total weight of cement and sand particles, similar to equations (2-14) and (2-15), the percolation threshold υ_c' by weight is

$$V_c' = \left[1 - exp\left(\frac{-8nt}{L+7nt}\right)\right] \times \frac{1+1+0.6}{1+1} = 1.3\left[1 - exp\left(\frac{-8nt}{L+7nt}\right)\right] \quad (2\text{-}17)$$

Substituting the average length L and average thickness t, the relations between υ_c' and particle overlapping layer number *n* for TC307 particles and 3775 particles are

$$V_c(TC307)' = 1.3\left[1 - exp\left(\frac{-8n\times3}{2600+7n\times3}\right)\right] = 1.3\left[1 - exp\left(\frac{-24n}{2600+21n}\right)\right] \quad (2\text{-}18)$$

$$V_c(3775)' = 1.3\left[1 - exp\left(\frac{-8n\times37}{8000+7n\times37}\right)\right] = 1.3\left[1 - exp\left(\frac{-296n}{8000+259n}\right)\right] \quad (2\text{-}19)$$

The curves for equations (2-18) and (2-19) are plotted in Figure 2.11 and Figure 2.12 respectively. It can be seen that agglomeration of GNP particles will lead to an increase in percolation threshold. This highlights the importance of good dispersion on fabricating conductive nanocomposites with a low nano-particle fraction.

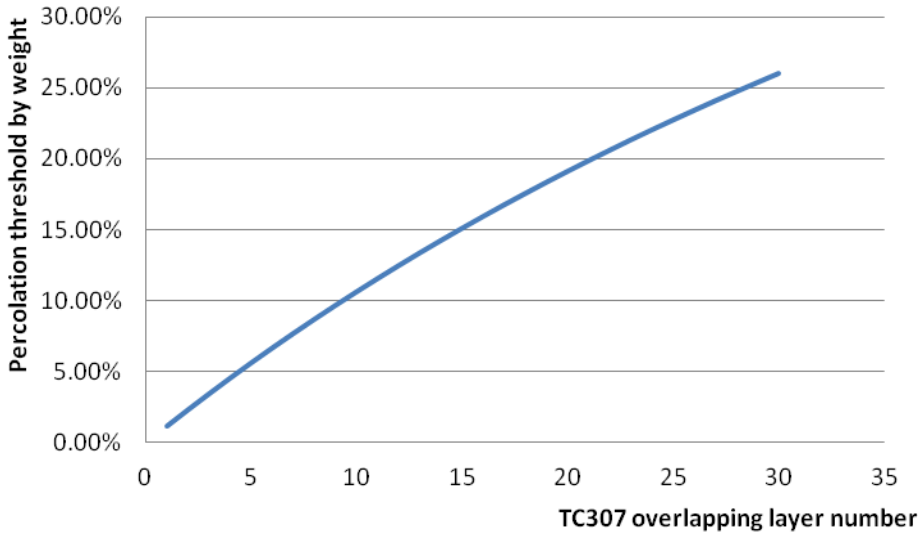

Figure.2.11 Relation between percolation threshold (by total weight of cement and sand) and particle overlapping layer number for TC307 particles.

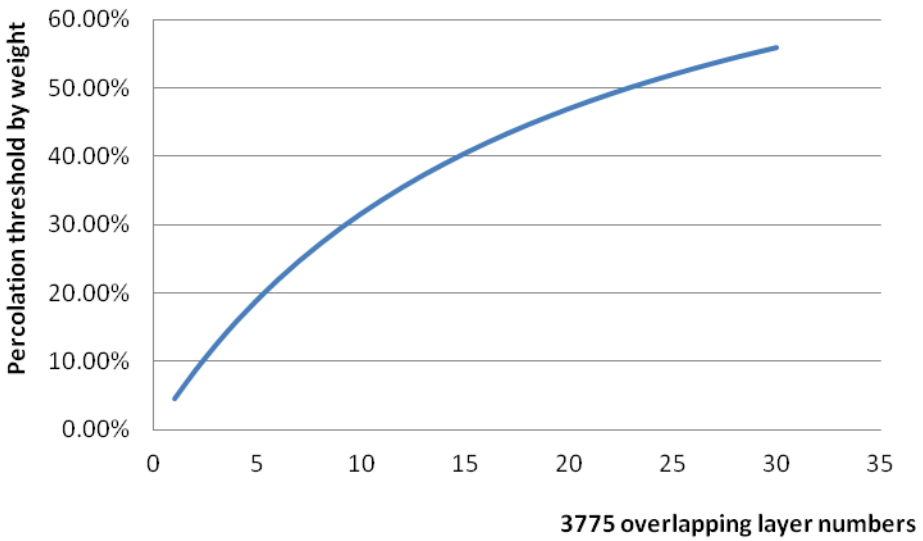

Figure.2.12 Relation between percolation threshold (by total weight of cement and sand) and particle overlapping layer number for 3775 particles.

2.4.2 Special Processing Technique for Addition of High Dose of GNP

From the fabrication of the mortar specimens discussed in section 2.3.1, it was found that when making GNP suspension with the amount of mixing water calculated from the w/c ratio, the dose of GNP should not exceed 1.5% by weight of the cement and sand particles to prevent the liquid to be too viscous that the free movement of solid particles would be blocked. For a GNP dose higher than 1.5%, the suspension became "jam-like" which drastically increases the impedence for the transfer of ultrasonic wave energy. In order to prevent the "jam-like" problem, two possible ways may be considered. The first involves increasing the dose of Darex Super 20. However, the target of GNP dose in this study is as high as 5%, under the limiting amount of mixing water it was found that the large gap between 1.5% and 5% could not be supplemented by solely increasing the dose of Darex Super 20. Therefore a second method, which involves introducing additional

water, was applied. The dose of Darex Super 20 was kept as 0.4% by weight of cement which is consistent with the amounts of other dispersants such as methylcellulose and gum arabic that are reported in the literatures (Sihai W. and Chung D. D. L., 2000; David G. M. et al., 2010; Rajdip B. et al., 2001), enabling comparison among the effects of different dispersants. This Darex Super 20 dose was proved to be enough in dispersing GNP particles when acting with additional water since stable GNP suspension could be obtained and no particle floating or precipitation was observed. In order to include the additional water for fabricating mortar with a GNP dose as high as 5%, and at the meantime keep the design w/c ratio unchanged, an alternative processing technique has to be introduced. In this study, a novel technique was proposed which allows for addition of more water during sonication while retaining the design w/c ratio in the specimen. This new processing technique is described as follows:

Step 1: Dispersant (Darex Super 20), GNP and sufficient water for ultra-sonication (mixing water as well as additional water) were mixed to get the GNP suspension. Based on the observation during mixing, to prevent the "jam-like" problem, the maximum GNP to water ratio by weight is in the order of 10^0;

Step 2: The suspension was ultra-sonicated for 2 hours. During sonication, the beaker was kept in a water bath with normal environment temperature to cool down the suspension. As the heat generated during sonication may cause rapid evaporation, more water may need to be added to maintain adequate consistency for sonication. The amount of water need not be monitored at this stage, as they will be removed subsequently when sonication is completed.

Step 3: Mixing sand particles were sieved and separated into two groups for sizes larger and smaller than 1mm respectively. Sand particles with sizes smaller than 1mm were mixed with the sonicated GNP suspension in a mixer for about 3 minutes. The mixture was stirred to ensure homogeneity and after that it was put into a 90-centigrade oven for 24 hours to remove all the water. The exfoliated GNP particles were kept from re-agglomeration due to the presence of fine sand particles.

Step 4: The mixture was taken out of the oven, crushed and then ground into fine particles using Retsch Model RM100 Mortar Grinder. After grinding, all the particles in the mixture passed the 1mm sieve; this is the rationale for splitting the sand particles into two groups in step 3. If the sand particles were not separated, the grading curve of the sand cannot be retained in the final cement mix.

After step 4, conventional casting procedures were carried out to complete the mortar fabrication:

1. Cement, GNP/sand mixtures, and the remaining sand particles with sizes larger than 1mm, were placed into a 5 liter rotary mixer and dry–mixed for 3 min at a low mixing speed of 1 revolution per second, to create a more homogeneous mixture.
2. Mixing water, based on the design w/c ratio, was slowly added to the mixer with the mixing speed unchanged.
3. Additional Darex Super 20 was added until cohesiveness of the fresh mixture was increased to a level that the fresh mixture could be gripped into a mass and did

not spread apart, and workability of the mixture was increased to a level that it could be cast without a consolidation problem.

4. The final mixture was further mixed for 1min at a medium speed of 2 revolutions per second.

In this study on the electrical resistance, 5% of GNP by weight of cement and sand particles was used in all specimens that were cast in steel molds. To prevent consolidation problems, ready mixtures were cast in three layers and were consolidated using a vibration table. After placement of each layer, tamping as recommended by ASTM Standard C109/C109M-08 was performed before each round of vibration. All specimens were covered with a plastic sheet immediately after casting to prevent loss of moisture and thus prevent drying shrinkage. All specimens were kept in the molds for 24 hours until the specimens were hardened. Demolded specimens were cured in the fog room for 10 days and then placed in the air-con room for setting electrical contacts (see section 4.1.3). The air-con room had a temperature that was around 25 centigrade and a normal environment relative humidity that was around 70%.

2.4.3 Basic Testing Method for Electrical Resistance Measurement

Electrical resistance measurements were conducted using the two-probe method under a DC (direct current) setup, due to the convenience and low cost of the testing system. For all specimens, except those used for self damage sensing property test under compression (see section 5.2), the two end surfaces normal to the longitudinal direction were first flatten with a sand paper, then the dust on the surfaces was brushed, and followed by a

coat of conductive epoxy to serve as electrical contacts (see Fig. 2.13). Therefore, the voltage drop was measured across the two silvery end surfaces, which were 50mm apart for the cubes and 160mm apart for the prisms as shown in Fig 2.13.

(a) Cube (b) Prisms

Fig.2.13. Specimens for the electrical property tests

When the specimens were being cured in the fog room, moisture would continuously diffuse into the interface between the electrical contacts (conductive epoxy) and the mortar surface. It impaired their bonding and destroyed the electrical contacts by causing bubbles and crimples to form (see Fig. 2.14). To avoid this problem, the specimens were painted with conductive epoxy only after they were removed from the fog room, that is, on the 11^{th} day after they were cast. For this reason, the electrical resistances were only recorded after 10 days.

Fig.2.14. Destroyed electrical contacts

A FLUKE 111 multimeter was used to test the electrical resistance of the specimens. The readings were taken within a short time period of 5 seconds to minimize the effects of electric polarization, which are described in details in Section 4.2.1.3. For each specimen, voltage drop was applied across the two end surfaces in two opposite directions to further negate the effects of electric polarization and the average value was recorded.

CHAPTER 3 MECHANICAL PROPERTIES OF GNP REINFORCED CEMENT PASTE AND MORTAR

The feasibility of using GNP as a nano-reinforcement strategy to improve the mechanical properties of cementitious materials will be studied in this chapter. In section 3.1 the test results will be shown and discussions will be made for both cement paste batches and mortar batches. In section 3.2 and 3.3, the strengthening mechanism and potential problem in the nano-reinforcement will be discussed respectively.

3.1 Experimental Results and Discussion

3.1.1 28 Day Strength and Stiffness

28 day strength of cement paste and mortar are shown in Table 3.1, Fig. 3.1 and Fig. 3.2, which are attached at the end of this section.

No increases in compressive strength were observed for cement paste batches compared to pure cement paste. On the other hand, the compressive strengths of mortar batches were all higher than that of plain mortar batch. The most significant increase was observed in batch M4 (0.5% GNP of TC307 with dispersion and without sonication) which was 20%.

The flexural strengths of cement paste batches were comparable or higher than that of

pure cement paste. The maximum flexural strength was 6.2 MPa which was founded in batch P8 (0.05% GNP of T15 sonicated through Darex Super 20) indicating a strength increase of 82% as compared to the flexural strength of pure cement paste. It is also from here that the effects of sonication and good dispersion are manifested. Considerable increase in flexural strength was also observed for all the mortar batches and the maximum increase was observed for batch M2 (Darex Super 20 control batch) which was 23%.

As for stiffness, for cement paste batches, the inclusion of GNP particles has resulted in both increase and decrease of stiffness. The maximum increase was shown in batch P8 (0.05% GNP of T15 sonicated through Darex Super 20) with an increase of 20%. And the maximum decrease occurred in batch P4 (0.05% GNP of TC307 unsonicated through Darex Super 20) where a 42% decrease was founded. Stiffness for mortar was generally higher than that of cement paste, with the highest occurred in batch M6 (dry mixed with 1.0% GNP of TC307) where an increase of 14% was found compared to plain mortar. No significant variation in stiffness was observed.

It is concluded that the enhancement in mechanical properties can be achieved by nano-reinforcement through using dispersant and applying ultra-sonication technique. The most significant improvement was found in flexural strength of the cement paste batches with an increase of 82%. However, judging the test results from an overall view it is concluded that in most cases the enhancement gained from nano-reinforcement was not significant, since the extent of increase in strength can also be attained by other methods

such as decreasing w/c ratio or adding mineral admixtures, which are more convenient and cost-effective. Further discussions will be made in later sections. The strengthening mechanism for GNP reinforced cementitious materials as well as the potential problems will be discussed deeply.

Table 3.1. Compressive and flexural strength of hardened mixtures

Group ID	Type of GNP	GNP Content (GNP/cement)	Dispersing agent Content	Sonication (hrs)	Density (kg/m^3)	Compressive strength (MPa)	Flexural strength (MPa)	Stiffness/ Stiffness of pure cement
Paste P1	-	-	-	-	1980	75.33	3.38	1.0
P2	-	-	Darex S20 2mL	-	2030	69.85	3.66	1.2
P3	Asbury TC307	0.05%	-	-	1990	57.60	3.96	0.6
P4	Asbury TC307	0.05%	Darex S20 2mL	-	2020	63.73	3.04	0.6
P5	Asbury TC307	0.05%	Darex S20 2mL	2	2030	66.08	5.29	0.7
P6	Asbury TC307	0.25%	Darex S20 2mL	-	2040	73.04	3.76	0.8
P7	Timrex T15	0.05%	Darex S20 2mL	-	2040	70.94	3.28	0.7
P8	Timrex T15	0.05%	Darex S20 2mL	2	2040	74.47	6.25	1.2
P9	Timrex T15	0.25%	Darex S20 2mL	-	2020	62.02	4.45	1.0
P10	Timrex T15	0.50%	Darex S20 2mL	-	2060	70.99	3.37	1.2
Mortar M1	-	-	-	-	2240	49.81	6.93	1.4
M2	-	-	Darex S20 2mL	-	2250	55.90	8.51	1.5
M3	Asbury TC307	0.50%	-	-	2280	58.93	7.18	1.6
M4	Asbury TC307	0.50%	Darex S20 2mL	-	2280	59.77	7.10	1.3
M5	Asbury TC307	0.50%	Darex S20 2mL	2	2250	55.39	7.54	1.3
M6	Asbury TC307	1.00%	-	-	2270	58.62	7.94	1.6
M7	Asbury TC307	1.00%	Darex S20 2mL	-	2250	56.63	8.08	1.5
M8	Asbury TC307	1.00%	Darex S20 2mL	2	2260	55.04	7.84	1.4
M9	Asbury TC307	1.50%	-	-	2250	58.09	7.63	1.4

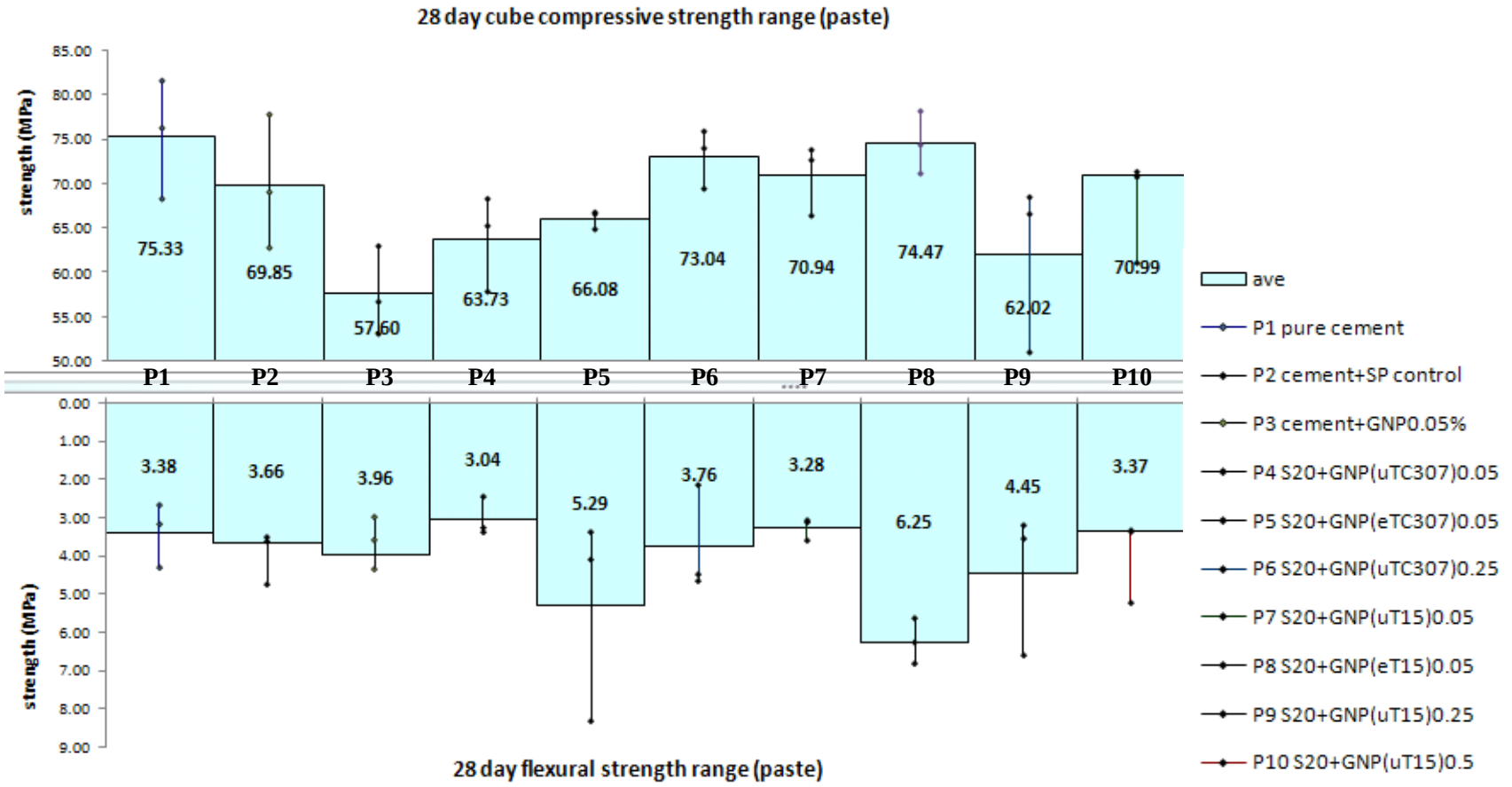

Fig.3.1. 28 day strength of cement paste batches

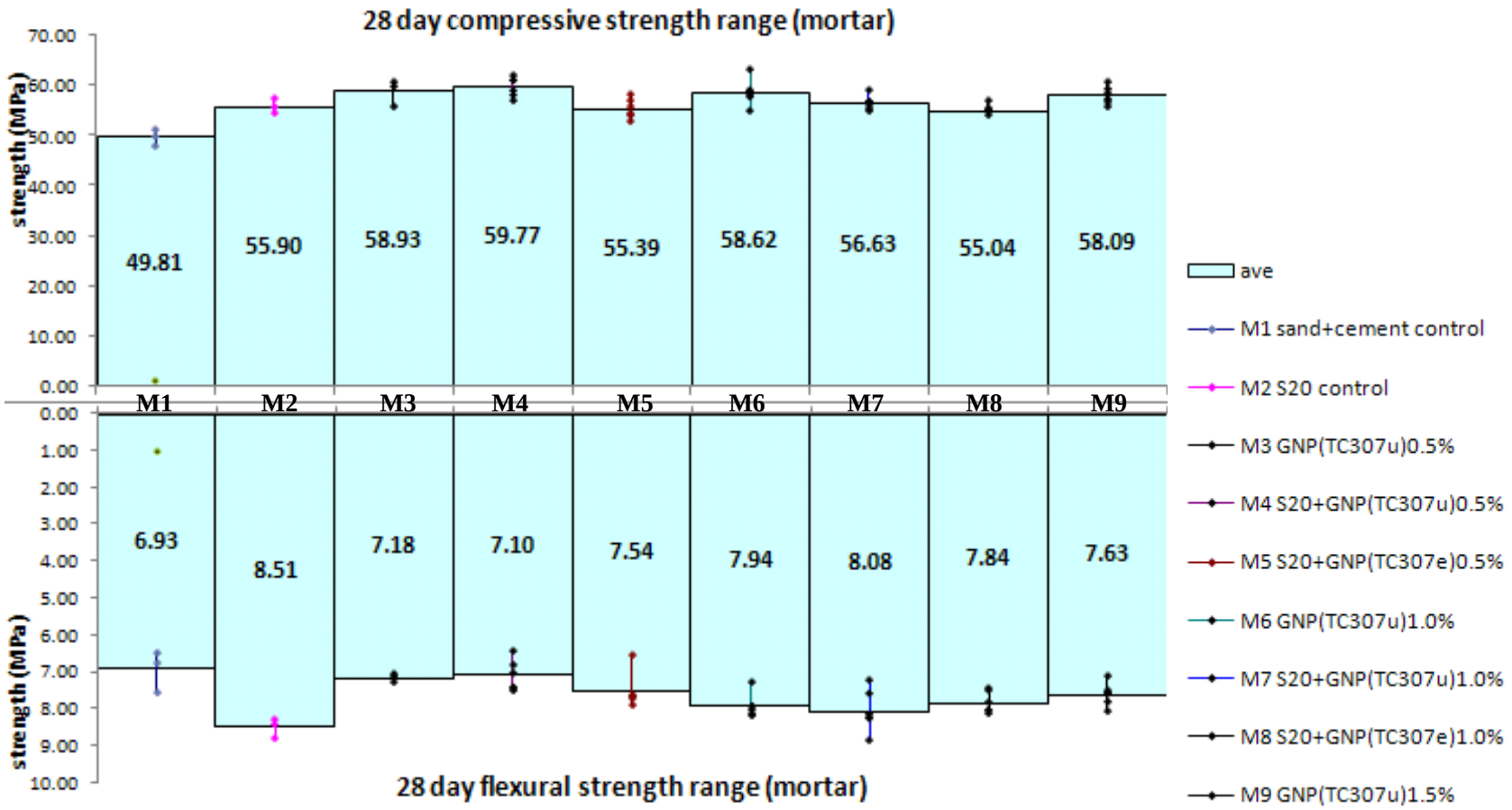

Fig.3.2. 28 day strength of mortar batches

3.1.2 Discussions on Strength and Stiffness of Hardened Mixtures

3.1.2.1 Discussions on Hardened Cement Paste Mixtures

1. Degree of GNP dispersion is in accordance with the strength of hardened mixture. As shown in Figure 3.3, by comparing strengths of batches P3 and P1 it is concluded that poorly dispersed GNP particles can affect the compressive strength adversely due to the formation of weak zones in the hardened matrix. Beneficial effects of dispersion and ultra-sonication are demonstrated by comparing P3 with other batches (P4 and P5) containing GNP particles. As shown in Figure 3.4, exfoliation and ultra-sonication have been proven to be effective in nano-reinforcement creating particles with finer sizes and improved properties in terms of strength and stiffness. This claim can be confirmed by observing that for batch P8, sonication of T15 GNP particles through the dispersant has resulted in a flexural strength increase of 82%.

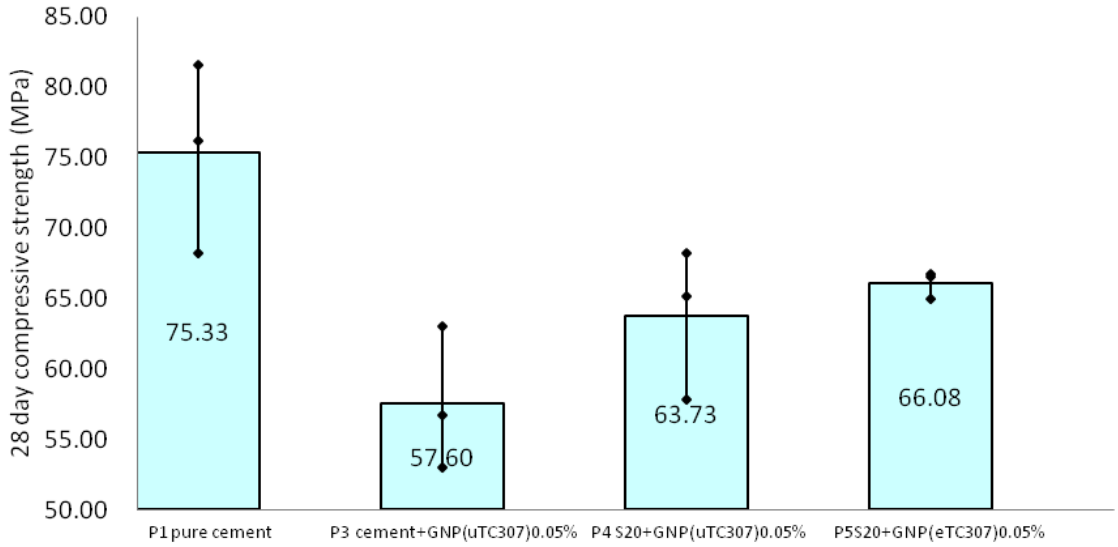

Fig.3.3. 28 day compressive strength comparison among batches P1, P3, P4 and P5

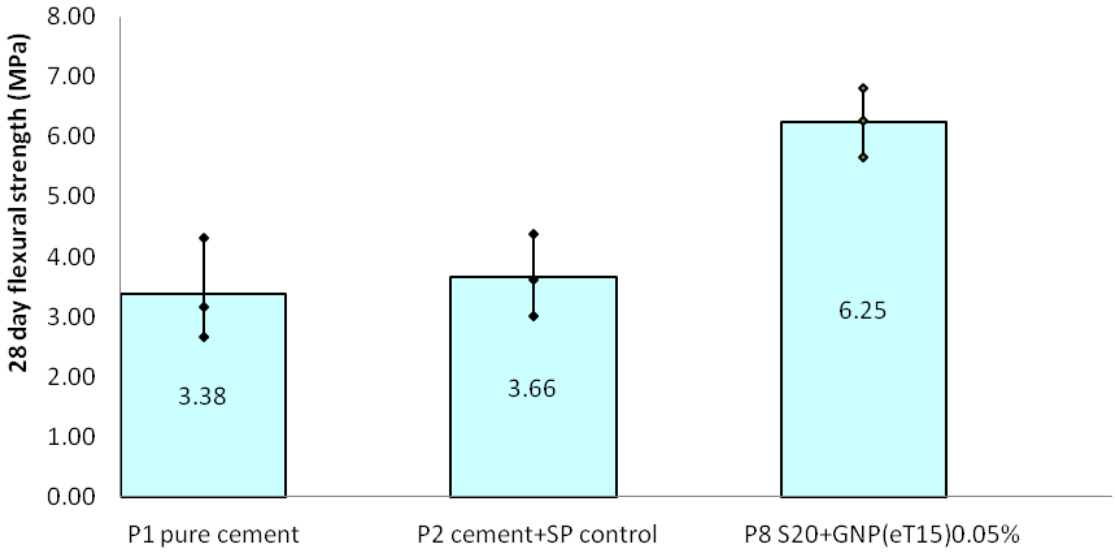

Fig.3.4. 28 day flexural strength comparison among batches P1, P2 and P8

2. As can be seen from comparing of P1 and P2 in Figure 3.5, inclusion of dispersants but without GNP particles resulted in a reduction in compressive strength. This is probably due to the excessive bleeding problem in batch P2. During casting it was found that workability of the mixture in batch P1 had already been high enough to prevent consolidation problem that no water-reducing agent was needed. Therefore in batch P2, when Darex Super 20 was added, too high a flowability of the mixture and bleeding problem were observed, which were manifested by the water moving upwards to the surface of the mixture before it set. This bleeding problem ended in a weak surface of the specimens and therefore decreased the compressive strength. However, after GNP particles were added to the mixture, it was found that the bleeding problem could significantly be reduced, due to that the GNP particles have a large surface area and are able to absorb a large amount of water. The adverse effect of incorporating dispersants can therefore be offset by increasing dosage and better dispersion of GNP particles, as can be observed by comparing batches P6 and P2 in Figure 3.5, or P7, P8 and P2 in Figure 3.6.

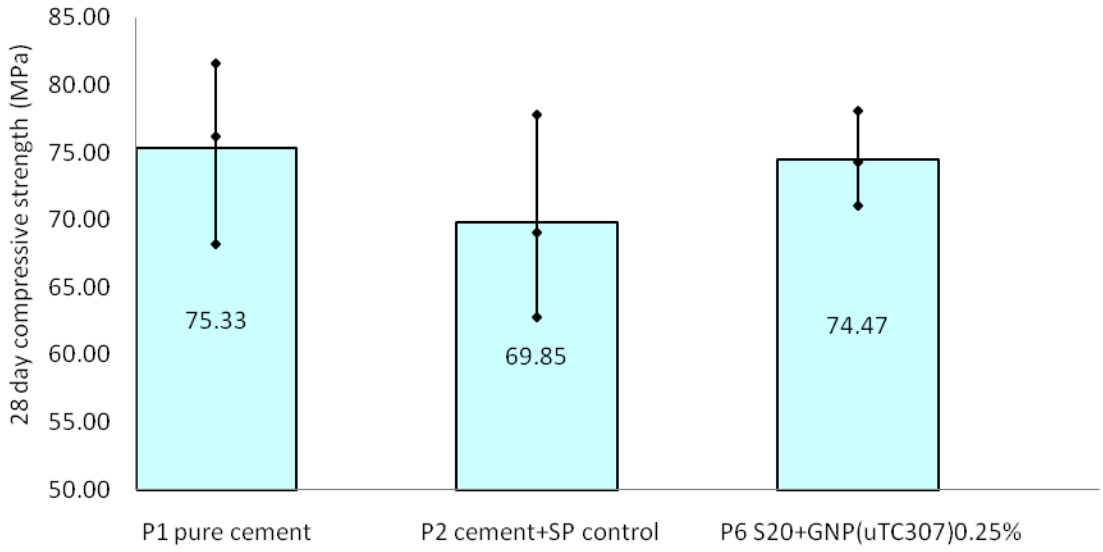

Fig.3.5. 28 day compressive strength comparison among batches P1, P2 and P6

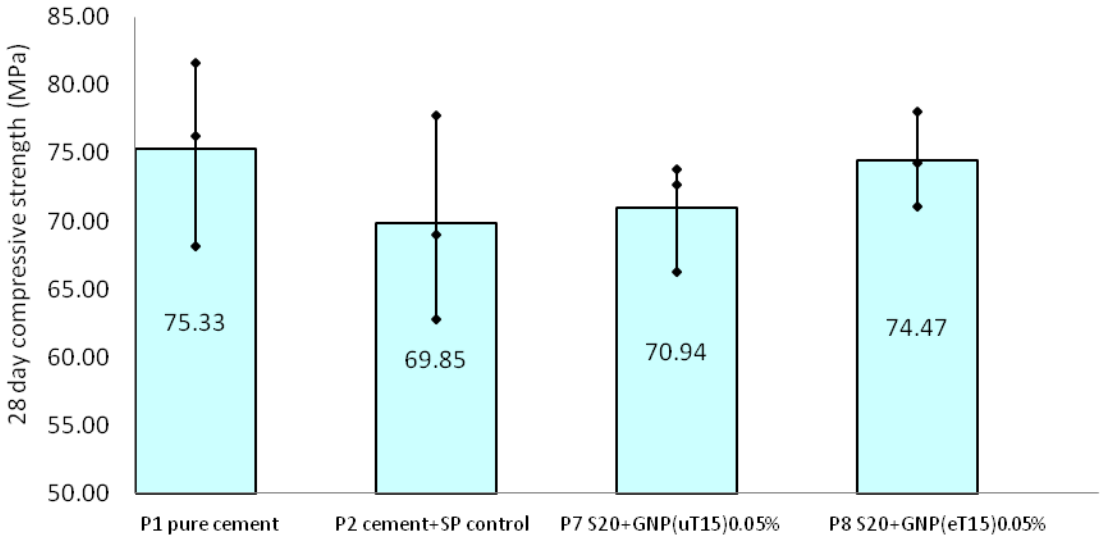

Fig.3.6. 28 day compressive strength comparison among batches P1, P2, P7 and P8

3. Batches with GNP reinforcement exhibit larger variations in flexural strength and very high strength was observed for some specimens as shown in Fig.3.1. Possible explanations for this phenomenon is for cementitious material with low

tensile strength, crack in flexural failure is normally initiated at the weakest point within the tensile region, and cracks can propagate easily through if no stiff materials are present to divert the crack path. In three-point loading, the critical point is found at the mid-span of the specimen. Therefore, flexural strength of the specimen largely depends on the degree of dispersion and the strength of stiff particles at the small mid-span region, leading to test results with a large variation.

3.1.2.2 Discussions for Hardened Mortar Mixtures

1. The inclusion of GNP particles has resulted in a consistent increase in both compressive strength and flexural strength for the mortar mixtures, which is expected to be mainly due to the filler effect of GNP. High porosity is anticipated for mortar batches owing to their low workability and high w/c ratio, which provides ample room for nano-particles to be effective fillers. From the test results it can be found that the inclusion of GNP particles increased compressive strength for mortar but not for cement paste. There may be two reasons for this. Firstly, the mean size of Portland cement particles is 10-15μm (Mindess S. et al., 2003) while the average effective diameter of TC307 GNP particles is 2.6μm. These two values are at the same level of magnitude; therefore the filler effect of GNP particles in cement paste is not as obvious as that in mortar mixtures although their estimated thickness is small. Secondly, pore size in cement paste ranges from 0.5nm to only around 10μm (Mindess S. et al., 2003), with the upper limit close to the average effective diameter of GNP particles. While in the mortar, the pore size is enhanced due to the existence of interfacial transition zone around the fine

aggregates. This also leads to more effective filler effect of GNP particles in mortar mixtures than in cement paste.

2. The results obtained from mortar batches exhibited much better consistency than cement paste batches also due to their high porosity. Because for mortar batches, the large defects are distributed throughout the whole specimen, their strengths are controlled by the whole block, while for cement paste batches, their strengths are very sensitive to the randomly distributed local large defects which will lead to the most severe stress concentration.

3. Although weaker in compressive strength, mortar mixtures general exhibit higher flexural strength than cement paste mixtures. This is due to the inclusion of fine aggregate, which helps to redirect the crack paths and provides interlocking effect resulting in improved crack resistance. The failure pattern of mortar is less brittle as compared to the cement paste because of a wider size spectrum of different particles in the matrix.

4. Since the water reducing agent can free the water absorbed by the particles to improve the workability of the fresh mixture, and thus generate mixtures with better homogeneity, the control Darex Super 20 batch has shown better flexural strength than the rest. Although Darex Super 20 was also added to mixtures with GNP particles, no comparable improvement in the test results was obtained because the water can be easily absorbed by the GNP particles, which possess

large surface area. Therefore less water can be mobilized for the workability or even cement hydration, resulting in mixtures with reduced mechanical properties.

3.2 Strengthening Mechanisms for GNP Reinforced Cementitious Composites

As one type of nano-particle, GNP possesses the "small size effect" and "surface effect" which are beneficial for mechanical properties of cementitious composites. Besides, GNP also can enhance mechanical properties of these composites via filler effect, crack-arresting effect and improvement in the interfacial transition zone (ITZ). The strengthening mechanisms for GNP reinforced cementitious composites will be summarized and discussed in detail in this section.

3.2.1 Small Size Effect

Under certain conditions, qualitative changes in particle properties can occur along with quantitative changes in particle size. Small size effect refers to the phenomenon that materials reduced to the nanoscale can show different properties compare to what they exhibit on a macro scale. (Wikipedia, 2012). This is because when the size of particles is reduced to a level that it is comparable or even smaller than some physical characteristic sizes such as the light wavelength, the de Brogile wavelength, the coherence length or the penetration depth of the superconducting state, etc., the periodic boundary conditions of the crystal will be destroyed and the number of atoms near the particle surface will be

reduced. Since the size of GNP particles has reached the nanoscale, they have a very large interface along which the arrangement of the atoms is very confusing. When the material is subjected to an external force and deforms, these atoms can easily migrate, by which energy can be absorbed and material deformation can be resisted. Therefore when GNP particles are added into the intrinsically brittle cementitious materials, increases in mechanical properties can occur.

3.2.2 Surface Effect

As a particle becomes smaller, the proportion of its surface atom sharply increases and leads to changes in its properties, this is known as the surface effect for nano-particles (Gong S., 2008). When the size of a particle is far larger than the diameter of the atom, the number of its surface atoms is small and therefore their effects can be ignored. However, when the particle is reduced to the nanoscale, the large proportion of surface atoms provides a large surface area and high surface energy, leading to much stronger absorption ability and chemical reactivity compared to normal materials. Therefore, in cementitious nanocomposites, GNP particles can show good bonding with the cement matrix due to strong van der Waals force at the interface. Moreover, they serve as nuclei around which the network structure of cement hydration products is formed, which improves the homogeneity of the harden cement. All these effects help to modify the microstructure of the composites and hence increase their strength.

3.2.3 Filler Effect

It has been well known that concrete is a porous and non-homogeneous complex system, whose porosity has a decisive influence on its strength. In concrete the pores with a diameter of larger than 20nm are considered to be harmful to its mechanical properties (Wang Y., 2005). Moreover, hardened cement paste composed of hydrated calcium silicate gel which contributes most to the strength of concrete is identified as one type of primary nanomaterials with millions of gel pores inside (Wang Y., 2005). These indicate that nano-particles can be used to modify the structure of cementitious materials at the nanoscale. The small size, large surface area and high surface energy make GNP particles to be one kind of efficient fillers. Although they cannot act like silica fume to react with water and generate hydration products, their physical filler effect has already made them effective in reducing porosity of the matrix. The effect of GNP particles on reducing porosity can be judged from the densities in Table 3.1. For the mortar batches, the density of plain mortar (batch M1) is larger than the density of the GNP that is 2160kg/m^3; therefore, if GNP only replaces the solid particles of the plain mortar rather than fill in the pores, the density of the material would decrease. However, densities of batch M3 to M9 show that the additions of GNP particles do increase the density of the material; therefore the filler effect of GNP is confirmed. For cement paste batches, the dose of GNP particle is small, even by assuming that the weight of the pure cement paste (batch P1) is totally from the cement and neglecting the contribution of water to the weight, and assuming that all the GNP particles fill in the pores in the matrix, adding 0.50% GNP (by weight of cement) can only at most increase the density from 1980kg/m^3 to 1990kg/m^3, which is smaller than the actual densities in batch P2 to P10. The density increase in the cement

paste batches therefore is considered to be mainly from the enhanced workability by adding Darex Super 20, and the filler effect of GNP is not as obvious as that in the mortar batches. Besides reducing porosity, GNP particles also improve the particle size distribution and decrease the size and connectivity of the pores. In conclusion, the filler effect of GNP provides a higher density (see Table 3.1) and less stress concentration for the cement matrix, therefore helps to improve mechanical properties of the composites.

3.2.4 Improvement in ITZ

There are three components in hardened concrete: hydrated cement paste, aggregates and interfacial transition zone (ITZ). ITZ plays the most critical role since it connects the other two components that have completely different natures. ITZ has a less crack resistance than either the aggregate or the hydrated cement paste; therefore, fracture occurs preferentially in the ITZ to constitute the "weak link" in the concrete. One reason causing this is that ITZ is a porous weak zone due to the inability of the cement particles to pack efficiently around the aggregates, a well-known phenomenon called the "wall effect". Furthermore, due to the bleeding phenomenon in cement mortar, water in the fresh mixture migrates upwards and this migration is blocked when the water comes across an aggregate. In this situation water film is formed under the aggregate and the bond between cement paste and the aggregate is weakened. When GNP particles are added into the cementitious composites, their large surface area and high surface energy make them absorb a large amount of water, by which bleeding of cement mortar is reduced and the possibility of forming water films is significantly decreased. These strengthen the bond between aggregates and cement paste and meanwhile improve the

crack resistance of ITZ. Although thickness of ITZ is only 20-40μm, it nearly occupies 20-40% of the total volume of the cementitious matrix (Mindess S. et al., 2003). Therefore, if ITZ is modified by nano-particles, significant improvement in strength and stiffness of the cementitious composites can be anticipated.

3.2.5 Crack-arrest and Particle-interlocking

When a force is applied to concrete, in most instances cracking originates internally, gradually forms a network of micro cracks and at last failure of concrete is identified with multiple cracks or major cracks cut through it. Therefore to improve strength of concrete, arresting crack propagation is an effective way. Incorporating GNP particles into concrete can achieve this by two effects. Firstly, their large aspect ratio and plate shape provide them strong ability in blocking and diverting the micro cracks, which slow down crack propagation and formation of the crack network. Secondly, the bridge effect of GNP particles can delay crack origination and prevent crack opening up. By these two effects as well as the interlocking between GNP slip planes, a large amount of energy can be absorbed in the loading condition, leading to increased strength of the cementitious composites.

3.3 Potential Problems for GNP Reinforced Cementitious Composites

Although the results for both cement paste batches and mortar batches show some

improvement in mechanical properties, it is found that the enhancement is not significant enough for industrial purposes. The potential problems are discussed here as references for future study.

3.3.1 Material Incompatibility

Though has not been addressed in published documentations regarding cementitious nanocomposite, the incompatibility between cement matrix and GNP particles was identified as an influencing factor for insignificant strength enhancement. It was postulated that GNP particles exhibit double sided effects on cementitious materials meaning its good strength and stiffness make concrete stronger, but its thermal and elastic modulus incompatibility increase the probabilities of defects and internal cracks of concrete. Due to this thermal incompatibility, formation of effective bonding between cement matrix and the nano-particles may be difficult. Although thermal expansion is never seen as a key parameter of cementitious material, it indeed affects the effectiveness of reinforcement both at the macro and micro level (Mindess S. et al., 2003). The internal restraining stresses caused by differential strain and stresses can be crucial especially when concrete is coupled with materials of high elastic modulus. A rough calculation can show how much stress could be developed because of thermal incompatibility. Coefficient of thermal expansion for GNP particles is $1x10^{-6}/℃$ and coefficient of thermal expansion for saturated cement paste α_{cement} with w/c of 0.4 is 18~20E-6 /^{o}C (Administration U. S. F. H., 2010). Calculations of restraining stress for each degree of temperature change are shown as follows:

Difference in thermal strain $\Delta\varepsilon = (\alpha_{cement} - \alpha_{GnP})\Delta T = (18-1)1 = 17$ micro strain

GNP restraining stress $\sigma_{remain} = \Delta\varepsilon E_{GNP} = 17 \times 0.03 = 0.51MPa$

Therefore, the restraining thermal stress of cement matrix for each degree of temperature change will be approximately 0.51MPa; assuming appropriate values of Young's modulus for cement and GNP are 30GPa and 1000GPa respectively. As cement hydration is an exothermic reaction and the temperature rise is approximately 12^{o}C for every 100g of cement, the resultant restraining stress could be far larger than the tensile strength of the cement matrix. Thus, cracks might have been developed even before external loading and the flaws and defects caused by internal crack could be opened up very easily upon stressing. Internal cracking is particularly detrimental to tensile strength of concrete because the failure mechanism of concrete in tension is very sensitive to defects and notches and is generally governed by micro-cracking, associated especially with the interfacial transition zone (Mindess S. et al., 2003). Defect detecting technology should be implemented to verify the postulations on thermal incompatibility and to further monitor the differences between conventional and nano-particle reinforced cementitious composites.

3.3.2 Formation of Weak Zones due to Insufficient Dispersion

The strength of GNP particles is likely to be weakened due to particle entanglement and overlapping owing to insufficient dispersion. As can be seen from the SEM images, considerable overlapping of GNP particles were observed for all types of GNP products leading to a possible weakening mechanism due to slippage and disintegrating of overlapping graphite layers under stress which can result in formation of weak zones

within the cement matrix. This argument can be validated by examining the test results obtained for the cement paste batches where the most significant improvement of 82% in flexural strength was attributed to the mixtures with good ultra-sonication and meanwhile the compressive strength also shows a consistent trend of increase with alleviated overlapping of GNP particles through dispersion and ultra-sonication process.

3.3.3 Insufficient Multi-axial Rigidity of GNP Particles

The directional strength capacity and insufficient rigidity of GNP particles may also introduce potential difficulties in their composite implementations. Hitherto, the structural strength obtained for GNP particles were all based on direct tensile test and this reveals only their mechanical behavior parallel to the stronger plane of graphite which is characterized by strong sigma bonding among carbon atoms (Asbury, 2010). However, high uniaxial tensile strength and stiffness may not mean high strength under multi-axial loading because graphite sheets are likely to bend hence their structural potential may be only limited to directional loading. Since the orientation of GNP particles inside the composite matrix are not necessarily directional it is likely that a great portion of the GNP particles are exposed to multi-axial loading resulting in limited strengthening effects due to the low multi-axial rigidity of GNP particles.

3.3.4 Insufficient GNP Dosage

There is a high probability that the dosage of GNP particles is too little to be able to

manifest their potential in strengthening effect. The maximum dosage of GNP particles was 0.5% by weight of cement for cement paste mixtures and 1.5% by weight of cement and sand for mortar mixtures which may not be sufficient to alter the averaged mechanical behavior of the composite product since the limited presence of GNP particles can neither block the crack path nor strengthen the hydration products effectively. If this were to be the real reason the incorporation of nano-particles for the strengthening effect of concrete will require complicated processing technique before being feasible for commercial applications.

The potential problems discussed here in Section 3.3 not only have negative effects on mechanical properties of the nanocomposites, but also impair their electrical properties, which will be discussed in Chapter 4 and Chapter 5, since all these problems will lead to degradation in conductive network formed by GNP particles. Further study is needed in the future to minimize the effect of these problems so that both the mechanical and electrical properties of the nanocomposites can be improved.

CHAPTER 4 STUDY ON ELECTRICAL RESISTANCE OF GNP REINFORCED MORTAR

In section 4.1, the conducting mechanism of GNP reinforced cementitious materials will be studied, based on which the effects of different factors on the electrical resistance will be investigated and discussed in section 4.2. This chapter serves as the basis for Chapter 5, in which the self damage sensing properties of the materials will be explored.

4.1 Conducting Mechanism of GNP Reinforced Cementitious Composite

The electrical conduction model of GNP reinforced mortar is shown in the schematic diagram in Fig.4.1 where **A**, **B** and **C** represent the fine aggregates, cement matrix and GNP particles dispersed in the cement matrix respectively. The fine aggregates are good electrical insulators while the cement matrix containing capillary pores has electrical resistivity that is highly dependent on the moisture content. For example, dry hardened cement is a good electrical insulator with a resistivity of about 10^{15} ohm.cm while moist hardened cement has a much lower resistivity of about 10^{8} ohm.cm, which is in the range for semiconductors (Mindess S. et al., 2003). The increase in conductivity is due to the presence of water in the capillary pores, which contains dissolved salts and therefore acts as an electrolyte.

GNP particles have pi-electrons that participate in interlayer pi bonding, which make it a good electrical conducting material. Besides, the carbonation process with temperature up

to 1050 ℃ during fabrication of GNP left a large excess of holes in the valence band (Sun M. et al., 1998). When the GNP content is low, there are hardly any contacts between GNP particles in the cement matrix. In this condition, the pi-electrons or the holes could be excited and make a leap from one GNP particle to another, which is called tunneling effect. With increasing GNP content, the connectivity of GNP particles is improved and a conductive network can be formed, along which the pi-elections and holes can transport.

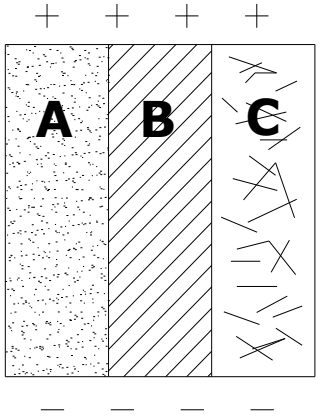

Fig.4.1. The electrical conduction model of GNP reinforced mortar containing **A**, the fine aggregates, **B**, the cement matrix, and **C** the GNP.

When the amount of GNP particles exceeds the percolation threshold, the electrical conduction model of GNP reinforced mortar can be considered as a composite consisting of three components in parallel. In this model, the conduction of electric current can follow three paths:

1. Ionic conduction through the free evaporable water in the cement matrix;
2. Electronic conduction and hole conduction through GNP and cement matrix in series by tunneling effect;

3. Electronic conduction and hole conduction through conductive network formed by GNP particles.

When the GNP content is too low, the distance between GNP particles is too large for tunneling effect to occur and the current is conducted mainly through path 1. As the GNP content increases, both paths 1 and 2 are operative. When conductive network is formed by the GNP particles, path 3 will be the dominating one. The collaboration of tunneling effect in path 2 and particle-particle contact conduction in path 3 is also similar to that in epoxy/GNP composites (Jovic N. et al., 2008).

4.2 Parametric Study on Electrical Resistance

4.2.1 Effect of Type of GNP

In this section, the electrical resistances of the specimens with different types of GNP were compared in Tables 4.1 and 4.2 for the cubes and prisms respectively, to provide knowledge for the selection of GNP to enhance the electrical conductivity of the composites. The composite can thus be fabricated with a lower dose of GNP to achieve the same conductivity, which could imply lower cost and workability loss for the fresh mixture.

Table 4.1 Electrical resistivity of the cubes (kΩ.cm)

Age	TC307 cube	[a]3775 cube
16 days	0.813	3.80

30 days	0.813	4.30

Table 4.2 Electrical resistivity of the prisms (kΩ.cm)

Age	[a]TC307 prism	[a]3775 prism 1	[a]3775 prism 2
16 days	[b]–	3.60	4.60
30 days	4.00	9.84	11.20

[a]Although readings up to three decimal places are taken, the values are shown for two decimal places due to the larger fluctuations in the third decimal place.
[b]There was no measurement due to the damage of the electrical contacts.

Electrical resistance of the plain mortar cube was not measurable since it was beyond the upper measuring limit of the multimeter of 40 MΩ, which corresponds to a resistivity of 200 MΩ.cm. On the other hand, it can be seen from Tables 4.1 and 4.2 that the resistivities for mortar specimens with either type of GNP were of the order of kΩ.cm. From here, it can be concluded that both types of GNP have greatly enhanced the electrical conductivity of mortar specimens.

However, the degree in enhancing the electrical conductivity of the mortar composites for different types of GNP was different. It was observed that the mortar reinforced with 3775 GNP had a much higher resistivity than mortar reinforced with TC307 GNP (see Tables 4.1 and 4.2). For the prisms it was more than 100% higher and for the small cubes it was up to 400% higher. The greater effectiveness of TC307 GNP in enhancing the electrical conductivity of the mortar composites could be explained by their differences in physical properties. TC307 GNP has a smaller average size of 2.6μm, a much larger surface area of 352m^2/g and a much larger average aspect ratio of 986 as compared to those of 3775, which are 8.0 μm, 24m^2/g and 215, respectively. For the same amount of GNP that was properly dispersed within the matrix, there will be more of the smaller

TC307 particles with a larger surface area compared to 3775 particles, resulting in smaller average inter-particle distance. Therefore, it is easier for the tunneling effect to occur in the specimens reinforced with TC307 particles. Besides, a larger surface area and aspect ratio of TC307 particles mean higher chance for the GNP particles to contact each other and form conductive network. Interactions of these effects resulted in a better electrically conducting material for mortar composites reinforced with TC307 GNP.

4.2.2 Effect of Dimensions of the Specimens

Comparing values of resistivity for the cubes and the prisms in Tables 4.1 and 4.2, it was found that at the later age, resistivity of the prisms was more than twice that of the cubes, which was true for both TC307 and 3775 specimens. The results imply that dimensions of specimens have a significant effect on its own conductivity. Despite the process of ultra-sonication with the use of dispersant, fully homogeneous dispersion can never be achieved due to the difficulties in quality control and the inhomogeneous microstructure of the cement matrix. GNP particles were randomly distributed inside the specimen and conductive paths were randomly formed. For the prisms, the distance between the two electrical contacts normal to the longitudinal direction of the prism is 16cm, while the corresponding distance for the cubes is only 5cm. The chance of forming continuous conductive paths between the electrical contacts is thus much higher for a cube than for a prism, which explains the lower resistivity of the cube.

Comparing the resistivity of the two geometrically identical prisms containing 3775 GNP, it was found that their resistivity differed significantly even though they were cast in the

same batch. At 16 days, resistivity of prism 2 was 27.8% higher than that of prism 1; at 30 days, the difference was only 14.1%. There are mainly three reasons causing this difference:

1. Inhomogeneity in microstructure of the cement matrix – Hydration products, sand particles as well as capillary pores distribute randomly inside cementitious composites resulting in microstructure that varies from specimen to specimen. This has already been known as a reason for strength variation in concrete specimens that will similarly lead to variation in resistivity. Hydration product and sand particles form barriers between GNP particles and affect the tunneling effect, while connectivity of the capillary pores and the evaporable water in it affect the ionic conduction in the cement matrix.
2. Inhomogeneous dispersion of GNP particles – This can also be considered as another form of inhomogeneity in microstructure of the composites. However, the role of GNP dispersion is much more significant than the other factors when the percolation threshold is exceeded since it is the GNP that dominates the conductivity of the composites. Inhomogeneous dispersion of GNP will result in different forms of conductive networks inside the matrix, leading to difference in resistivity.
3. Unavoidable quality control problems during specimen fabrication. Examples of these errors are: inaccuracy in specimens dimension control, difference in cement hydration extent although the specimens are cured under the same condition, difference of contact resistance between conductive epoxy and the specimen, etc.

In conclusion, it was found that the different specimen dimensions could lead to significant difference in resistivity; even when the specimens had the same dimensions, large variation in their resistivity values could still be observed. Compared to the test results in literatures (Chung D. D. L., 2003), the difference in the intrinsic electrical resistance could possibly be higher than the change in electrical resistance caused by damage. Therefore it is proposed that the resistivity of a specimen cannot be simply represented or predicted either by an average value of a batch or by a value of another specimen. When analyzing the self damage sensing property of a specimen, its electrical resistance change should be calculated based on its own original value which should have been stable with age before the self sensing test (see Section 4.2.4).

4.2.3 Effect of Electric Polarization

4.2.3.1 General

Electric polarization refers to the phenomenon in which the centers of positive and negative charges do not coincide. It commonly occurs in a dielectric material when it is exposed to an electric field (Cao J. and Chung D. D. L., 2004). For GNP reinforced cementitious composites, electric polarization could happen involving ionic conduction in the cement matrix. During electrical resistance measurement under direct current (DC) condition, migration of the positive and negative ions occurred in response to the applied electric field. However, the ions could not enter the external circuit and thus gathered at the two ends of the specimen, which resulted in internal electric field that was opposite to

the applied one. This slowed down the flow of the charges and caused the electrical resistance to increase with time.

The effect of electric polarization, which causes temporal variation in the electrical resistance, is undesirable for the tests on self damage sensing properties in Chapter 5, since it complicates the assessment of damage. There are possibly two obvious methods to exclude the effect of electric polarization; one is to maintain polarization at the same level throughout the test, while the other is to perform prompt measurement before the effect of polarization becomes significant. A long- and short-duration electric polarization tests were carried out to investigate these two methods in this study.

4.2.3.2 Long-Duration Monitoring

The electric resistance was continuously monitored for 100 minutes under an external electric field of less than 0.6V generated by the multimeter (see appendix E) on the TC307 prism to investigate how long it took for the polarization to reach steady state, if it existed. It was observed that the electrical resistance increased with time throughout the entire test, meaning that the electric polarization did not complete within a period of time as long as 100 minutes. However, due to the polarization-induced internal electric field that was opposite to the external applied one, the rate of increase in electrical resistance was reduced with time, which could imply that the extent of polarization was approaching a steady state. It was observed that while the electrical resistance increased by 20.93% within the total period, more than 70% of this increase occurred in the first 20 minutes. Subsequently, the increase for the second to fifth 20 minutes intervals were only

2.94%, 1.66%, 1.15% and 0.83% respectively, which were small enough to be neglected when compared to the increase in electrical resistance caused by a damage or crack, as detailed in Chapter 5.

Therefore, the determination of electrical resistance when the polarization has nearly stabilized provides a consistent measurement where variation due to polarization is minimized. However, the disadvantages of this method are obvious. It requires a setup where the probes must be kept in good contact with the specimen and the electric field must be supplied continuously. Since electric polarization does not reach steady state rapidly, long waiting time is required before measurement can be taken. Although using a higher voltage can help to accelerate the electric polarization process because the rate of this process is determined by both the mobility of the ions and the magnitude of the electric field (I. L. H. Hansson, 1983), it also increases the steady state polarization to a higher level since the internal electric field formed by the migrated ions tends to balance the applied electric field (Qizhao M. et al., 1997; Lee C.-Y. and Wang S.-R., 2010). Therefore, it is not necessary that using a higher voltage would help to shorten the waiting time before polarization reaches the steady state. Besides, using a higher voltage means an additional source is required to generate the higher voltage since the built-in voltage in the multimeter for measuring electrical resistance is fixed.

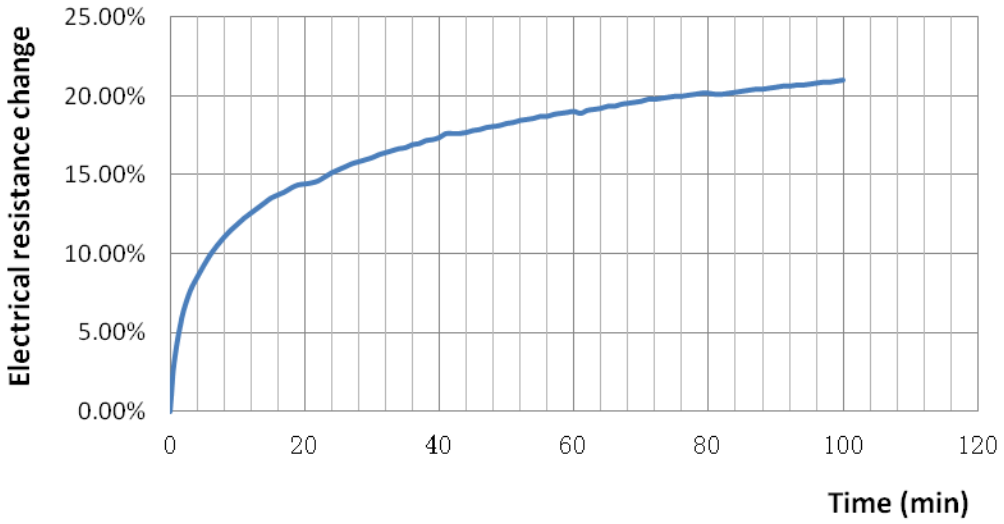

Fig.4.2. Increase in electrical resistance due to polarization.

Immediately following the long-duration monitoring, reversibility of the electric polarization was studied. The external electric field was removed to allow electric polarization to reverse under the internal electric field and its electrical resistance was measured every 10 minutes by taking prompt readings of within 5 seconds in order to avoid significant additional electric polarization (see Section 4.2.3.3). Due to the internal electric field formed by the migrated ions inside the specimen, electric polarization began to reverse immediately after the external electric field was removed, leading to decreased electrical resistance (See Fig. 4.3). However, when the electrical resistance had finally decreased to a stable level, it was found that the new steady state was about 3.70% higher than the original value. This means that the electric polarization resulting from the long duration monitoring was not fully reversible when a constant electrical source is absent.

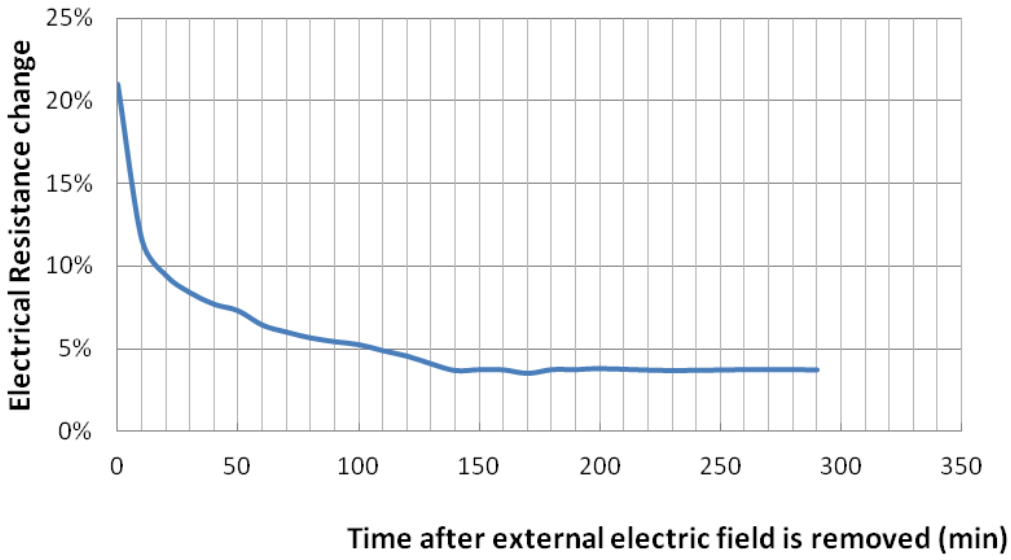

Fig.4.3. Reversibility of electric polarization when a constant electrical source is absent.

To study whether the irreversibility of the electric polarization can be eliminated by applying an electric field in the reversed direction, another test was carried out in which the external electric field was switched immediately after being applied in the first direction (direction 1 in Fig.4.4) for 100 minutes. Since the external electric field was generated by the digital multimeter, the electrical resistance measured was always in the same direction with the external electric field, i.e. before 100 minutes the electrical resistance in direction 1 ($R_1(t)$) was measured while after 100minutes the electrical resistance in direction 2 ($R_2(t)$) was measured (see Fig.4.4). The test results are shown in Fig.4.5. To be convenient, we define "resistance change $\Delta R_i(t)$" at time t with the following equation:

$$\Delta R_i(t) = \frac{R_i(t) - R_0}{R_0} \times 100\% \qquad (4\text{-}1)$$

where *i* equals to 1 or 2 representing direction 1 or 2. $R_i(t)$ is the electrical resistance reading at time t, when $t \leq 100$min, $R_i(t)=R_1(t)$ and when $t>100$min, $R_i(t)= R_2(t)$. R_0 is the

original electrical resistance reading (at the time of 0 min), which is the same for both direction 1 and 2 since electric polarization has not occurred, i.e. $R_0=R_1(0)=R_2(0)$. Under equation (4-1) a positive value for ΔR means an increase in electrical resistance while a negative value means a decrease in electrical resistance.

In Fig.4.5, the abrupt drop in measured electrical resistance during switching of external electric field confirmed the occurrence of polarization in the first 100 minutes, which caused $R_1(t)$ to increase and $R_2(t)$ to decrease. After the external electric field was switched, $R_2(t)$ started to increase, and at $t=T_1\approx110$min it increased back to the original value, having $\Delta R_2(T_1)=0\%$. However, this does not mean that electric polarization inside the specimen had been eliminated at this time, because it was found that $\Delta R_1(T_1)\approx5\%$ rather than also equaled to 0% when $R_1(T_1)$ was also measured. If the test were ended and the external electric field were removed at this time T_1, the residual internal electric field would continue to cause ΔR_1 to decrease and ΔR_2 to increase, finally ΔR for both directions would become stable at a value between 0% and 5% rather than exactly equal to 0%, which means the specimen would not be stable at its original state. Therefore, this point at $t=T_1$ which has a feature of $\Delta R_2(t)=0\%$ cannot be simply taken as the point representing full polarization elimination.

After $t=T_2=200$min when electric field had been applied to each direction for a same duration (100 minutes) and then removed, it was found that the electrical resistance of the specimen finally became stable at a value with -4.10% change compare to the value at the time of 0 min, which means it was lower than the original value. Therefore it is inferred

that there is a point T_3 between T_1 and T_2, at which if the switched electric field were stopped, the electrical resistance of the specimen would be exactly the same as the original value when it becomes stable. However, finding T_3 would not be easy because it is not a point with significant features in the curve in Fig.4.5. Moreover, whether the polarization is fully reversed when the electrical resistance of the specimen comes back to its original value is still another question because the polarization and depolarization processes have disturbed the arrangements of the ions (I. L. H. Hansson, 1985).

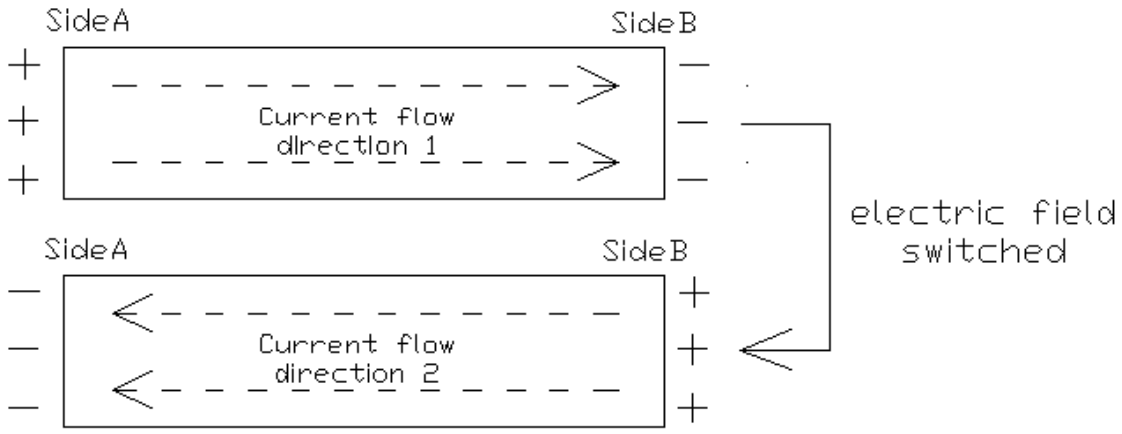

Fig.4.4. Directions for measuring electrical resistance

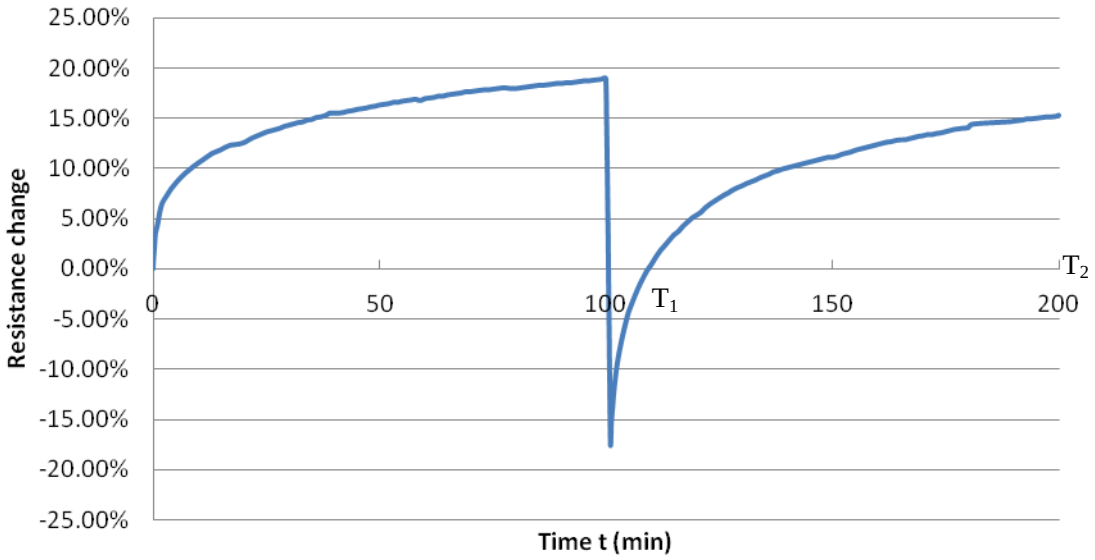

Fig.4.5. Variation of the measured electrical resistance with time before and after voltage polarity switching.

It was due to those disadvantages mentioned above that the long-duration monitoring method was not adopted in the later studies but a rapid measurement method described in the following section was adopted.

4.2.3.3 Rapid Measurement

The commonly used rapid measurement is an alternative approach in determination of electric resistance. The electrical resistance of the specimen was taken at the end of a 5s measurement. Due to the inhomogeneous pores and ions arrangement inside the specimen, electrical resistance measured from two opposite directions (see Fig.4.4) could show up to 5% difference, therefore the average electrical resistance of the two directions was taken (B. G. Han, 2004). The electrical resistances of the specimens were from two

opposite directions in sequence with an interval of 5s between successive measurements to allow for switching of the external electric fields. This rapid measurement approach was evaluated for the level of electric polarization in GNP reinforced cementitious composites.

Electric polarization level at the steady state of a long-duration electrical resistance measurement depends on the applied potential because the internal opposite electric field formed by the migrated ions tends to balance the external electric field (I. L. H. Hansson, 1985). Also, it has been known that electric polarization develops more slowly in specimens with higher conductivity (Wen S. and Chung D. D. L., 2008); this means that the mortar specimens reinforced with GNP of TC307, which have a lower resistivity (see Section 4.2.2) than those reinforced with GNP of 3775, would take more time to develop a steady state in a long-duration test when under the same applied voltage. This explains why specimen of TC307 was used in the long-duration test. On the other hand, during rapid electrical resistance measurement, the mortar specimens reinforced with GNP of 3775 would more likely experience greater electric polarization because they develop electric polarization much faster. Therefore, specimens reinforced with GNP of 3775 were used in this rapid measurement test. Also, prism has a higher resistivity than the cubes reinforced with the same type of GNP particles (see Section 4.2.3), which means electric polarization is more severe for prisms than for cubes, therefore, 2 prisms (3775 prism 1 and 3775 prism 2) were used in this test while only one cube (3775 cube) was used.

Due to the sluggishness of ion movement, electric polarization takes time to build up under DC condition. Therefore, the use of prompt electrical resistance measurement can avoid the problem of electric polarization (Sihai Wen and D. D. L. Chung, 2006). During the test it was found that in a period of 5s, electric polarization resulted in only around 0.5% increase in measured electrical resistance in the mortar specimens containing GNP. When compared to the electrical resistance increase due to damage as shown in Chapter 5, this 0.5% increase is negligible. Therefore it was concluded that the electric polarization built up within a 5s duration was negligible and correspondingly it led to negligible irreversible polarization. Furthermore when taking the second reading, the reversed external electric field caused electric polarization in the opposite direction and tended to diminish the irreversible polarization caused when taking the first reading. It could be approximately considered that after one set of electrical resistance measurement (measurement was taken once for each direction) the specimen was around its undisturbed state since the durations for applying the external electric field in the two directions were the same. As can be seen in Table 4.3, when three consecutive sets of electrical resistance measurements were taken from the specimens, it was found that the variations of the readings for each specimen in the same direction were only in the range of 0.46%-1.10%, and the variations for the average values, and the average values of each set of measurement, were less than 1%. When compared to the electrical resistance increase caused by internal damage in the self damage sensing test in Chapter 5, the variations of the readings were small enough to be neglected. Therefore it was concluded that the effect of electric polarization during prompt electrical resistance measurement is negligible and this approach was used throughout the study.

Table 4.3. Results of repeated short-duration electric polarization test (Unit: kΩ)

Steps	3775 cube		
	Direction 1	Direction 2	Average
1	1.017	1.020	1.019
2	1.022	1.012	1.017
3	1.023	1.022	1.023
Variation	0.59%	0.98%	0.59%

Steps	[a]3775 prism 1		
	Direction 1	Direction 2	Average
1	6.33	6.54	6.44
2	6.30	6.50	6.40
3	6.37	6.54	6.46
Variation	1.10%	0.61%	0.93%

Steps	[a]3775 prism 2		
	Direction 1	Direction 2	Average
1	8.65	8.36	8.51
2	8.63	8.32	8.48
3	8.67	8.35	8.51
Variation	0.46%	0.48%	0.35%

[a]Although readings up to three decimal places are taken, the values for prisms are shown for two decimal places due to the larger fluctuations in the third decimal place.

4.2.4 Effect of Age of the Specimens

It has been well known that the strength of cementitious materials increases at the early age as cement hydration process goes on, and gradually becomes stable after about 28 days when cement hydration is about to complete. Similarly, electrical resistance of GNP reinforced mortar also increases with age mainly due to three reasons: (1) the evaporable water is continuously consumed during cement hydration. Also, the hydration products decrease connectivity of capillary pores, reducing the effect of ionic conduction in the cement matrix; (2) the cement hydration products form barriers between GNP particles,

reducing tunneling effect for electrical conduction; (3) the cement hydration products have the chance to break the contact or increase the distance and barrier between GNP particles, thus degrading the conductive network and the effect of electronic conduction.

Since the age of the specimens also leads to electrical resistance increase, its effect is to be excluded in the study of self-sensing properties based on electrical resistance changes. For this purpose, experimental tests were carried out to investigate the variation of electrical resistance of the specimens with age. The 3775 cube and the two 3775 prisms were used in this test. The specimens were stored in the air-con room with a temperature of around 25℃ and a humidity of around 70%, and their electrical resistances were determined daily at a fixed time. Fig. 4.6 shows the development of the electrical resistivity of the 3775 batch specimens, which was measured after the 10th day when the specimens were removed from the curing room.

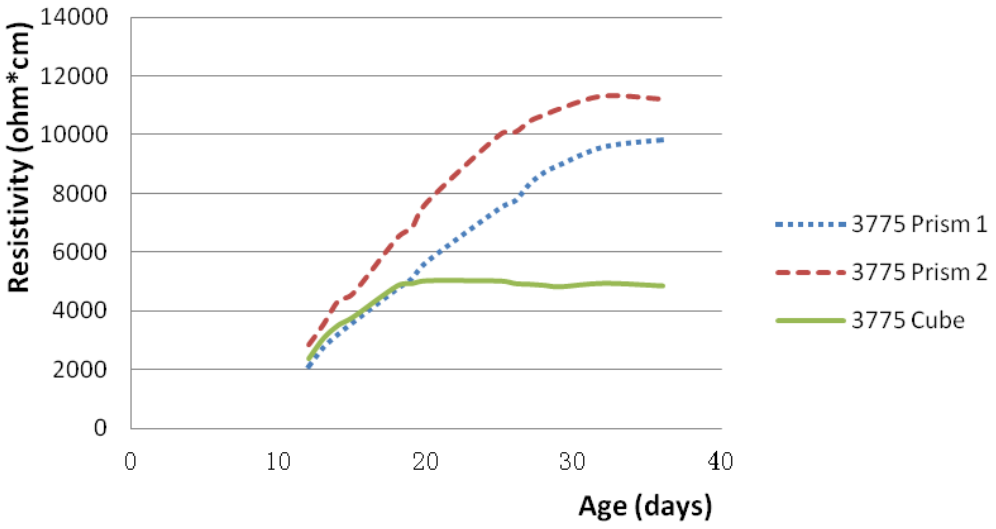

Fig.4.6. Electrical resistance development curves for 3775 batch specimens

It can be seen that the curves have shapes similar to the cement hydration degree curve of concrete (Mindess S. et al., 2003), which increases rapidly in the early ages but slows down and reaches a plateau in the later ages. Since during the cement hydration process, the consumption of the free water, the generation of the cement hydration products, the reduction in the size and the connectivity of the pores inside the cement matrix directly lead to electrical resistance increase, it is reasonable to infer that the degree of cement hydration can be judged by testing electrical resistance of the specimens, which means that when the electrical resistance of the specimens becomes stable with age, it may be taken to indicate that the rate of hardening of cement has slowed to a negligible level. This may provide an alternative way in monitoring the cement hydration process. Traditionally the cement hydration stages were identified by the heat liberation measurement, however it was pointed out that the liberated heat content was neither simply proportional to the cement hydration degree nor to the development of physical properties (Gartner et al., 2002). Therefore the calorimetric method only provides an approximation in understanding cement hydration and leaves space for exploring more accurate ways to understand the process (Lianzhen Xiao and Zongjin Li, 2009). For the electrical resistance method, its accuracy would largely depends on the fraction of GNP, which means an optimum GNP fraction needs to be found, because if the GNP fraction is too low, conductivity of the specimen would be mainly through ionic conduction and severe polarization problem would be met, and if the GNP fraction is too high, conductive network would be too well formed and a small change in cement hydration degree would not be reflected by an significant increase in electrical resistance.

Although the cube and the prisms had similar electrical resistances in the early age, their electrical resistance stabilized at different ages as the cement hydration process went on. It can be seen in Fig.4.6 that after an age of about 16 days, the electrical resistance of the cube had reached a steady state, while those of the prisms still kept increasing until an age of about 30 days. This phenomenon can be explained with the conduction mechanism of GNP reinforced cementitious composites. It can be considered that the ionic conduction and the conduction through GNP are in parallel. If we assume that the electrical resistance through ionic conduction is R_i and the electrical resistance through GNP is R_G, the equivalent electrical resistance for the whole system would be

$$R = \frac{R_i \times R_G}{R_i + R_G} = \frac{R_G}{1 + \frac{R_G}{R_i}} \tag{4-2}$$

As cement hydration process went on, the consumption of evaporable water together with the decrease in size and connectivity of the capillary pores reduced the effect of ionic conduction, R_i. Meanwhile, the forming of cement hydration product weakened the tunneling effect and caused degradation in the GNP conductive network, which means R_G also increased with age. How fast the electrical resistance of the specimen became stable depended on how long it took for the ratio of R_G to R_i to diminish, under which condition R approached the following limit:

$$R = \frac{R_G}{1 + \frac{R_G}{R_i}} \approx \frac{R_G}{1 + 0} = R_G \tag{4-3}$$

In section 4.2.2 it has been discussed that due to the dimensional effect, there were more continuous networks in the cube than in the prism, i.e. R_G was smaller in the cube than in the prisms. Furthermore, for the same degree of cement hydration, there are more continuous networks in the cube which means that the degradation in the conductive network was less severe in the cube than in the prisms, thereby a slower increase in R_G in

the cube than in the prisms. Since the cube had a smaller R_G as well as a lower R_G increasing rate, as cement hydration went on the ratio of R_G to R_i came to the negligible level faster in the cube than in the prism, this explains why the electrical resistance of the cube became stable at an earlier age than the prisms.

In conclusion, the age of the specimens has different effects on specimens with different dimensions. The electrical resistance of the specimens should have been stable with age before they are used to perform the self-sensing property tests.

4.2.5 Effect of Temperature

The effect of temperature was investigated with the TC307 cube. It was first put into a 90℃ oven for 24 hours (Beer F. C. d. et al., 2004) to get a stable high temperature as well as to eliminate the evaporable water within the specimen to exclude the effect of moisture. After the cube was taken out from the oven, its temperature and electrical resistance were simultaneously monitored with a thermometer and a multimeter respectively. The specimen was wrapped by a layer of foil to insulate it from moisture in the environment.

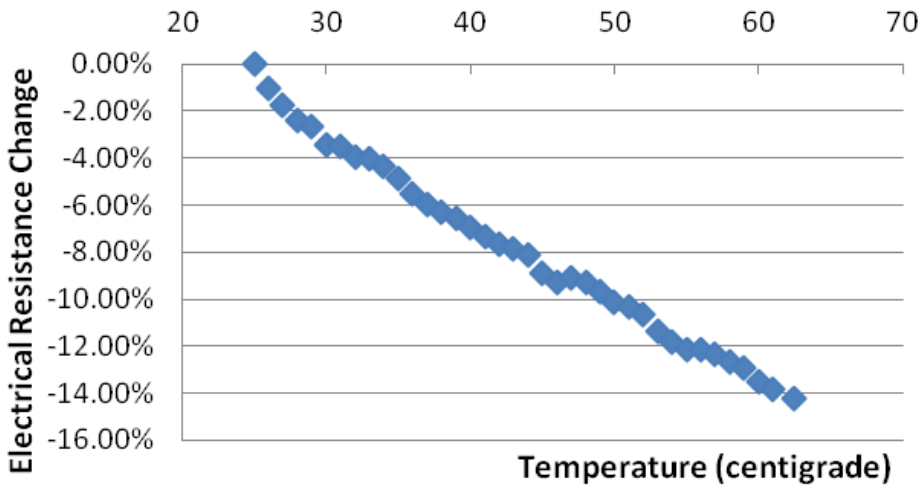

Fig. 4.7. Relation between electrical resistance change and temperature

Fig. 4.7 shows the relation between electrical resistance change and temperature for the TC307 cube. The electrical resistance change was based on the reference to the resistance value at a temperature of 25℃. It was found that the electrical resistance decreased nearly linearly as the temperature increased in the range from 25 to 62 centigrade.

There are two reasons causing the electrical resistance to decrease when temperature increases. The first involves the conducting mechanism of GNP. GNP made from graphite is composed of series of stacked parallel graphene layers. Within each layer, the carbon atom is bonded to three others with covalent (sigma) bonds, which have a high strength (524 kJ/mol). The hybridized fourth valence electron is paired with another delocalized electron of the adjacent plane by a much weaker van der Waals bond of only 7 kJ/mol (pi bond) (Hugh, 1993). The high electrical conductivity of GNP is attributed to these delocalized electrons. When temperature increases, an increasing number of electrons from the pi bonds is freed and becomes available for conduction. Also, a higher

temperature provides more energy for the tunneling effect to occur. The second reason involves the ionic conduction. High temperatures increase conductivity because the rates of diffusion for the ions increase (Hamann C. H. et al., 1998). The first reason is the dominating one since the conductive network of GNP has been formed in the specimen and electron conduction is much easier than ion conduction due to the low mass of electrons (Jingyao Cao and D. D. L. Chung, 2004).

The temperature dependence of electrical resistance for graphite is different from metals. The metallic elements have electropositive atoms that donate their valence electrons to form a "sea" of electrons surrounding the atoms. These electrons are not tightly bound to any atom and are able to move freely in the metals, resulting in their high electrical conductivity (D. R. Askeland and P. P. Phule, 2003). When the temperature of a metal increases, thermal energy causes the atoms to vibrate. At any instant, the atom may not be in its equilibrium position, and it therefore interacts with and scatters electrons. Therefore, for metals their electrical resistivity increases with increasing temperature rather than decreases.

Although there is an existing equation showing the linear relationship between electrical resistance and temperature for metals (D. R. Askeland and P. P. Phule, 2003), it cannot be used to justify the reasonableness of the linear relationship in this study since the temperature dependences of electrical resistance for GNP and metals are different. However, by referring to previous literatures, reasonableness of the linear relationship in this study can still be proved. It was reported that electrical resistivity of graphite

decreased linearly with temperature increased in the range investigated in this study (Thmas J. Horn and Amanie N. Abdelmessih, 2000; S. Mrozowski, 1951).

The linear relationship between temperature and electrical resistance under the normal temperature range means that it is easy to exclude the effect of temperature when measuring electrical resistance change. Also, after the specimen was cooled down to the room temperature, its electrical resistance was found to be almost the same as the value before heated up. This implies that the variation of temperature did not lead to variation in conductive network or structure degradation within the specimen. However, the testing results here are only validated in the temperature range of 25 to 62 centigrade. Further study is needed to study the effect of temperature over a wider range.

4.2.6 Effect of Moisture

The effect of moisture was also investigated with the TC307 cube. Besides, a plain mortar cube was also tested to serve as a control. The electric resistance of the specimens was tested for two extreme conditions, i.e. the wet and the dry conditions. The specimens were first immersed in water for 1 hour during which the electrical contacts were protected with a layer of plastic sheet to prevent damage by moisture. The specimens were then taken out of water and exposed to the air in the air-con room, with free water on their surfaces removed. Their electrical resistance versus drying time were tested and tabulated in Table 4.4. After 4 hours, the specimens were dried in the oven at 90℃ for 1 day and the final electrical resistances under dry condition were tested when they were cooled to the room temperature.

From Table 4.4, it is evident the conductivity of plain mortar could be attributed fully to its moisture content. This led to severe electric polarization, causing the electric resistance to increase rapidly even within just 5 seconds. The readings recorded for the plain mortar cube were thus only accurate to one hundred. The polarization effect was much smaller in TC307 cube since its conductivity is contributed mainly by electron conduction and tunneling effect.

Table 4.4. Electrical resistance of plain mortar versus TC307 at different drying time

Time	Electrical Resistance (Ohm)	
	Plain mortar cube	TC307 cube
0h	1000	183
1h	1800	173
2h	2000	165
3h	2000	160
4h	2000	159
24h	$>4*10^7$	163

For TC307 cube, moisture only affected the electrical resistance slightly, which is favorable for a self sensing property test where the effect of moisture is to be excluded. It confirms that conductive networks have been formed by the GNP inside the cube, and by the theory of parallel circuit, the contribution of ionic conduction can almost be negligible. Referring to previous literature (Wen S. and Chung D. D. L., 2008), for carbon fiber reinforced cement with a fiber fraction below the percolation threshold, its electrical resistance increases when the moisture is lost. However, the results for TC307 cube in this study show that as the moisture was lost, electrical resistance of TC307 cube

showed a slight decreasing trend. Therefore it is concluded that the GNP fraction in this cube has gone beyond the percolation threshold. The presence of moisture weakens the contact between GNP particles, resulting in decrease in the conductivity of the specimen.

CHAPTER 5 SELF DAMAGE MEMORIZING PROPERTIES OF GNP REINFORCED MORTAR

In this chapter, the smart material property of the GNP reinforced mortar, which is its ability to respond to internal damage, is exploited. Section 5.1 is a study on the electrical resistance change when a major crack occurs and develops at its central plane. Section 5.2 is a study on the correlations between the electrical resistance behavior and mechanical behavior for the specimens under uniaxial compression. In both sections, experimental results will be reported and discussions will be made.

5.1 Studies on Self Crack Memorizing Property

5.1.1 Experimental Program

Due to the low tensile strength and brittleness of concrete, cracks can happen easily in concrete structures. Although they usually do not affect the loading capacity of the members, they can lead to corrosion and durability problem; and also, decrease in stiffness may occur. Therefore, it is important to monitor the crack growth in concrete members. It is expected that electrical resistance change of GNP reinforced mortar is responsive to the growth of a traction-free crack and thus can be used to monitor the crack growth and estimate the crack length. To investigate this, experimental tests were carried out in this study, for the simplest crack situation that contains a major crack, which initiates and propagates at the central plane of the specimens. In real structures, a

major crack can be found in members such as concrete pavements or concrete beams under a flexure load.

The test was performed with the TC307 cube and a 3775 prism outside the air-con room where the environment conditions could change. The two specimens were selected as they represent specimens with different aspect ratios. The different types of GNP would not affect the relation between electrical resistance change and growth of crack since when the other factors keep unchanged; the shape of the current streamlines in a specimen only depends on its geometry. In these tests, for each specimen, a major crack was created by sawing it at the central plane perpendicular to the longitudinal direction, as shown in Fig. 5.1. For each crack depth, the corresponding electrical resistance of the specimen was recorded.

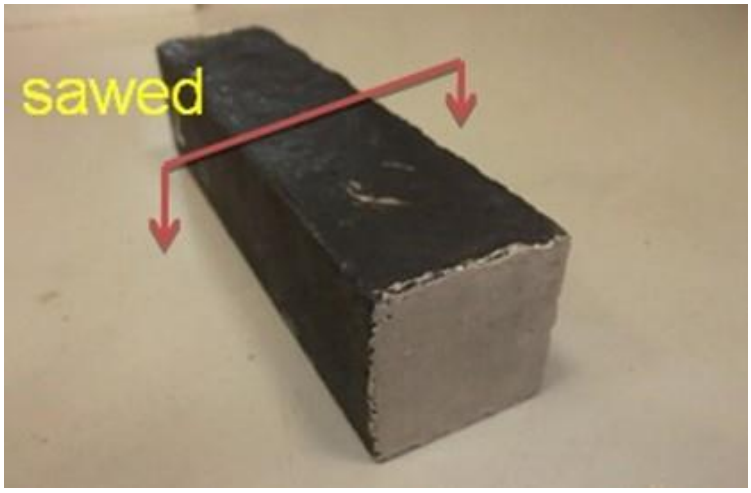

Fig.5.1. Illustration of self crack memorizing property test

5.1.2 Testing Results and Discussion

Fig. 5.3 shows the relations between electrical resistance change and relative crack depth for both the TC307 cube and the 3775 prism. The electrical resistance change was calculated with respect to electrical resistance before the test, that is, when the crack depth was 0. Relative crack depth (d/D) is defined as the ratio of the absolute crack depth (d in Fig. 5.2) to the overall height of the specimen (D in Fig. 5.2).

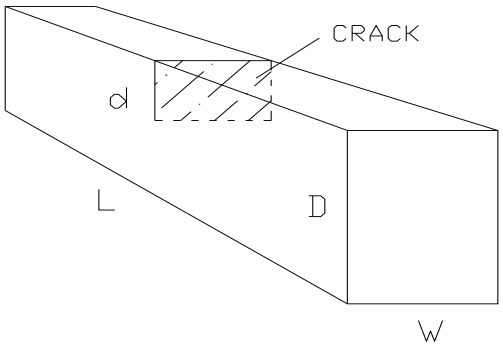

Fig.5.2. Specimen dimensions for self crack memorizing property test

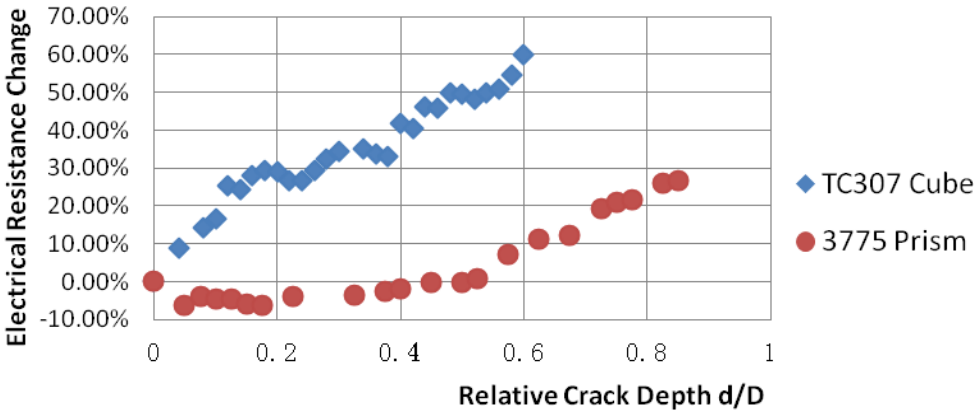

Fig.5.3. Relation between electrical resistance change and crack depth

It is found in Fig. 5.3 that for both the specimens, electrical resistance increased as the crack depth became larger. The principle is quite simple: in the crack plane it comprises of an uncracked area where the matrix is intact and an empty zone representing the crack. In the empty zone, there is no means of electrical conduction across the crack. Therefore the electric field in a cracked specimen with a current flowing through it is a function of the specimen geometry, and in particular the crack depth. For a constant voltage drop, the current across the crack plane will decrease with increasing crack size due to modification of the electrical field and associated perturbation of the current streamlines. Therefore an increase in the crack depth should logically increase the overall electrical resistance.

For the TC307 cube, the electrical resistance increased nearly linearly as the relative crack depth d/D increased up to a value of 0.6, and when the relative crack depth reached 0.6, the electrical resistance change was as large as 60%. The linear behavior is consistent with the test results for carbon fiber reinforced cement composite specimens under compact tension tests (Reza F. et al., 2004), where the specimens also developed a major crack at the central plane as the tests went on due to an initial notch that was prepared before the compact tension test. It is also noted that for the TC307 cube and those specimens in literature, they had similar aspect ratios, i.e. the ratio of the longitudinal dimension between the two electrical contacts to the height of the specimen (L/D) was close to 1. For the 3775 prism, it was observed that initially the electrical resistance decreased a bit, which is an abnormal phenomenon. This might be caused by the change in the environment conditions such as temperature and moisture since the test could not

be operated inside the air-con room. However, it still confirms that a small relative crack depth does not cause obvious change in electrical resistance for this prism. The electrical resistance changed only slightly until d/D is larger than 0.4, after which it also began to show significant increase with d/D developed. When d/D reached 0.85, the electrical resistance increase was about 30%.

Comparing the performances of the TC307 cube and the 3775 prism, it can be found that for the same relative crack depth d/D, the electrical resistance change for the TC307 cube was always more significant than the change for the 3775 prism. This is believed to be due to their different aspect ratios. Although these two specimens also have different widths (W in Fig. 5.2), the width of the specimen is not expected to affect the extent of electrical resistance change, since the crack had cut along the whole width of the specimen and only a plane perpendicular to the crack can represent its behavior. In other words, when analyzing the extent of electrical resistance change for the specimen, it can be simplified to be a 2D problem.

To explain the effect of the aspect ratio L/D of the specimen on the extent of electrical resistance change, the migration paths of the conducting particles and equivalently the geometry of the current streamlines can be used. For the TC307 cube, its aspect ratio is 1; while for the 3775 prism, its aspect ratio is 4. Before a crack occurs in the specimen, it can be assumed that all the conducting particles can migrate along straight lines so the current streamlines are all parallel to the bottom of the specimen (see Fig.5.4 (a)). When a crack with a certain relative crack depth d/D appears in the specimen, it blocks the

migration of some of the conducting particles and diverts their migration paths, leading to the change in the geometry of the current streamline (see Fig.5.4 (b)). It is obvious that for a certain specimen, the extent of the change in the geometry of the current streamlines depends on the angle **a** as shown in Fig.5.4 (b). For the specimen with a smaller aspect ratio, it has a larger **a** for the same relative crack depth and therefore has a larger change in the geometry of the current streamlines, resulting in a higher extent of electrical resistance change as compared to the specimen with a larger aspect ratio.

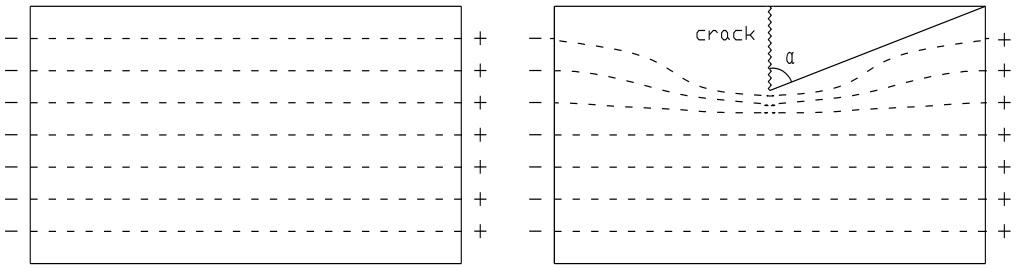

(a) Before a crack (b) After a crack

Fig.5.4. Geometry of current streamlines before and after a crack

There is also a hypothesis that a crack only disturbs the current streamlines in its vicinity, which means it only affects the geometry of the streamlines up to a certain distance along the longitudinal direction, shown as the critical length in Fig. 5.5. Therefore for a specimen with a large aspect ratio, a small d/D can only cause change in the geometry of the current streamlines within the critical length and judging from an overall view, this change is insignificant; while for a specimen with a small aspect ratio, even a small d/D can cause perturbation of current streamlines beyond its overall length. This explains why for the 3775 prism, there was only little electrical resistance change when the d/D was

small; while for the TC307 cube, the electrical resistance increase was significant once the crack initiated. All the discussions above indicate that a specimen with a smaller aspect ratio has a better self crack sensing ability than a specimen with a larger aspect ratio.

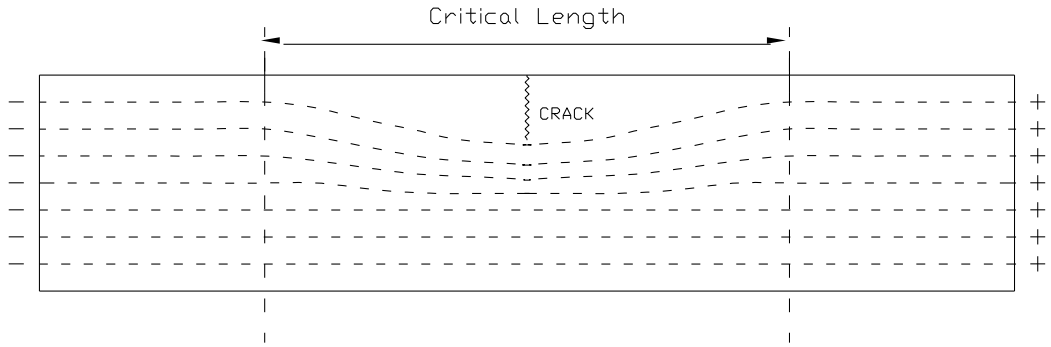

Fig.5.5. Current streamlines affected by a crack with the critical length

5.1.3 Comparison of Existing Models for Studying Crack Growth

Base on theory, a model describing the relation between electrical resistance change ΔR and crack growth d/D for a specimen should satisfy the following two boundary conditions:

(1) For the initial condition, i.e. when d/D = 0, ΔR = 0;

(2) For the final condition, i.e. when d/D = 1, ΔR = + ∞.

Here $\Delta R = \frac{R - R_0}{R_0}$, where R is the electrical resistance according to a certain crack depth, and R_0 is the original electrical resistance of the specimen. These two conditions also indicate that the model is nonlinear for the overall range of d/D.

Furthermore, based on the test results in this study and literatures, and also discussions in section 5.1.2, the model should also reflect the following features:

(1) The effect of the aspect ratio of the specimen should be reflected, i.e. under the same d/D, the electrical resistance change for a specimen with a smaller d/D should always be more significant than the electrical resistance change for a specimen with a larger d/D;

(2) Although for the whole range of d/D, the model is not linear, judging from the test results in this study and previous literatures (Li C.-Y. and Wei R. P., 1966; Reza F. et al., 2004), for specimens with small aspect ratios (approximately 1 or less), the electrical resistance changes nearly linearly with the d/D increases in the small range (0 ~ approximately 0.5). It is preferable that the model can also capture this feature.

Two existing models from previous literatures will be presented here and their fitness to the test results in this study will be discussed. Both of these two models were derived from studies on metal specimens. The first model (Reza F. et al., 2004) has the form of

$$R = \frac{d - d_0}{d_f - d_0}(R_f - R_0) + R_0 \tag{5-1}$$

where d_0 is the initial crack depth, d_f is the final crack depth and R_f is the final measured electrical resistance. In this study, the initial crack depth was 0, therefore equation (5-1) becomes

$$R = \frac{d}{d_f}(R_f - R_0) + R_0 \tag{5-2}$$

The second model has a closed form equation derived by Johnson (Johnson H. H., 1965) and appeared in ASTM E647 for compact tension geometry:

$$R = \cosh^{-1}\left[\frac{\cosh(\frac{\pi}{d}\times\frac{L}{2})}{\cos(\frac{\pi}{2}\times\frac{d}{D})}\right] \Big/ \cosh^{-1}\left[\frac{\cosh(\frac{\pi}{d}\times\frac{L}{2})}{\cos(\frac{\pi}{d}\times\frac{d_0}{2})}\right] \tag{5-3}$$

In this study $d_0 = 0$, therefore equation (5-3) becomes

$$R = \cosh^{-1}\left[\frac{\cosh(\frac{\pi}{d}\times\frac{L}{2})}{\cos(\frac{\pi}{2}\times\frac{d}{D})}\right] \Big/ (\frac{\pi}{d}\times\frac{L}{2}) \tag{5-4}$$

Fig. 5.6 and Fig. 5.7 show comparisons between the test results in this study and the models expressed with equation (5-2) and equation (5-4). Equation (5-2) fits the test results of TC307 cube well because it has a linear form. However, its linear form also makes it fit poorly with the test results for 3775 prism. This means that the first model presented with equation (5-2) has failed in reflecting the effect of the aspect ratio of the specimen. Its disadvantages also lie in that it cannot reflect the overall non-linear behavior of the specimens under a crack, and cannot satisfy the final boundary condition, which is the electrical resistance becomes infinite when the crack cut through the overall depth of the specimen. Therefore, this model is only applicable for studying specimens with small aspect ratios under small d/D.

The second model expressed with equation (5-4) has an opposite performance to the first model. It fits well with the test results for the 3775 prism while underestimates the results for the TC307 cube. This also indicates its failure in applicable to specimens with

different aspect ratios although the term d/D is included in equation (5-4). The model fits the test results of the TC307 cube poorly mainly because it is derived from only the test results for specimens with large aspect ratios. Besides, its disadvantages also lie in its complex equation and that it is derived from the test results provided under 4-probe method, which is different from the 2-probe method in this study. Therefore, although this model satisfies the boundary conditions and reflects the non-linearity of the test results, it is not a satisfactory model for all the specimens.

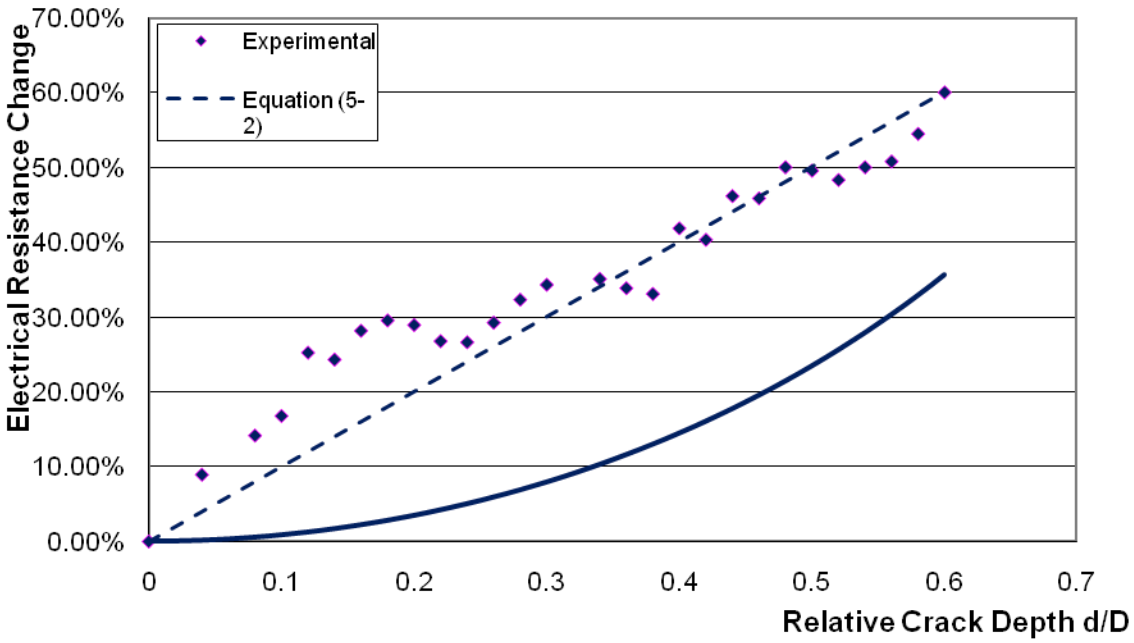

Fig.5.6. Comparison between test results and models for TC307 cube

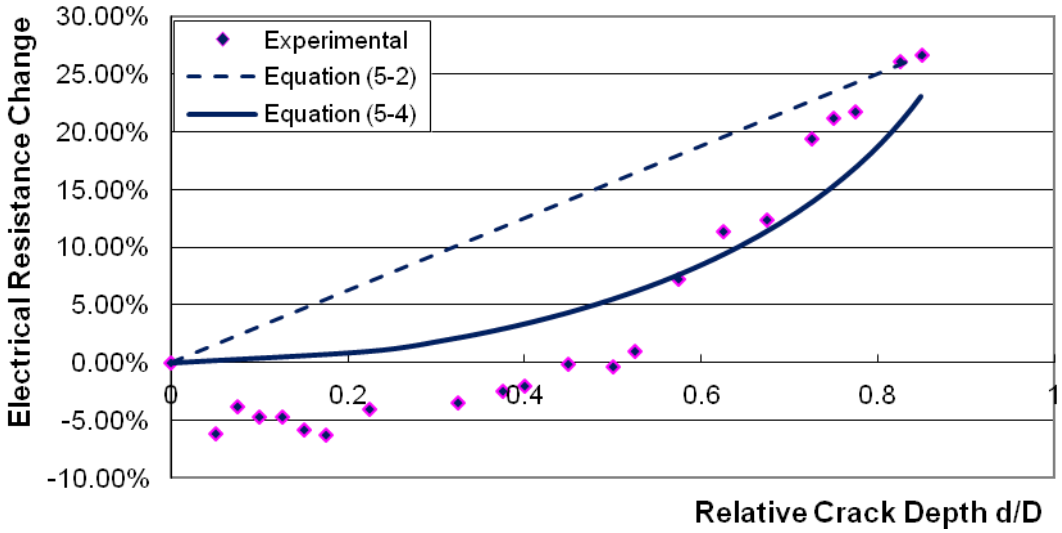

Fig.5.7. Comparison between test results and models for the 3775 prism

5.1.4 Proposed Model for Studying Crack Growth

Based on the law of electrical resistance, a preliminary model is proposed to simulate the relation between electrical resistance R and relative crack depth d/D. A function f(d/D) is introduced to modify the electrical resistance calculated with residual cross section area A_r when a crack occurs:

$$R = f\left(\frac{d}{D}\right) \times \frac{\rho L}{A_r} = f\left(\frac{d}{D}\right) \times \frac{\rho L}{(D-d)W} \tag{5-5}$$

where ρ is the resistivity when d = 0.

For 3775 prism, the curve of f(d/D) versus d/D plotted with experimental data was found to be nearly a straight line, with the intercept equals to 1, as shown in Fig. 5.8. f(d/D) is therefore expressed with a linear equation as

$$f\left(\frac{d}{D}\right) = k\frac{d}{D} + 1 \tag{5-6}$$

For each specimen, k is a constant got from linear regression of the experiment data with the intercept set to be 1 to satisfy the initial boundary condition, therefore k varies for different specimens. By substitute the relationship in equation (5-6) into equation (5-5), R can be further expressed as

$$R = f\left(\frac{d}{D}\right)\times\frac{\rho L}{A_r} = f\left(\frac{d}{D}\right)\times\frac{\rho L}{(D-d)W} = \frac{\rho L}{(D-d)W}\left[k\frac{d}{D}+1\right] \tag{5-7}$$

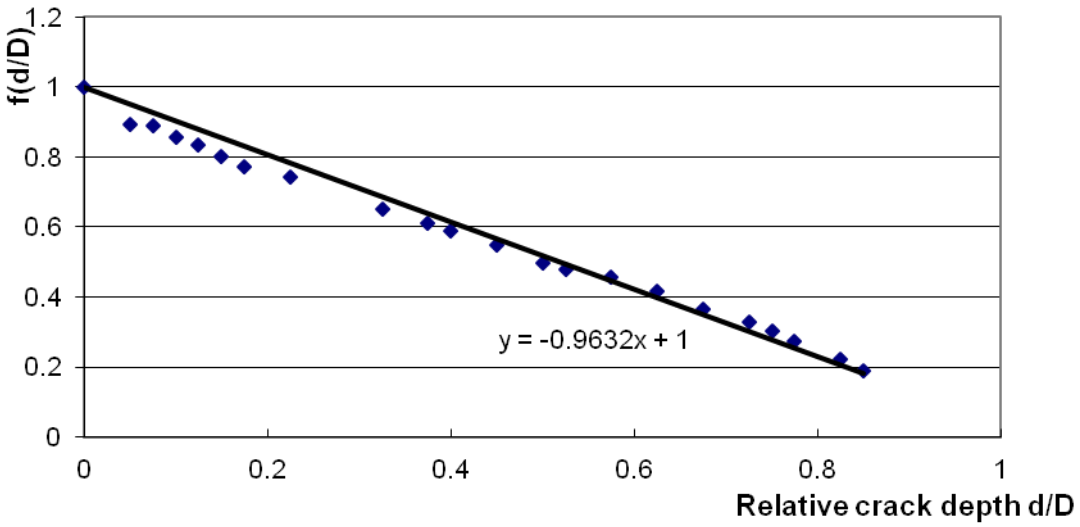

Fig.5.8. Relation between f(d/D) and d/D for 3775 prism

However, when f(d/D) versus d/D was plotted for the TC307 cube, which is shown in Fig. 5.9, the curve was found to be non-linear in the small range of d/D. This again confirms that specimens with different aspect ratios behave differently in the small d/D value range. According to the critical length hypothesis in section 5.1.2, it is reasonable to infer that corresponding to the critical length there exists a critical aspect ratio, below which the curve of f(d/D) versus d/D shows nonlinearity with an ascending part occurs first in the

small d/D range and then followed by a descending part, and beyond which the ascending part disappears and the whole curve becomes close to a descending straight line. This is consistent with the conclusion that a specimen with a smaller aspect ratio is more sensitive to a small crack, because when under the same d/D a specimen with a smaller aspect ratio will have a larger f(d/D) and therefore a higher electrical resistance increase as calculated by Equation (5-5). The curve of f(d/D) versus d/D for a specimen with a small aspect ratio is therefore expected to be divided into two segments, with each of the segment simulated by an individual expression. By looking at the curve in Fig. 5.9 and taking convenience into consideration, the dividing point for the two segments can be set to be the point at the end of the ascending part of the curve. Crack depth d at this point is represented as $d_{1\text{-}2}$. Obviously the second segment can be simulated with a linear equation in the form of

$$f\left(\frac{d}{D}\right) = a\frac{d}{D} + b \text{, when } d > d_{1\text{-}2}; \tag{5-8}$$

where a and b are the constants got from linear regression of the experiment data for the second segment.

For the first segment, although judging from the curve it can be found that a linear function will also fit the experimental data well, it is preferable that a 2nd order function is used because the linear increase of electrical resistance versus d/D in the small d/D range as shown in Figure 5.11 can be reflected. Through calculation it can be found that when f(d/D) has the form of

$$f\left(\frac{d}{D}\right) = \left(k_1\frac{d}{D} + 1\right)\left(1 - \frac{d}{D}\right) \tag{5-9}$$

the electrical resistance of the specimen will increase linearly as the d/D increases if k_1 is a constant, i.e.

$$\frac{R_2 - R_1}{\frac{d_1}{D} - \frac{d_2}{D}} = \frac{f\left(\frac{d_2}{D}\right) \times \frac{\rho L}{(D - d_2)W} - f\left(\frac{d_1}{D}\right) \times \frac{\rho L}{(D - d_1)W}}{\frac{d_1}{D} - \frac{d_2}{D}} = \frac{k_1 \rho L}{DW} \qquad (5\text{-}10)$$

Therefore, for the first segment of the curve of f(d/D) versus d/D, it is simulated with equation (5-9) to achieve the linearity. The constant k_1 is determined by substituting the point value at $d=d_{1\text{-}2}$into equation (5-9), through which the continuity between the first segment and the second segment is achieved.

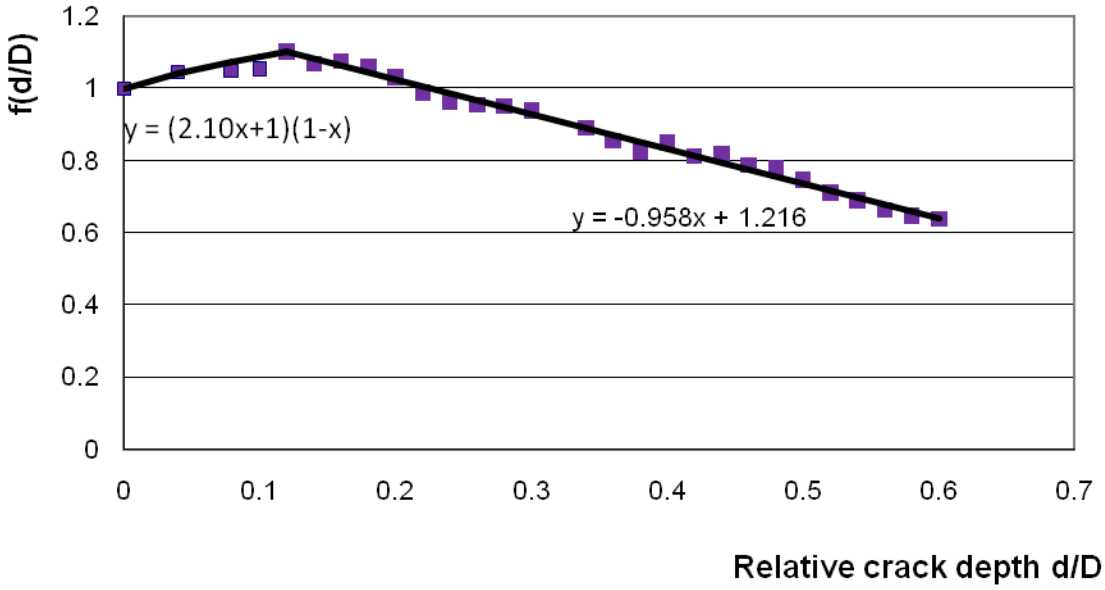

Fig.5.9. Relation between f(d/D) and d/D for 3775 prism

In conclusion, for a specimen that has a large aspect ratio and the curve of f(d/D) versus d/D displays linearity for the whole d/D range, the relation between electrical resistance

and relative crack depth can be expressed as

$$R = f\left(\frac{d}{D}\right)\times\frac{\rho L}{A_r} = f\left(\frac{d}{D}\right)\times\frac{\rho L}{(D-d)W} = \frac{\rho L}{(D-d)W}\left[k\frac{d}{D}+1\right] \qquad (5\text{-}7)$$

For a specimen with a small aspect ratio for which the curve of f(d/D) versus d/D shows non-linearity, the relation between electrical resistance and relative crack depth can be expressed as

$$R = f\left(\frac{d}{D}\right)\times\frac{\rho L}{(D-d)W} = \left(k_1\frac{d}{D}+1\right)\left(1-\frac{d}{D}\right)\times\frac{\rho L}{(D-d)W}, \text{ when } 0 \le d < d_{1\text{-}2}; \quad (5\text{-}12)$$

$$R = f\left(\frac{d}{D}\right)\times\frac{\rho L}{(D-d)W} = \left(a\frac{d}{D}+b\right)\times\frac{\rho L}{(D-d)W}, \text{ when } d_{1\text{-}2} \le d \le D; \qquad (5\text{-}13)$$

For the 3775 prism and the TC307 cube, the constants in their models have been shown in Fig 5.8 and Fig. 5.9 respectively. The comparisons between the experimental data and the proposed model are shown in Fig. 5.10 for 3775 prism and in Fig. 5.11 for TC307 cube, where satisfactory agreements can be found.

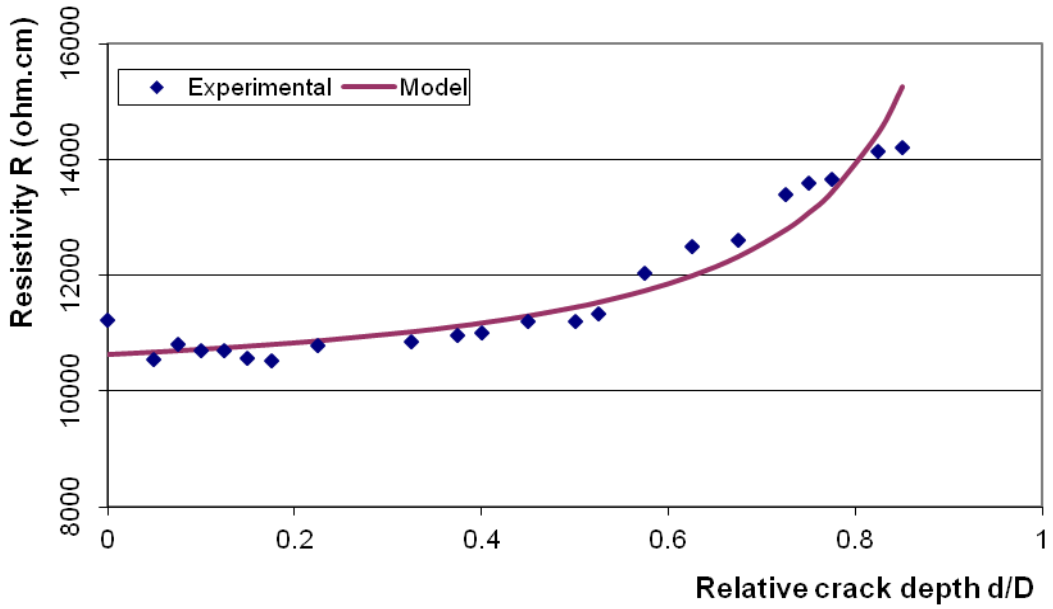

Fig.5.10. Comparison between experimental data and proposed model for 3775 prism

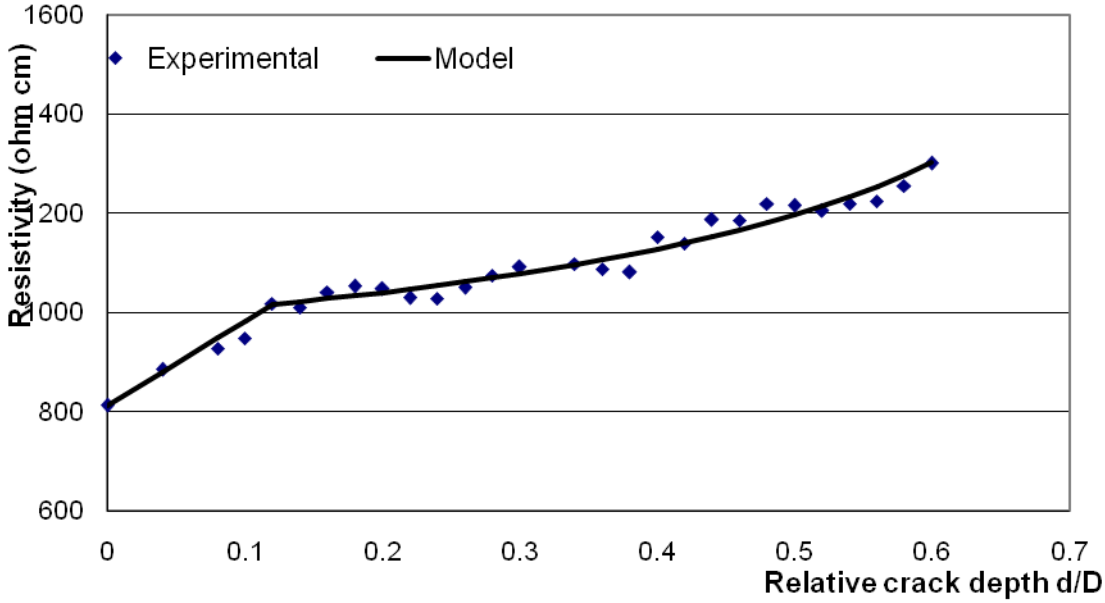

Fig.5.11. Comparison between experimental data and proposed model for TC307 cube

The model proposed in this study is reasonable because (1) when d=0, it goes back to the formula for the law of electrical resistance, and when d/D approaches 1, R tends to be infinity, which mean it satisfies the two boundary conditions; (2) the f(d/D) reflects the effect of the aspect ratio of the specimen. A specimen with a smaller aspect ratio has a larger f(d/D) according to the same d/D and therefore has more significant electrical resistance increase when compared to a specimen with a larger aspect ratio. Besides, the linear relation between R and d/D in the small d/D range is also reflected for specimens with small aspect ratios. However, due to the brittleness of the material, fracture of the specimen easily occurred when d/D approaches 1 due to the sawing process to generate the artificial crack. Therefore the test results in the range of d/D close to 1 were not obtained in this study and future research is needed to assess and improve the proposed model.

5.2 Study on Self Damage Memorizing Property under Compression

5.2.1 Experimental Program

Compressive strength of concrete is so much greater than its tensile strength, therefore compressive strength is widely considered to be the most important property of concrete; and concrete is used primarily in a compressive mode. In this study, experimental tests were also carried out to investigate the self damage memorizing property of GNP reinforced mortar under compression.

The tests were performed to study how electrical resistance changes with the

development of compressive damage. 3775 cube and one half part of 3775 prism obtained after self crack memorizing property test in the last section were used in this test. All the specimens were tested under uniaxial compression, during which their two opposite surfaces in the longitudinal direction directly contacted the platen of the testing machine and were directly under compression. To avoid damage of the electrical contacts during the tests, the electrical contacts were designed in the form of a “peripheral strip”, as shown in Fig. 5.12.

During testing, the compression force was applied by the Instron machine (see Fig. 2.9) at a loading rate of 20N/s for the 3775 cube and by the servo-hydraulic testing machine (see Fig. 2.8) at a loading rate of 800 N/s for the 3775 half prism. The different loading rates were used in order to assess whether the electrical resistance change can reflect the effect of loading rate since it is well known that crack growth is a time-dependent nature relative to the loading rate (Mindess S. et al., 2003).The compression force was applied by repeated steps, which is like incremental cyclic compression, with each step went to a higher stress level of around 5MPa more than the former step, and finally came to compressive failure of the specimen. After each step, the compressive force was removed, the stress of the specimen came back to 0 and the electrical resistance of the specimens was measured under the 0 stress state. At the beginning of each step, the compressive force was reapplied from the 0 stress condition. For the half prism, its sawed surface was rough, therefore before testing the dental stone was pasted on the sawed surface to make it flat, allowing the compressive stress to be uniformly applied to the specimen.

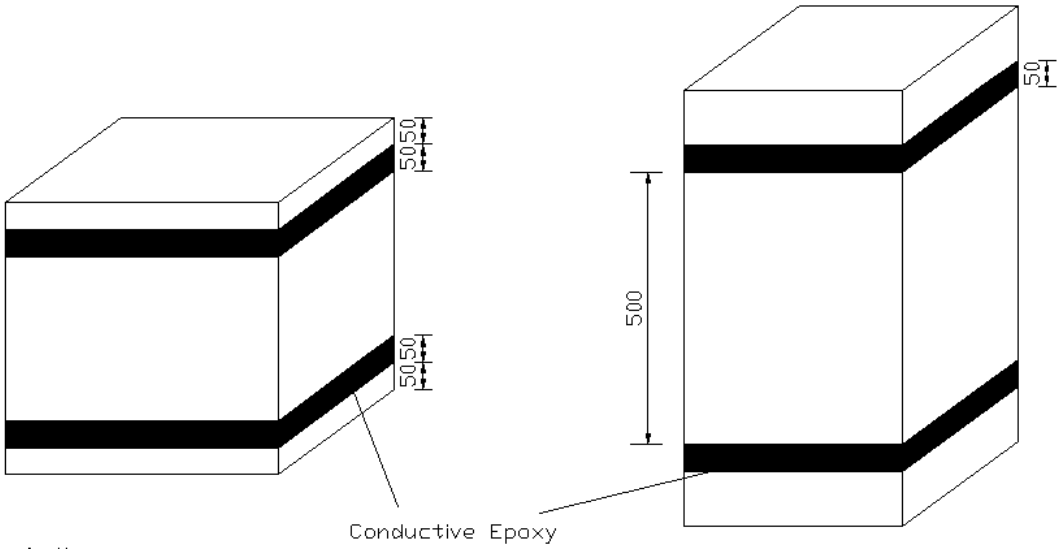

Fig.5.12. Specimens for self damage memorizing property test

5.2.2 Discussions on the Form of Electrical Contacts

For the specimens under compression, their electrical contacts were in the "peripheral strip" form to avoid direct contact with the testing machine and being destroyed. Actually, this form of electrical contacts also helps to increase the sensitivity of the specimen to its internal damage under uniaxial compression, which can be illustrated as follows.

If we neglect the friction between the platens of the testing machine and the specimen ends, which means the ends of the specimen are not restrained from lateral expansion and thus are free to move, when under uniaxial compression, the secondary tensile stress induced in the specimen will be at right angles to the axis of the specimen, causing a splitting failure in which all the cracks are parallel to the axis of the compressive force (see Fig. 5.13).

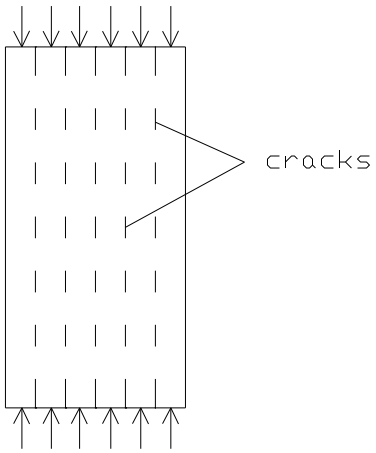

Fig.5.13. Splitting failure under uniaxial compression

When electrical contacts of the specimen are in the form as shown in Fig. 2.11 that conductive epoxy is painted to the whole area of the two end surfaces, the equivalent circuit for electrical resistance measurement can be modeled as in Fig. 5.14. In this situation, since the electrical contacts have covered the whole area of the two end surfaces, the current can go directly along straight lines from one electrical contact to the other. Therefore the specimen can be modeled as a series of resistance in parallel, i.e. the specimen is equivalent to *n* layers that are stacked in the thickness direction, and each resistance represents one layer of the specimen. According to this model, when the specimen has suffered splitting failure, the cracks are in the longitudinal direction that is parallel to the direction of each branch circuit; therefore none of these branch circuits is cut off and by theory the electrical resistance of the specimen will remain unchanged.

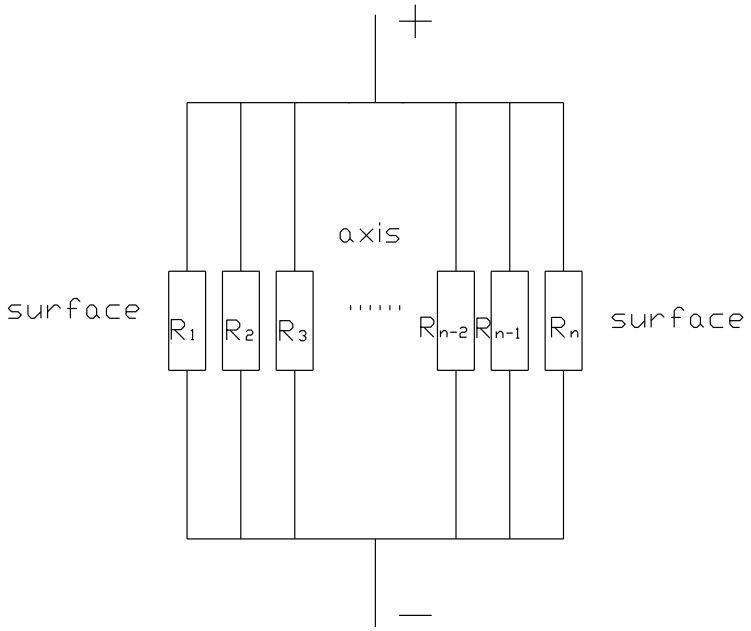

Fig.5.14. Equivalent circuit for electrical resistance measurement when electrical contacts are at the two end surfaces of the specimen

On the other hand, when electrical contacts of the specimen are in the "peripheral strip" form as shown in Fig.5.12, the current will need to penetrate into the specimen in the through-thickness direction to go from one electrical contact to the other. In this situation, the equivalent electrical circuit will consist of a series of longitudinal resistance (R_{li}) and a series of through-thickness resistance (R_{ti}), as shown in Fig. 5.15. The specimen is divided into n peripheral layers with the first layer surrounding the surface and the n^{th} surrounding the longitudinal axis. Each layer is represented by a longitudinal resistance R_l and the contact resistance between two layers is represented by through-thickness resistance R_{ti} and R_{ti}'. When splitting failure happens, the cracks along the longitudinal direction are able to cut off the branch circuits that are in the through-thickness direction and therefore, increase in electrical resistance of the specimen will be observed.

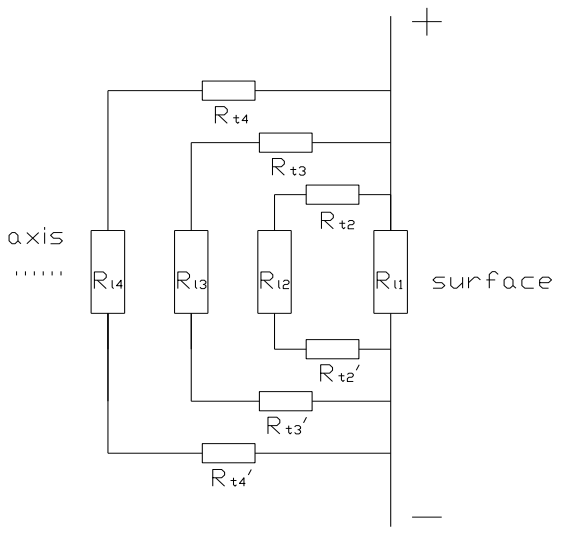

Fig.5.15. Equivalent circuit for electrical resistance measurement when electrical contacts are in the “peripheral strip” form

These two equivalent circuits explain why electrical contacts in the “peripheral strip” form are more sensitive to the internal damage for specimens under uniaxial compression. In short, under an ideal condition, the cracks propagate in the longitudinal direction, therefore do not interrupt the current streamlines when electrical contacts are set at the two end surfaces; but they will block and divert the current streamlines when the electrical contacts are in the “peripheral strip” form, leading to electrical resistance increase. However, in a real test, the specimen is not under pure compression due to the friction between the platen of the testing machine and the surface of the specimen, also, the pre-existing pores inside the specimen cause stress concentration which also affects direction of the cracks, therefore increase in electrical resistance can also be observed even when the electrical contacts are at the two ends of the specimen.

5.2.3 Testing Results and Discussions for 3775 Cube

Fig. 5.16 shows the test result for 3775 cube, the test results for Carbon Fiber Reinforced Cement Composites (CFRC) (Chen B. and Liu J., 2007) is also shown for comparison. For 3775 cube, as discussed in Section 5.2.1, the compressive load was applied by repeated steps and the load was removed after each step for the electrical resistance to be measured under 0 stress state, so the electrical resistance measured after each step reflected the damage inside the specimen with a monotone incremental compressive load history. On the other hand, the curve for CFRC is a real-time sensing curve for which electrical resistance of the specimen was continuously measured with the compressive load gradually increased to its maximum. The electrical resistance change was calculated with respect to the original value at the start of the test. The load values were normalized with respect to the peak load.

It can be found in Fig. 5.16(a) that the curve of electrical resistance change for 3775 cube obviously shows two stages: there is little to no observable increase in electrical resistance before normalized load goes to 0.5, and after that, electrical resistance started to increase with the rate of increase becoming larger. This is because under the low compressive load levels, the specimen behaved almost elastically, its deformation was largely reversible and there was little additional damage occurred inside it. The test of CFRC also showed consistent results. As can be seen in Fig. 5.16(b), the first stage in the curve for CFRC also stopped at a normalized compressive load level of around 0.5, with the electrical resistance decreased almost linearly mainly due to the “push-in” effect of the carbon fibers and the strengthened tunneling effect with smaller distance between

carbon fibers.

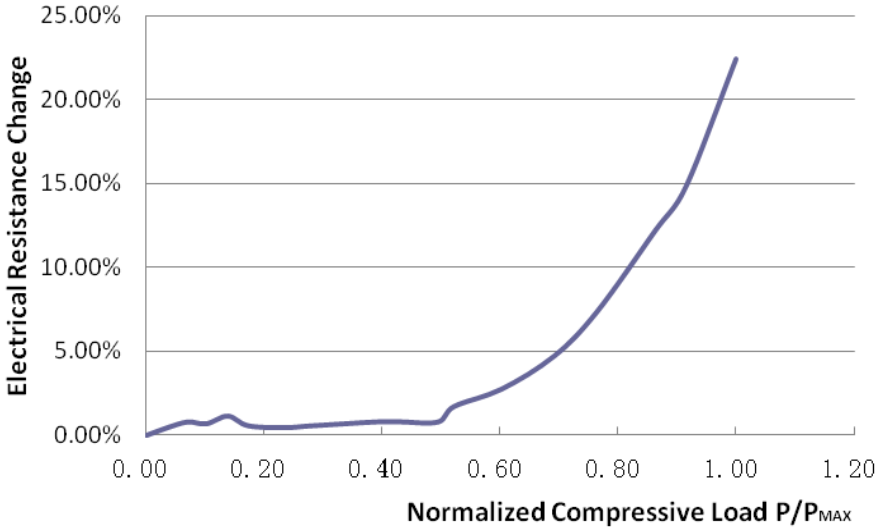

(a) Testing results for 3775 cube

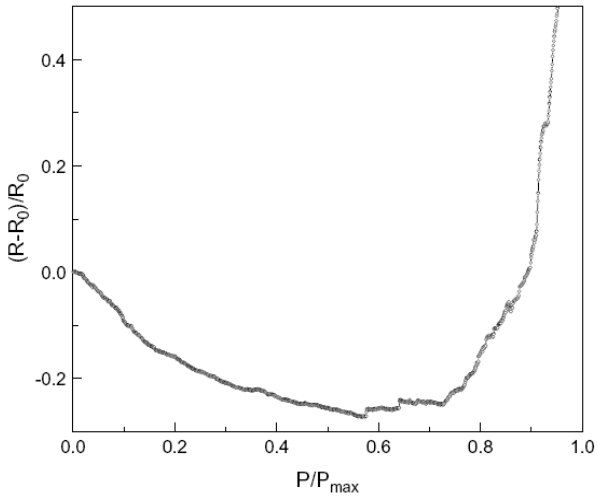

(b) Testing results for CFRC (Chen B. and Liu J., 2007)

Fig. 5.16 Electrical resistance change versus compressive load for (a) mortar cube reinforced with GNP of 3775; (b) CFRC

However, the damage memorizing testing method showed its advantages over the real-time testing method at the later stages. When the curve for CFRC showed a plateu around normalized load level of 0.5-0.7, the curve for 3775 cube showed a gradual increase in electrical resistance, which means the 3775 cube could capture the development of internal damage at an earlier stage than the CFRC specimen. This is because for CFRC, the development of internal damage interacts with the "push-in" and the strengthened tunneling effect of carbon fibers, and whether the electrical resistance will increase or decrease depends on which effect plays the more important role. However, for the 3775 cube, its electrical resistance was tested under the 0 stress condition when the external force had been removed, which allowed its strain to reverse in a greatest extent; this excludes the "push-in" effect and strengthened tunneling effect due to the absence of the external force and accelerates the internal damage to be dominant in controlling the electrical resistance change.

As the load level continued to increase and the specimen started to fail, there was a sharp increase in the electrical resistance. It can be seen that electrical resistance of CFRC had tended to infinity when the normalized compressive load level was just around 0.9, while increase of electrical resistance for 3775 cube could be captured until the maximum load, indicating that the 3775 cube could monitor the damage development during the whole ascending part of the compressive load while the CFRC specimen could not. This is because in the CFRC specimen, fraction of carbon fiber was lower than the percolation threshold; its conducting mechanism was dominated by the tunneling effect that can be easily broken down by internal cracks. On the other hand, the GNP fraction in 3775 cube

was higher than its percolation threshold, conductive network had been well formed inside the specimen and therefore conductivity could still remain even when the damage grew to a large extent. The comparison between 3775 cube and CFRC specimen verifies the ability of GNP reinforced mortar to monitor the development of its internal damage, and also shows the advantages of the damage memorizing method over the real-time damage sensing method.

The reasonableness of the test results can also be confirmed when compared to the studies on development of microcracking by researchers from the Cornell University (Mehta, P., and Monteiro, P.J.M., 2006). In regard to the relationship between stress level (expressed as percent of the ultimate load) and microcracking in concrete, Fig.5.17 shows that concrete behavior can be divided into four stages. Under normal atmospheric exposure conditions when a concrete element is subjected to drying or thermal shrinkage effects, due to the differences in their elastic modulus differential strains are set up between the matrix and the aggregate, causing cracks in the interfacial transition zone. Therefore, even before the application of an external load, micro cracks already exist in the interfacial transition zone between the matrix and the aggregate. Below about 30 percent of the ultimate load, the interfacial transition zone cracks remain stable. This is Stage 1 in Fig.5.17. It is consistent with the results of this study shown in Fig.5.16 (a), where no increase in electrical resistance in the load level range of 0%-30% ultimate load was observed, meaning negligible microcracking development at this stage.

Above 30 percent of the ultimate load, with increasing stress, the interfacial transition

zone micro cracks begin to increase in length, width and number. However, until about 50 percent of the ultimate stress, a stable system of microcracking appears to exist in the interfacial transition zone. This is Stage 2 and at this stage the matrix cracking is negligible. Judging from the curve in Fig 5.16(a), in the load level range of 30%-50% ultimate load, there is still no significant electrical resistance increase can be observed, which means that the material is not sensitive to the cracking development at this stage. This is because that the microcracking development at this stage mainly occurs at the interfacial transition zone and little cracking develops in the matrix. The cracking development in the interfacial transition zone has little effect on disturbing the continuity of the GNP conductive networks and therefore does not lead to significant increase in electrical resistance. This indicates that there is still some space to improve the sensitivity of the nanocomposites to its early development of micro cracks. Optimizing the composition of the nanocomposites and thus to strengthen the interfacial transition zone might be one of the method.

At 50 to 60 percent of the ultimate load, cracks begin to form in the matrix. With further increase in stress level up to about 75 percent of the ultimate load, not only does the crack system in the interfacial transition zone become unstable but also the proliferation and propagation of cracks in the matrix increases. This is Stage 3. Above 75percent of the ultimate load, with increasing stress very high strains are developed, indicating that the crack system is becoming continuous due to the rapid propagation of cracks in both the matrix and the interfacial transition zone. This is the final stage (Stage 4). Cracking development in both Stage 3 and Stage 4 are well reflected in Fig.5.16 (a). It can be seen

that electrical resistance begins to show significant increase in the load level range of 50-75% ultimate load, and after load level of 75% it shows sharp increase that indicates rapid crack propagation.

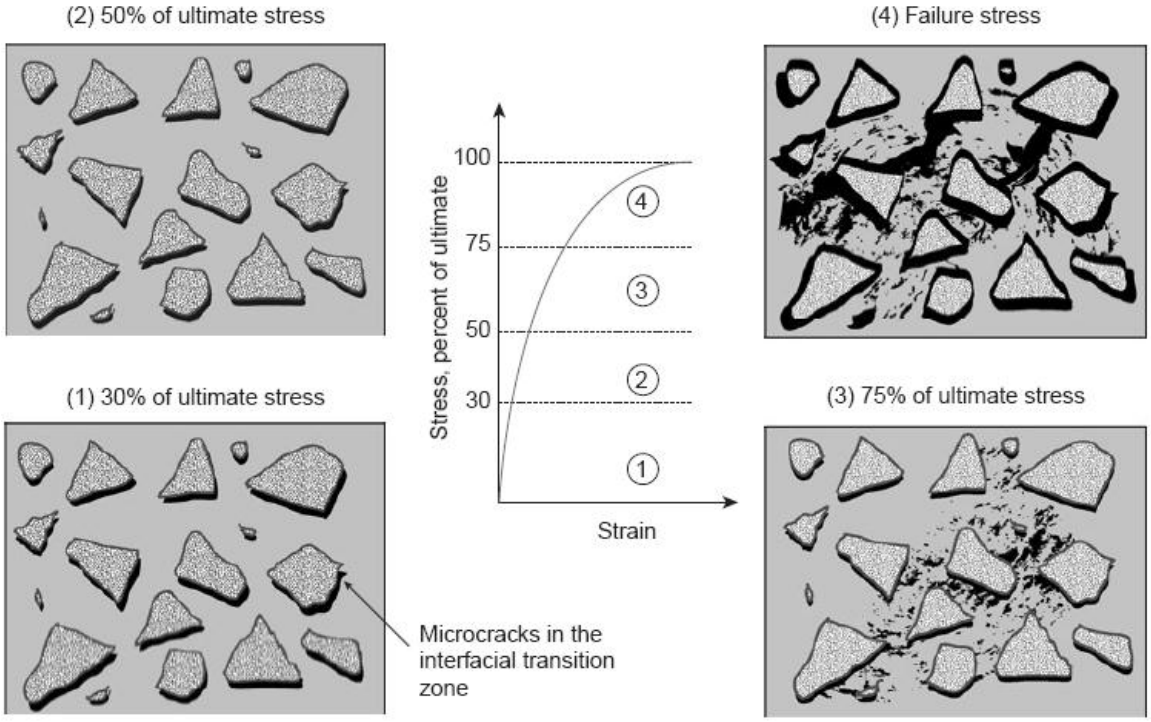

Fig.5.17. Diagrammatic representation of the stress-strain behavior of concrete under uniaxial compression. The progress of internal microcracking in concrete goes through various stages, which depend on the level of applied stress. (Mehta, P., and Monteiro, P.J.M., 2006)

5.2.4 Testing Results and Discussions for 3775 Half Prism

Table 5.1 shows the test results of the 3775 half prism under a similar repeated compression test, with the performance of the specimen after the peak load also tested.

The steps before the peak load is called as ascending part and those after the peak load called as descending part. It is observed that during the ascending part, electrical resistance of the 3775 half prism changed in the same trend as the 3775 cube. Initially there was little decrease in electrical resistance due to the improvement in tunneling effect and contacts between GNP particles; when the normalized load level came to around 0.5, increase of electrical resistance occurred and the increase became rapid after the normalized load level reached 0.7. These confirm the reasonableness of the test results and also verify the self damage memorizing ability of the specimen.

Table 5.1 Resistance change for 3775 half prism under repeated compression

	Normalized Compressive Load	Electrical Resistance Change
Ascending	0	-0.01%
	0.2935	-0.04%
	0.5371	0.12%
	0.6931	0.49%
	0.8071	0.67%
	0.9527	2.20%
Peak Load	1	3.41%
Descending	0.9993	11.36%
	0.8364	15.10%

However, the electrical resistance increase for 3775 half prism during the ascending part was not as significant as that for the 3775 cube in last test. While the electrical resistance increase for the 3775 cube was more than 22% at the time that compressive failure just occurred (the applied compressive stress equaled to its compressive strength), the corresponding electrical resistance increase for the 3775 half prism was just 3.41%. There are mainly two reasons causing this insignificant electrical resistance increase. The first, which is also the most important reason involves the loading rate. For 3375 half prism,

the loading rate is 800N/s, which is 0.5MPa/s, compared to that of only 20N/s, which is 0.0125MPa/s for the 3775 cube. The much higher loading rate prevented more subcritical crack growth to occur, hindering damage accumulation inside the 3775 half prism. This claim can be supported by referring to the results shown by Cao J. and Chung D.D.L. (2001), which by performing compressive tests on mortar with loading rates up to 0.575MPa/s, concluded that the loading rate affects the damage evolution all the way from the early part of the loading, and a higher loading rate results in less time for microstructure change, thereby leading to less damage built-up. The second reason involves the aspect ratio of the specimen. As has been mentioned, for a specimen under a uniaxial compressive test, the friction between the testing platens and the surfaces of the specimen produces considerable lateral confinement within the specimen. This confining pressure is greatest right at the specimen end and gradually dies out at a distance from each end of approximately 0.866*d*, where *d* is the dimension of the end surfaces (Mindess S. et al., 2003). Therefore, for the 3775 cube, actually the whole specimen was in a state of tri-axial stress, causing the cracks to propagate in the directions that form angles with the longitudinal direction. According to the equivalent circuits discussed in section 5.2.2, this form of cracks can effectively cut off the conductive network and lead to significant electrical resistance increase. On the other hand, the center of the 3775 half prism has a distance of *d* to either of its surface ends, which is larger than the value of 0.866*d*, meaning that the central portion of the specimen is in true uniaxial compression. Therefore the cracks at the center of the 3775 half prism propagate in the longitudinal direction, which is parallel to some of the branch circuits (see Fig. 5.15) and less interruption occurs in the conductive network, leading to less significant electrical

resistance increase.

To verify the ability of the 3775 half prism to memorize the accumulated internal damage, the compressive test was carried on after the compressive load had reached the compressive strength. It was found that during the descending part, the electrical resistance increase became significant, which means that the repeated re-loading after the peak load had led to dramatically increasing damage inside the specimen, although the damage was not obvious when observed from the surface of the specimen (see Figure 5.18). It is inferred that there is certain correlation between electrical resistance increase and residual loading capacity of the specimen during the descending part, which can be used to help in assessing the safety of a structure after an unexpected accident such as an earthquake. This provides a possible direction for future studies.

Fig.5.18. Surface view of 3775 half prism after self damage memorizing property test

CHAPTER 6 SUMMARY AND CONCLUSIONS

6.1 Summary of Present Study

The objective of this study is to investigate the feasibility of developing intrinsically smart construction materials by using GNP as a novel conductive admixture for cementitious nanocomposites. The GNP particles were added into the cement matrix and both the mechanical and electrical properties of the nanocomposites were studied. In particular, the self damage memorizing properties of the new materials were investigated.

The first part of this study focused on solving the agglomeration problem of the nanoparticles when they are added into the matrix. Two methods were investigated to facilitate the dispersion of GNP particles: by using dispersants and applying ultra-sonication technique. The effects of different dispersants on preparing stable GNP suspension were compared to select the most suitable one. The effect of ultra-sonication technique on further dispersing GNP particles was studied by SEM technique. The dispersing mechanism of the dispersant and the mechanism of ultra-sonication were also studied.

In the second part of this study, 10 batches of cement paste specimens and 9 batches of mortar specimens were fabricated, with each batch including six 50*50*50mm cubes and six 40*40*160mm prisms. Compressive strength tests were carried out with the small cubes and flexural strength tests were carried out with the prisms, to study the mechanical

properties of GNP reinforced cementitious composites. The strengthening mechanisms for these nanocomposites were analyzed and in addition, the potential problems preventing further improvement in mechanical properties were discussed.

The third part of this study started to work on electrical properties of GNP reinforced mortar. Firstly the processing technique for incorporating a high dose of GNP into the cement matrix was studied, to facilitate fabricating specimens with high conductivity. The conducting mechanism for GNP reinforced cementitious composites were analyzed, based on which experimental tests were carried out to study the effects of different factors on electrical resistance of the specimens, including electric polarization, type of GNP, age and dimensions of the specimen, as well as temperature and moisture content.

In the last part of this study, the self damage memorizing property of the GNP reinforced mortar specimens were studied. The first experimental test was carried out with a small cube and a prism to study the relation between electrical resistance increase and growth of a major crack. To simulate the performances of the specimens under the crack, models from previous literatures were compared and a new model was proposed. The second experimental test studied the electrical resistance increase of the specimens under repeated uniaxial compression. The reasonableness of the test results was discussed and the advantages of damage memorizing method over real-time damage sensing method were analyzed.

6.2 Conclusions

6.2.1 Dispersion of GNP

Agglomeration problem occurs in GNP particles due to their nano size and high surface energy. To solve this problem two measures were taken in this study: firstly, using a dispersant and secondly, applying ultra-sonication technique.

The study on dispersant selection was carried out. Compared to acetone, gum arabic and tap water, Darex Super 20 was able to prepare GNP suspensions with good stability and meanwhile had minimal alteration on fresh cement mixtures, therefore it was selected as the only dispersant for GNP particles throughout this study. This is the first time that Darex Super 20 is used as a dispersant for carbon-based nano-particles in cementitious composites. Its dispersing mechanism involves making the GNP particles carry uniform charges of like sign and thus repel each other.

Besides using a dispersant, better dispersion of GNP particles can be achieved by applying ultra-sonication technique. During ultra-sonication energy is imparted into GNP particles, resulting in the breakage of the weak interlayer pi-bonds. In this way the graphene layers in GNP particles can be separated and smaller GNP particles can be obtained. The effect of ultra-sonication was verified by looking at SEM images. It was found that a time period of 2 hours has been beyond the sonication threshold, with which satisfactory expansion, peeling and fractionation of the GNP particles had been achieved.

6.2.2 Mechanical Properties of GNP Reinforced Cement Paste and Mortar

After the GNP particles were added, for cement paste batches there was no increase in the compressive strength, but a maximum increase of 82% in the flexural strength was observed. For the mortar batches both the compressive strength and the flexural strength were increased. The most significant increase in compressive strength was 20% and the maximum increase in flexural strength was 23%. No significant variation in stiffness was observed for both cement paste and mortar. By comparing the test results of the mixtures in different batches, the effects of incorporating GNP particles and enhancing their dispersion on improving mechanical properties of cementitious composites were confirmed.

There are basically five effects making GNP particles able to enhance the mechanical properties of cementitious composites. (1) The small size effect that makes GNP particles have atoms that can easily migrate and absorb energy when under an applied force. (2) The surface effect that makes GNP particles to have a large surface area and high surface energy. These help to strengthen the bond between GNP particles and cement matrix. (3) The filler effect of GNP particles that helps to reduce porosity, pore size and connectivity of pores in the cement matrix. (4) GNP particles absorb large amount of water and reduce the bleeding problem, by which interfacial transition zone is improved. (5) The GNP particles bridge, block and divert micro cracks, which delay crack origination and slow down crack propagation.

However, in this study, the enhancement in mechanical properties of GNP reinforced cementitious composites was not significant enough for industrial purposes. There are probably four potential problems leading to this. (1) The thermal incompatibility between cement matrix and GNP particles may have caused flaws and defects due to the heat generated during cement hydration. (2) Insufficiently dispersed GNP particles may have formed weak zones in the matrix. (3) Insufficient multi-axial rigidity of GNP particles may limit their strengthening effect when under multi-axial loading. (4) The dosage of GNP particles may be too low to manifest their potential in strengthening effect.

6.2.3 Study on Electrical Resistance of GNP Reinforced Mortar

After GNP particles were added into the mortar mixtures, electrical properties of the material were significantly enhanced and the material became highly conductive. The conducting mechanism in GNP reinforced mortar involves three conducting paths: (1) the ionic conduction through the free evaporable water in the cement matrix; (2) the electronic conduction and hole conduction through GNP and cement matrix in series by tunneling effect; and (3) the electronic conduction and hole conduction through conductive network formed by GNP particles connecting each other. The third conducting path is the dominated one since the GNP fraction in this study has been larger than the percolation threshold.

Parametric studies were carried out to investigate the factors having effects on electrical resistance of GNP reinforced mortar, including the effect of electric polarization, the type of GNP, the specimen dimensions, age of the specimen, temperature and moisture. The

following conclusions have been made: (1) Electric polarization was found to cause-electrical resistance of the material to keep increasing with time. To exclude the effect of electric polarization, electrical resistance could be measured within a short period of 5 seconds before polarization became significant. (2) The inclusion of GNP particles helped to decrease the resistivity of the composites. GNP of TC307 was more effective than 3775 because its smaller particle size led to better dispersion, and its larger surface area and larger aspect ratio increased the chance of forming a conductive network. (3) Specimens having different dimensions showed different resistivity. Furthermore, even two specimens having the same dimensions from the same batch showed significant different resistivity. Therefore resistivity of a specimen cannot be simply represented by an average value of a batch or by a value of another specimen. (4) Electrical resistance of GNP reinforced mortar increased with age as the cement hydration process went on. The electrical resistance development curves had a similar shape to the strength development curves. (5) The electrical resistance of GNP reinforced mortar decreased linearly as the temperature increased in the range of 25 to 62 centigrade. This is due to the accelerated movements of electrons in GNP and ions in cement matrix moisture when the temperature increases. (6) The moisture content in the GNP reinforced mortar affected its electrical resistance only slightly. This shows that the GNP fraction has been larger than the percolation threshold and conductive networks have been formed inside the material.

6.2.4 Self Damage Memorizing Properties of GNP Reinforced Mortar

GNP reinforced mortar has the potential in being used as a damage sensing material due to its enhanced electrical properties. Experimental results showed that electrical

resistance of a specimen increased as a crack developed at its center. However, specimens with different dimensions behaved differently when the crack developed. For TC307 cube, the electrical resistance increased nearly linearly as the crack developed until 60% of its whole height, while for 3775 prism, the electrical resistance changed only slightly until the crack depth is larger than 40% of the specimen height. The different performances of the two specimens are believed to be due to their different aspect ratios. Under the same relative crack depth (the ratio between crack depth to the height of the specimen), the current streamlines in the specimen with a smaller aspect ratio is disturbed more significantly, therefore lead to a more significant electrical resistance increase. By observing the disadvantages of the existing models that were developed for metallic materials, a new model based on the law of electrical resistance was proposed to study the electrical resistance change when under the crack development. A function based on the relative crack depth was introduced to modify the electrical resistance calculated with residual cross section area of the specimen. The proposed model was found to be reasonable and it provided a good match with the experimental data.

The damage sensing property for specimens under uniaxial compression was also studied. It was found that electrical resistance of the specimens increased as their internal damage developed. By looking at the electrical resistance change curves the internal damage developing stages could be identified, and they were proved to be consistent with the reported results based on a micro cracking theory. In this study the internal damage of the material was measured using the “damage memorizing method”, whose advantages lie in continuous real-time electrical resistance measurement is not needed, early internal

damage can be captured and internal damage development during the whole loading process can be monitored. Moreover, it was found that internal damage development could also be well monitored for a specimen having a larger aspect ratio and under a higher loading rate.

6.3 Recommendation for Future Work

1. Processing conditions affect significantly the mechanical properties of the nanocomposites and percolation threshold of the conducting fillers. There is still a large room for improvements in nanocomposite fabrication towards optimization of various processing variables. More uniform dispersion of GNP particles in the cement matrix and higher extent of exfoliation may be achieved by using strong chemicals such as nitrate or sulphate acid as the dispersant. Besides, the interfacial adhesion between GNP particles and the matrix may be improved by implementing surface treatments such as UV/O_3 treatment technique or organo-silanes processing technique.

2. In this study, fraction of GNP for specimens in electrical property tests was selected as 5% to achieve high conductivity. This value is beyond the percolation threshold but probably not the optimum. The optimum fraction of GNP will not only form satisfactory conductive network within the matrix but also increase the sensitivity of the network to internal damage. Therefore the optimum fraction of GNP is desired to be found in future researches to improve the self damage sensing property of the composites.

3. This study serves as a preliminary development for smart construction materials that can monitor their internal damage by showing electrical resistance change. However, the greatest challenge for future works involves the application of the test results into real structures. To achieve this, further researches are needed to study the responses of electrical resistance under multi-crack condition, tri-axial stress condition and so on, and also the form of the smart material as well as the form of electrical contacts in the real structures.

References

Administration U. S. F. H., Portland Cement Concrete Pavements Research: Thermal Coefficient of Portland Cement Concrete, Retrieved 2010, from http://www.fhwa.dot.gov/pavement/pccp/thermal.cfm

Ajayan P. M., Schadler L. S. and Braun P. V., Nanocomposite science and technology, Strauss Offsetdruck GmbH, Modenbach, Germany, 2003.

Asbury, Structure and bonding, Retrieved 2010, from http://www.asbury.com/structure-and-bonding.html

Balberg I., Anderson C. H., Alexander S. and Wagner N., Excluded volume and its relation to the onset of percolation, Physical Review B, Vol. 30(7), 1984, pp. 3933-3943.

Banthia N., Djeridane S. and Pigeon M., Electrical resistivity of carbon and steel micro-fiber reinforced cements Cement and Concrete Research, Vol. 22(5), 1992, pp. 804-814.

Beer F. C. d., Strydom W. J. and Griesel E. J., The drying process of concrete: a neutron radiography study, Applied Radiation and Isotopes, Vol. 61(4), 2004, pp. 617-623.

Cao J. and Chung D. D. L., Electric polarization and depolarization in cement-based materials, studied by apparent electrical resistance measurement Cement and Concrete Research, Vol. 34(3), 2004, pp. 481-485.

Chacko R. M., Banthia N. and Mufti A. A., Carbon-fiber-reinforced cement-based sensors Canadian Journal of Civil Engineering, Vol. 34(3), 2007, pp. 284-290.

Chen B. and Liu J., Damage in carbon fiber-reinforced concrete, monitored by both electrical resistance measurement and acoustic emission analysis, Construction and Building Materials, Vol. 22, 2007, pp. 2196-2201.

Chen P.-W. and Chung D. D. L., Carbon Fiber Reinforced Concrete as a Smart Material Capable of Non-Destructive Flaw Detection, Smart Materials and Structures, Vol. 2(1), 1993, pp. 22-30.

Chen P.-W. and Chung D. D. L., Carbon fiber reinforced concrete as an intrinsically smart concrete for damage assessment during static and dynamic loading, ACI Materials Journal, Vol. 93(4), 1996, pp. 341-350.

Chiou J.-M., Zheng Q. and Chung D. D. L., Electromagnetic interference shielding by carbon fibre reinforced cement Composites Vol. 20(4), 1989, pp. 379-381.

Chung D. D. L., Self-monitoring structural materials. Material Science and Engineering, Material Science and Engineering, Vol. 22, 1998, pp. 57-78.

Chung D. D. L., Damage in cement-based materials, studied by electrical resistence measurement, Material Science and Engineering, Vol. 42, 2003, pp. 1-40.

Drzal L. T. and Fukushima H., Nanographite: a multifunctional nanomatrial for polymers and composites, Paper presented at the High performance fillers 2006: the 2nd International Conference on Fillers for Polymers, 2006

Gogotsi Y., Nanomaterials handbook, CRC Press, 2006.

Gong S., Study on the long-term mechanical properties and pressure-sensitivity of concrete containing nano-sized carbon black or carbon fibers, B. Eng. Thesis, Department of Civil Engineering, Shantou University, Shantou, 2008.

Grobert N., Carbon nanotubes - becoming clean, Materialstoday, Vol. 10(1-2), 2007, pp. 28-35.

Hamann C. H., Hamnett A. and Vielstich W., Electrochemistry, Weinheim, New York, 1998.

Hilding J., Grulke E. A., Zhang Z. G. and Lockwood F., Dispersion of carbon nanotubes in liquids Journal of Dispersion Science and Technology, Vol. 24(1), 2003, pp. 1-41.

Hugh, Hankbook of carbon, graphite, diamond and fullerenes, Noyes Publications, New Jersey, 1993.

Hussain M., Choa Y. H. and Niihara K., Fabrication process and electrical behavior of novel pressre-sensitive composites, Composites: Part A, Vol. 32, 2001, pp. 1689-1696.

Ibarra Y. S. d., Gaitero J. J., Erkizia E. and Campillo I., Atomic force microscopy and nanoindentation of cement pastes with nanotube dispersions, physica status solidi (a), Vol. 203(6), 2006, pp. 1076-1081.

Jia W., Tchoudakov R., Narkis M. and Siegmann A., Performance of expanded graphite and expanded milled-graphite fillers in thermosetting resins, Polymer Composites, Vol. 26(4), 2005, pp. 526-533.

Johnson H. H., Calibrating the electric potential method for studying slow crack growth, Material Research and Standards, Vol. 5, 1965, pp. 442-445.

Jovic N., Dudic D., Montone A., Vittori Antisari M., Mitric M. and Djokovic V., Temperature dependence of the electrical conductivity of epoxy/expanded graphite nanosheet composites, Scripta Materialia, Vol.58, 2008, pp. 846-849.

Konsta-Gdoutos M. S., Metaxaa Z. S. and Shah S. P., Multi-scale mechanical and fracture characteristics and early-age strain capacity of high performance carbon nanotube/cement nanocomposites Cement and Concrete Composites, Vol. 32(2), 2010, pp. 110-115.

Lee C.-Y. and Wang S.-R., Analysis of resistance characteristics of conductive concrete using press-electrode method, International Journal of Environmental and Earth Sciences, Vol. 1, 2010, pp. 7-10.

Li C.-Y. and Wei R. P., Calibrating the electrical potential method for studying slow crack growth, Material Research and Standards, Vol. 6, 1966, pp. 392-394.

Li G. Y., Wang P. M. and Zhao X., Mechanical behavior and microstructure of cement composites incorporating surface-treated multi-walled carbon nanotubes, Carbon, Vol. 43(6), 2005, pp. 1239-1245.

Li G. Y., Wang P. M. and Zhao X. H., Mechanical behavior and microstructure of cement composites incorporating surface-treated multi-walled carbon nanotubes, Carbon, Vol. 43, 2005, pp. 1239-1245.

Li G. Y., Wang P. M. and Zhao X. H., Pressure-sensitive properties and microstructure of carbon nanotube reinforced cement composites, Cement and Concrete Composites, Vol. 29, 2007, pp. 377-382.

Li H., Xiao H. and Ou J., Electrical property of cement-based composites filled with carbon black under long-term wet and loading condition, Composites Sicence and Technology, Vol. 68, 2008, pp. 2114-2119.

Li J., Kim J. K. and Sham M. L., Conductive graphite nanoplatelet/epoxy nanocomposites: effects of exfoliation and UV/ozone treatment of graphite, Scripta Materialia, Vol. 53, 2005, pp. 235-240.

Li J., Sham M. L., Kim J.-K. and Marom G., Morphology and properties of UV/ozone treated graphite nanoplatelet/epoxy nanocomposites Composites Science and Technology, Vol. 67(2), 2007, pp. 296-305.

Luo J., Fabrication and functional properties of multi-walled carbon nanotube/cement composites, Ph.D. Thesis, Department of Civil Engineering, Harbin Institute of Technology, Harbin, 2009.

Mehta, P., and Monteiro, P.J.M., Concrete Microstructure Properties and Materials, 3rd Edition, McGraw-Hill, New York, 2006.

Mindess S., Young J. F. and Darwin D., Concrete: Second Edition, pearson Education, Inc, United States of America, 2003.

Nan C.-W., Physics of inhomogeneous inoganic materials, Progress in Materials Science, Vol. 37, 1993, pp. 1-116.

Nanoamor, Nano scale and amorphous products, Retrieved April 14, 2010, from http://www.nanoamor.com/home

Pierson H. O., Handbook of carbon, graphite, diamond and fullerenes: properties, processing, and applications, New Jersey, Noyes, 1993.

Pike G. E. and Seager C. H., Percolation and conductivity: a computer study I, Physical Review B, Vol. 10(4), 1973, pp. 1421-1434.

Qi W. H. and Wang M. P., Size effect on the cohesive energy of nanoparticle Journal of Materials Science Letters Vol. 21(22), 2002, pp. 1743-1745.

Qizhao M., Binyuan Z., Darong S. and Zhuoqiu L., Influence of polarization on the conductivity of carbon fibre reindorced cement, Chinese Journal of Materials Research, Vol. 11(2), 1997, pp. 195-198.

Reid R., Roofing and Cladding Systems Handbook: A Guide for Facility Managers, The Fairmont Press, Lilburn, GA, 2000.

Reza F., Batson G. B., Yamamuro J. A. and Lee J. S., Volume electrical resistivity of carbon fiber cement composites, Materials Journal, Vol. 98(1), 2001, pp. 25-35.

Reza F., Yamamuro J. A. and Batson G. B., Electrical resistance change in compact tension specimens of carbon fiber cement composites, Cement and Concrete Composites, Vol. 26(7), 2004, pp. 873-881.

Saafi M., Wireless and embedded carbon nanotube networks for damage detection in concrete structures Nanotechnology, Vol. 20(39), 2009, pp.

Sanchez F. and Ince C., Microstructure and macroscopic properties of hybrid carbon nanofiber/silica fume cement composites, Composites Science and Technology, Vol. 69(7-8), 2009, pp. 1310-1318.

Seager C. H. and Pike G. E., Percolation and conductivity: a computer study II, Physical Review B, Vol. 10(4), 1973, pp. 1435-1446.

Sengupta R., Bhattacharya M., Bandyopadhyay S. and Bhowmick A. K., A review on the mechanical and electrical properties of graphite and modified graphite reinforced polymer composites, Progress in Polymer Science, Vol., 2010, pp.

Shah S. P., Konsta-Gdoutos M. S., Metaxa Z. S. and Mondal P., Nanoscale Modification of Cementitious Materials Nanotechnology in Construction 3 Vol. Part 2, 2009, pp. 125-130.

Sun M., Li Z., Mao Q. and Shen D., Study on the hole conduction phenomenon in carbon fiber-reinforced concrete Cement and Concrete Research, Vol. 28(4), 1998, pp. 549-554.

Toutanji H. A., El-Korchi T. and Katz R. N., Strength and reliability of carbon-fiber-reinforced cement composites Cement and Concrete Composites, Vol. 16(1), 1994, pp. 15-21.

Viculis L. M., Mack J. J., Mayer O. M., Hahn H. T. and Kaner R. B., Intercalation and exfoliation routes to

graphite nanoplatelets, Journal of Materials Vol. 15, 2005, pp. 974-978.

Wang Y., Study on mechanical properties and pressure-sensitivity of cement-matrix composites containing nano-sized carbon black, B. Eng. Thesis, Department of Civil Engineering, Shantou University, Shantou, 2005.

Wang Y., Study on mechanical properties and electrical behaviors of carbon fibers/carbon-black nanoparticles reinforced composites, M. Eng. Thesis, Department of Civil Engineering, Shantou University, Shantou, 2007.

Wen S. and Chung D. D. L., Effect of moisture on piezoresistivity of carbon fiber-reinforced cement paste, ACI Materials Journal, Vol. 105(3), 2008, pp. 274-280.

Wikipedia, Nanomaterials, Retrieved 22 February, 2011, from http://en.wikipedia.org/wiki/Nanomaterials

Wu X., Qi S., He J. and Duan G., High conductivity and low percolation threshold in polyaniline/graphite nanosheets composites, Journal of Material Science, Vol. 45(2), 2010, pp. 483-489.

Xiao H. and Li H., A study on the application of CB-filled cement-based composite as a strain sensor for concrete structures, Proceeding of SPIE, Vol., 2006, pp.

Yu A., Ramesh P., Sun X., Bekyarova E., Itkis M. E. and Haddon R. C., Enhanced thermal conductivity in a hybrid graphite nanoplatelet - carbon nanotube filler for epoxy composites, Advanced Materials, Vol. 20(24), 2008, pp. 4740-4744.

Publication

Conference

1. S. Huang, P. Wang, S. D. Pang and S. T. Quek, Mechanical and electrical properties of graphite nano-platelet (GNP) reinforced cement paste/mortar, 23rd KKCNN Symposium on Civil Engineering, 13-15 November 2010, pp. 441-444.

APPENDIX A: PRODUCT SHEET FOR ASBURY 3775

ASBURY CARBONS

Product Data Sheet
3775

General Product Description

	Min	Max	Target
%Carbon (LOI)	95	100	☐
%Moisture	0	1	☐
MT%50 (Microns)	5	10	☐
Surface Area m2/g	20		☑

Type: SURFACE ENHANCED FLAKE GRAPHITE

Typical Analysis

(U.S. Standard Test Sieves)

%Carbon (LOI)	97.96
%Moisture	0.32
%Sulfur	0.07
%+325 Mesh (44 Micron)	0.01
%-325 Mesh (44 Micron)	99.99
MT%10 (Microns)	3.1
MT%50 (Microns)	8.04
MT%90 (Microns)	18.13
Surface Area m2/g	23.7

Test Methods

Carbon	E4-1
Microtrac	E3-5B
Moisture	E4-7
Sieve Analysis	E2-3
Sulfur	E4-9
Surface Area	E36/9

The PDS lists percentages which are only guaranteed following specific agreement between Asbury and the customer. They are listed here only to indicate approximate physical and chemical analysis. Purchasers should thoroughly test and independently verify satisfactory results before application. The user assumes the risk and liability for loss, damage, or injury arising from the application of the goods furnished.

UNCONTROLLED DOCUMENT: Prior to placing an order based on this PDS, contact the Asbury Sales Department to confirm that the information contained herein is current.

Revision Level: Revision 3 **Revision Date:** 4/27/2009

Asbury Graphite Mills, Inc.
PO Box 144 405 Old Main St.
Asbury, New Jersey 08802
Tel: (908) 537-2155 **Fax:** (908) 537-2108 **http://** www.asbury.com

APPENDIX B: PRODUCT SHEET FOR ASBURY TC307

ASBURY CARBONS

Product Data Sheet
TC307

General Product Description

	Min	Max	Target
%Carbon (LOI)	99.8		☐
MT%50 (Microns)		5	☐
Surface Area m2/g	200		☐

Type: PRIMARY ARTIFICIAL

Typical Analysis

(U.S. Standard Test Sieves)

%Carbon (LOI)	99.92
%Moisture	0.96
%Sulfur	0.009
MT%10 (Microns)	0.73
MT%50 (Microns)	2.59
MT%90 (Microns)	5
Surface Area m2/g	352
True Density g/cc	2.16

Test Methods

Carbon	E4-1
Microtrac	E3-5B
Moisture	E4-7
Sieve Analysis	E2-5
Surface Area	E3-9

Revision Level: Revision 1 **Revision Date:** 5/28/2009

Asbury Graphite Mills, Inc.
PO Box 144 405 Old Main St.
Asbury, New Jersey 08802
Tel: (908) 537-2155 **Fax:** (908) 537-2108 **http://** www.asbury.com

APPENDIX C: PRODUCT SHEET FOR TIMREX_T15

TIMCAL
GRAPHITE & CARBON

TECHNICAL DATA SHEET

TIMREX® T15
Graphite

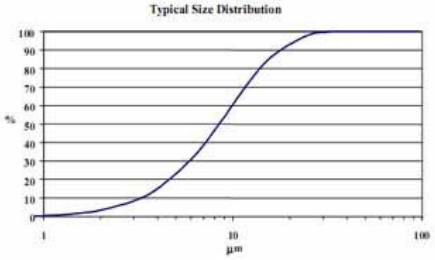

General Characteristics
Formula: Carbon
Aspect: Fine black powder
CAS number: 7782-42-5

Standard Packaging
-20 kg paperbags, 39 bags on one pallet (780 kg)

Guaranteed Values

Ash	**0.1**	**% max**
Moisture	**0.5**	**% max**
Crystallite Height	**80**	**nm min**
Interlayer Distance	**0.3354-0.3360**	**nm**
D90 (Laser Malvern)	**15.5-20.5**	**µm**

Typical Values

Purity		
Ash	0.08	%
Moisture	0.1	%
Al	10	ppm
As	<0.5	ppm
Ca	100	ppm
Co	<1	ppm
Cr	<1	ppm
Cu	<1	ppm
Fe	60	ppm
Mo	<1	ppm
Ni	2	ppm
Pb	<2	ppm
Sb	<0.1	ppm
Si	80	ppm
Ti	160	ppm
V	20	ppm
S	50	ppm
Cristallinity		
Lc	90	nm
c/2	0.3355	nm
Density		
Scott	0.1	g/cm³
Xylene	2.24	g/cm³
Specific Surface Area		
BET	13	m²/g
Particle Size Distribution		
Laser Malvern		
D10	3.2	µm
D50	8.5	µm
D90	17.7	µm

DOC.3.01.1.1129
Version 09/06

This product is in compliance with the EC Directive 2002/95/CE (Restriction Of Hazardous Substances, ROHS).

The information contained herein is believed to be correct. However, no warranty is made, either expressed or implied regarding the accuracy or the results to be obtained from the use of such information.

The user assumes all risk and liability for loss, damage or injury to property or others resulting from the use of the material.

No statement is intended or should be construed as recommendation to infringe any existing patent.

TIMCAL Group
TIMCAL Ltd., CH-6743 Bodio, Switzerland
Phone: +41 91 873 20 10 – Fax: +41 91 873 20 19 – http://www.timcal.com

a member of IMERYS

APPENDIX D: PRODUCT SHEET FOR DAREX SUPER 20

Grace Concrete Products

GRACE

Darex® Super 20

Superplasticiser for the Production of High Workability Concrete

Description

Darex® Super 20 is a high range water reducer based on naphthalene sulfonate. It is a low viscosity liquid which has been formulated by the manufacturer for use as received. Darex Super 20 contains no added chloride. Darex Super 20 is formulated to comply with the following chemical admixture specifications for concrete: BS 5075: Part 3: 1985. One litre weighs approximately 1.2kg ± 0.02kg.

Advantages

- High slump flowable concrete at no loss in strength.
- Low water/cement ratio concrete and therefore, high strengths.
- In prestress/precast work, can be used to substantially reduce or eliminate the high energy requirements of external heat for accelerated curing.
- Can be used with Type I cement to substitute for normal concrete produced with Type III cement to achieve early release strengths.
- Exhibits no significant segregation even at high slump.
- Aids in rapid discharge of concrete from truck mixers, thereby reducing time and improving mixer utilisation.

Dispersion

Darex Super 20 is a superior dispersing admixture having a marked capacity to disperse the cement agglomerates normally found in a cement-water suspension. The capability of Darex Super 20, in this respect, exceeds that of normal water-reducing admixtures.

Applications

Darex Super 20 produces concrete with extremely workable characteristics referred to as high slump, flowing concrete. Darex Super 20 also allows concrete to be produced with very low water/cement ratios at low or normal slumps.

Darex Super 20 is ideal for use in prestress, precast, bridge deck or any concrete where it is desired to keep the water/cement ratio to a minimum and still achieve the degree of workability necessary to provide easy placement and consolidation. Darex Super 20 will also fluidise concrete making it ideal for tremie concreting or other applications where high slumps are desired.

Addition Rates

Addition rates of Darex Super 20 can vary with type of application, but will normally range from 400 to 2,500ml / 100kg of cementitious material. In most instances the addition of 400 to 2,000ml / 100kg of cementitious material will be sufficient. At a given water/cement ratio, the slump required for placement can be controlled by varying the addition rate. Should job site conditions require using more than recommended addition rates, please consult your Grace Representative.

Compatibility with Other Admixtures

In concrete containing Darex Super 20, the use of an air-entraining agent (such as Daravair® or Darex® AEA®) is recommended to provide suitable air void parameters for resistance against freeze-thaw attack. Most water reducers or water-reducing retarders are compatible with Darex Super 20 as long as they are separately added to the concrete. Pretesting of the concrete should be performed to optimise dosages and addition times of these admixtures. Caution should be exercised when using Darex Super 20 together with a retarder, as excessive retardation can occur if the admixture dosages are too high. The admixtures should not be in contact with each other before they enter the concrete.

Dispensing Equipment

A complete line of admixture dispensers is available. Accurate and easy to maintain, the dispensers are easily adapted to new or existing batching plants.

Packaging

Darex Super 20 is available in bulk and in 205L drums. Darex Super 20 contains no flammable ingredients. It will begin to freeze at approximately 0°C, but will return to full strength after thawing and agitation.

In storage and for proper dispensing, Darex Super 20 should be maintained at temperatures above 0°C.

Health and Safety

See Darex Super 20 Material Safety Data Sheet or consult Grace Construction Products.

www.graceconstruction.com

Australia: Adelaide (61-8) 8261 8622, Brisbane (61-7) 3277 7244, Melbourne (61-3) 9359 2121, Perth (61-8) 9353 3433, Sydney (61-2) 9743 8811
Hong Kong (852) 2675 7898 Indonesia (62-21) 893 4260 Japan (81-3) 5405 2991 Korea (82-32) 814 2051
China Mainland: Beijing (86-10) 6786 3488, Guangzhou (86-20) 3833 0775, Shanghai (86-21) 5467 4678
Malaysia (60-3) 9074 6133 New Zealand: Auckland (64-9) 579 1320, Christchurch (64-3) 327 2173, Wellington (64-4) 238 2048 Philippines (63-49) 5497373 Singapore (65) 6265 3033 Taiwan (886-3) 461 5461
Thailand (66-2) 709 4470

GRACE

APPENDIX E: PRODUCT SHEET FOR GUM ARABIC

TIC GUMS
We're your Gum Guru

4609 Richlynn Drive, Belcamp, MD 21017 USA
(800) 899-3953 • (410) 273-7300
Fax (410) 273-6469 • www.ticgums.com

TIC Pretested® Gum Arabic FT Powder

Detailed Study (U. of MN) available on superior performance as encapsulation of flavor oils. High in soluble dietary fiber (85% typical). Used as a carrier in spray dried flavors, as a foam stabilizer in beer, as a clarifying agent in wines. Used in formulation of "cloud" emulsions and spray dried cloud powders. In confections will retard sugar crystallization and emulsify the fat — preventing the fat from rising to the surface to form an easily oxidizable, greasy film. Widely used in the panning process of many confections. In combination with hydrolyzed soy protein Gum Arabic functions as a whipping and stabilizing agent for aerated confections. In bakery Gum Arabic is used in a bun glaze, contributing to stability, flexibility and pliability. Just a few of the many applications of Gum Arabic.

Typical Usage Level	3% to 30%		
Solubility	Cold Water Soluble		
Suggested Uses	Flavor Encapsulation, Confection, Gum Arabic Replacement, Pet Food, Marshmallow, Tabletting		
Label Declaration	Gum Arabic		
Country of Origin	Made in the U.S.A. from Imported Acacia		
CFR #	21 CFR 184.1330		
CAS #	9000-01-5	Kosher Ⓤ	Y
EU #	414		
HS Tarrif #	1301.20.0000		
Standard Packing	50# Bags, 2,000 lbs. per pallet	All Natural	Y
Lead Time	Stock Product	Shelf-Life	3 years
Storage & Handling	Each container is identified with the product name and lot number. Store in cool dry place for maximum shelf life.		

NUTRITIONAL INFORMATION

Calories (Total)	348 Kcal	Calcium	1016 mg
%Calories from Fat	0.00 %	Total Carbohydrates	85.00 g
Calories from fat	0.00 g	Soluble Dietary Fiber	85 g
Total Fat	0.00 g	Insoluble Dietary Fiber	0.0 g
Trans Fat	0.00 g	Simple Carbohydrates	0 g
Cholesterol	0 g	Complex Carbohydrates	0 g
Sodium	441 mg	Protein	2 g
Potassium	298 mg	Vitamins, Other Minerals	*ND

(per 100 grams). This data is from analysis and calculation and should be considered "typical" and not a specification. Data is reported on an "as is" basis. Total fat and protein values are rounded to the nearest whole number.

* Calculated based on typical assay of component(s)

* N.D.; Not determined

**Total Calories are calculated in compliance with FDA Regulations requiring the inclusion of 4 Kcal/g for all soluble dietary fiber. However dietary fiber by definition consists of plant material that is resistant to hydrolysis by endogenous enzymes of the mammalian digestive tract. TIC GUMS has participated in discussions with the FDA as part of the Calorie Control Council to amend the FDA regulations to 2Kcal/g.

If all nutritional information is listed as "0" then these findings have yet to be evaluated.

SPECIFICATIONS

	Minimum	Maximum	
Bacteriological			
Aerobic Plate Count (AOAC 988.18)	0	500	cfu
Combined Yeast and Mold (BAM)	0	400	/g
E. coli (AOAC 989.11)	Negative /g		-
S. aureus (BAM)	Negative /10g		-
Salmonella - 25g (AOAC 990.13)	Negative /25g		-
Total Coliforms (AOAC 989.11)	0	10	/g
Mesh	**Minimum**	**Maximum**	
USS#80 Mesh Through	80	100	%
Physical and Chemical	**Minimum**	**Maximum**	
Flavor (Qualitative)	Bland		-
Moisture (Infrared)	0	11	%
Odor (Qualitative)	Odorless		-
pH (viscosity solution)	4	5.5	pH
Powder Color (Visual)	White-Off White		-
Solution Color	Lemon-Amber		-
Texture (Qualitative)	Free Flowing Powder		-
Viscosity (30.0%,LV@60rpm)	0	300	cps
Standard	**Minimum**	**Maximum**	
Total Ash Content (USP)	0	4	%
Total Dietary Fiber (Dry Weight Basis)	85% Minimum (Typical)		-

APPENDIX E: SPECIFICATIONS OF FLUKE 110 SERIES DIGITAL MULTIMETER

FLUKE®

Fluke 110 Series
True-rms Digital Multimeter
Extended Specifications

Model Differences
(all other specifications are the same for each model)

Feature	Model		
	110	111	112
Current Measurement		•	•
Backlight			•

Nominal Specifications

Function	Absolute Range or Description	
	Model 110	Models 111 and 112
AC Voltage, True-rms	1 mV to 600.0V (50 Hz to 500 Hz)	
DC Voltage	1 mV to 600.0V	
Continuity	Beeper guaranteed on < 20Ω, guaranteed off > 250Ω; detects opens or shorts of 250 µs or longer.	
Resistance	0.1Ω to 40.00 MΩ	
Diode Test	2.200V, 0.9% + 2 digits, audible feedback	
Capacitance	1 nF to 9999 uF	
AC Current, True-rms	NA	0.01A to 10.00A (20.00A overrange for 30 seconds)
DC Current	NA	0.001A to 10.00A (20.00A overrange for 30 seconds)
Frequency of Voltage	5 Hz to 50 kHz	
Frequency of Current	NA	50 Hz to 5 kHz
Basic DC Voltage Accuracy	0.7%	
Basic AC Voltage Accuracy	1.0%	

FLUKE®

Features

Feature	Description
Backlight (Model 112 only)	Automatically extinguishes after 2 minutes to save battery life The timeout feature can be disabled with a power-up option
HOLD	Display hold, freezes the display at the push of a button
MIN MAX AVG	Minimum, maximum, and average reading memory
Manual or auto ranging	In auto range, the meter selects the range with the best resolution for the present measurement value
Fast continuity/open detection	The beeper sounds with a stretched pulse for opens or shorts as brief as 250 µs
Beeper	Used in continuity and diode test functions, to signal new minimum and maximum in MIN MAX mode, and to signal valid and invalid button presses
Test lead alert	The message "LEAD" appears briefly on the display when the rotary switch is moved to or from any **A** (Amps) position
Power-up options	(1) Turn on all LCD segments, (2) Disable beeper, (3) Disable sleep mode, (4) Disable backlight timeout (Model 112 only)
Closed-case calibration	No internal adjustments needed
Probe holders	The standard-equipment protective holster has probe holders on the sides for probe storage and for convenience when making measurements
Battery access door	The battery is replaced easily by removing one Phillips head screw that fastens a battery door on the meter's back cover
Replaceable fuse (111 and 112)	A user-replaceable heavy-duty ceramic fuse protects the DMM from application of excessive current to the **A** (Amps) input jack. Use the exact replacement fuse as stated on the meter back cover
The high-impact case and protective holster	The 110 Series DMMs are tested to withstand a drop of 1 meter to a hard surface

Detailed Specifications

Accuracy is specified for 1 year after calibration, at operating temperatures of 18°C to 28°C, with relative humidity at 0% to 75%. The accuracy specifications take the form of: ± ([% of Reading] + [Counts])	
Maximum voltage between any terminal and earth ground	600V
Surge Protection	6 kV peak per IEC 61010-1-95
Fuse for A input (111 and 112)	11A, 1000V FAST Fuse, minimum interrupt rating 17000A
Display	Digital: 6,000 counts, updates 4/sec Bar Graph: 33 segments, updates 40/sec Frequency: 9,999 counts Capacitance: 9,999 counts
Temperature	Operating: -10°C to +50°C Storage: -30°C to +60°C
Temperature Coefficiant	0.1X (specified accuracy/°C) (<18°C or >28°C)
Electromagnetic Compatibility	Performance ≥ 3 V/m is not specified
Relative Humidity	Noncondensing < 10°C 0% to 95% @ 10°C to 30°C 0% to 75% @ 30°C to 40°C 0% to 45% @ 40°C to 50°C
Battery Life	Alkaline: 300 hrs typical, without backlight
Size, with Holster (H x W x L)	4.6 cm x 9.6 cm x 16.0 cm
Weight	350g
Safety Compliances	ANSI/ISA-S82.01-1988, CSA C22.2 No 231 and IEC 61010-1-95 Overvoltage Category III (CAT III), 600V
Warranty	Three years
Certifications	UL (3111), CE, CSA, TÜV, C (N10140)

FLUKE®

Function	Range	Resolution	Accuracy ±([% of Reading] + [Counts])		
			Model 110	Model 111	Model 112
AC Volts[1,2] — True-rms (50 Hz to 500 Hz)	6000 mV[3] 6.000V 60.00V 600.0V	1 mV 0.001V 0.01V 0.1V	1.0% + 3	1.0% + 3	1.0% + 3
DC Volts	6000 mV[3] 6.000V 60.00V 600.0V	1 mV 0.001V 0.01V 0.1V	0.7% + 2	0.7% + 2	0.7% + 2
Continuity	600Ω	1Ω	Beeper guaranteed on <20Ω, guaranteed off >250Ω; detects opens or shorts of 250 µs or longer.		
Ohms	600.0Ω 6.000 kΩ 60.00 kΩ 600.0 kΩ 6.000 MΩ 40.00 MΩ	0.1Ω 0.001 kΩ 0.01 kΩ 0.1 kΩ 0.001 MΩ 0.01 MΩ	0.9% + 2 0.9% + 1 0.9% + 1 0.9% + 1 0.9% + 1 1.5% + 3	0.9% + 2 0.9% + 1 0.9% + 1 0.9% + 1 0.9% + 1 1.5% + 3	0.9% + 2 0.9% + 1 0.9% + 1 0.9% + 1 0.9% + 1 1.5% + 3
Diode test	2.200V	0.001V	0.9% + 2		
Capacitance[4]	1000 nF 10.00 µF 100.0 µF	1 nF 0.01 µF 0.1 µF	1.9% + 2 1.9% + 2 1.9% + 2	1.9% + 2 1.9% + 2 1.9% + 2	1.9% + 2 1.9% + 2 1.9% + 2
	10000 µF	1 µF	100 µF - 1000 µF: 1.9% + 2 > 1000 µF: 10% + 90 typical		
AC Amps[5] — True-rms (50 Hz to 500 Hz) (Models 111 &112)	10.00A continuous or 20A overload for 30 seconds maximum	0.01A	NA	1.5% + 3	1.5% + 3
DC Amps (Models 111 & 112)	6.000A 10.00A continuous or 20A overload for 30 seconds maximum	0.001A 0.01A	NA	1.0% + 3	1.0% + 3
Hz[6] (V or A input)	99.99 Hz 999.9 Hz 9.999 kHz 50.00 kHz	0.01 Hz 0.1 Hz 0.001 kHz 0.01 kHz	0.1% + 2	0.1% + 2	0.1% + 2
MIN MAX AVG Accuracy and Response Time	Accuracy is the specified accuracy of the measurement function ±12 digits for changes >200 ms in duration (±40 digits in AC). Typical response time: 100 ms to 80% of signal, except V AC and A AC.				

1. AC voltage ranges are specified from 5% of range to 100% of range.
2. Crest factor of ≤3 at full scale up to 300V, decreasing linearly to crest factor ≤1.5 at 600V.
3. The 6000 mV range can only be entered in Manual Range mode. Use the 6000 mV range with accessories.
4. For film capacitors.
5. Crest factor of ≤3. AC current is not specified below 3A.
6. Hz is specified from 5 Hz to 50 kHz in volts, from 50 Hz to 5 kHz in amps.

Function	Input Impedance (Nominal)	Common Mode Rejection Ratio		Normal Mode Rejection
Volts AC	>5 MΩ <100 pF	>60 dB at DC, 50 Hz or 60 Hz		
Volts DC	>10 MΩ <100 pF	>100 dB at DC, 50 Hz or 60 Hz		>50 dB at 50 Hz or 60 Hz
		Full Scale Voltage		
	Open Circuit Test Voltage	**To 6 MΩ**	**40 MΩ**	**Short Circuit Current**
Ohms	<1.5V DC	<600 mV DC	<1.5V DC	<500 µA
Diode test	2.4 to 3.0V DC	2.400V DC		1.2 mA typical

Fluke. *Keeping your world up and running.*